DEVELOPMENT OF AN RNA-BASED THEOPHYLLINE-SPECIFIC MICROARRAY BIOSENSOR

by

Katherine M Jordan

A dissertation submitted in partial fulfillment
of the requirements for the degree of
Doctor of Philosophy
(Physics)
in the University of Michigan
2008

Doctoral Committee:

Associate Professor Jens-Christian D. Meiners, Chair
Professor Bradford G. Orr
Professor Duncan G. Steel
Associate Professor Nils G. Walter
Associate Professor Michal R. Zochowski

DEDICATION

To Mom and Nick,

For all of your support and encouragement.

ACKNOWLEDGEMENTS

It is with great honor and gratitude that I thank the people who have helped me so much throughout my life and without whose support the attainment of this degree would not have been possible.

I would like to express my sincere gratitude towards my advisor, Professor Chris Meiners, for his patience and support throughout my research career. I feel extremely fortunate to have had the opportunity to work with him on such an interesting and interdisciplinary project.

I would also like to thank my thesis committee for all their feedback and for having shown such genuine interest in my work. Specifically, Professor Nils Walter, who was also our main collaborator on this project, provided a great deal of support, as well as many of the resources necessary for the completion of this project. His expertise in catalytic RNA was instrumental to the conception and progress of this research.

Dr. Richard Miller and Dr. Robert Thompson, in the University of Michigan Geriatrics and Neuroscience Departments, respectively, provided unlimited access to their microarray scanners, which were crucial for sample imaging and data acquisition. Also, Lynn Winkelmann's instruction and advice regarding working with microarrays was invaluable during this stage of the research.

The post-docs that I have had the opportunity to work with have been phenomenal teachers without whom I would have been truly lost. I came into this project with a solid academic foundation in physics, but very little knowledge of molecular biology and biophysics. Ari Gajraj, Meredith Newby and David Rueda provided countless hours of mentorship and wet-lab training in the early years of my research. In the later years, Gerhard Blab provided many invaluable insights while helping to keep the project moving forwards and on track. Words cannot

truly express my appreciation of the hours that he spent, coding data analysis programs, teaching me MATLAB, and ducking from the edible projectiles that often pierce the air of the student office.

Throughout the years, I have met so many wonderful and intelligent people at the University of Michigan whose friendships made the graduate experience so enjoyable over the years. To all of my friends in the biophysics group, especially Hao, David, Yih-fan, Krishnan, Seth, Raj Kristin, Jeff, and Matt, thank you for making every semester go by faster than the last. I don't believe that I will ever understand your propensity towards drinking "icky" or why I was the only Meiners student who owned a pair of scissors, but I will miss seeing you every day. Also, Raj and Matt, thank you for making the conferences we attended together exceptionally fun and unpredictable. David, I have passed the tiara on to you, I am sure that you will wear it wisely. Also, I would like to thank my friends in the Walter Lab (Liz, Chamaree, Mark, John, Miguel, Rebecca and Afi) for letting me share your lab space and time on the instruments. Additionally, to my friends Heather and Craig, thank you for all of the times that we studied together or just hung out.

By far, the most memorable part of my graduate career was taking Plasma Theory, a class that ended up having no relevance to this dissertation, but which had the greatest impact on my life. There, I met my husband, Nick, for whom I am grateful for so many things. Mostly, I am thankful for your friendship, for your support during some of the most stressful times in graduate school, and for formatting this dissertation. I look forward to living out our lives together as Dr. and Dr. Jordan and bickering over who gets to be the first Dr.

Likewise, I would like to thank my mother for her support over the years. Mom, I have always admired your strength and courage to face and overcome life's obstacles. You have been there for me through many difficult times and I am truly grateful for that. Without your encouragement and strong support, none of this would have been even possible.

Finally, I would like to thank all of the project sponsors. Funding for this project was provided by The National Institutes of Health (GM 65934-01), the

NASA Fundamental Space Biology Program, the NASA Bioengineering Institute, and the Alfred P. Sloan Foundation. Additionally, throughout the years, I received financial support from other sources, all for which I am extremely grateful. Erie Scientific Company supplied materials necessary for sample preparation, such as the hundreds of coated microarray slides, free of charge. This support also included the Molecular Biology Training Grant and several teaching assistance-ships and grading appointments that I received from the Physics Department over the course of my graduate studies.

TABLE OF CONTENTS

LIST OF FIGURES

LIST OF TABLES

LIST OF APPENDICES

CHAPTER 1
INTRODUCTION

The ability to identify and quantify the concentrations of drugs, second messengers, hormones, proteins and pathogens is of fundamental biomedical importance. Although DNA microarray chips are revolutionizing biology by expanding our analyses from single-gene to genome-wide gene expression, analogous methods for the simultaneous study of the metabolome and proteome are not yet available. In addition, rapid monitoring of cellular events such as second messenger synthesis and hormone secretion in single cells is key to understanding cellular organization in higher organisms, yet is still not fully accomplished. Finally, early pathogen detection is of increasing urgency in clinical diagnosis and bio-defense in the face of newly emerging infectious diseases. For these applications, new biosensor technologies are needed.

1.1 Biosensors for Small Molecules

A biosensor is described as an analytical device that uses a biodetector, such as enzymes, antibodies, nucleic acids, microorganisms, or tissues to specifically detect a target analyte of interest without the need for complex specimen processing [Set94]. Traditionally, the biosensor has three parts: the sensitive biological element, a physiochemical detector element, and the transducer in between which associates both components [IUP07]. Ideally, a biosensor is extremely sensitive and highly specific for the target of interest, with the capability for specificity based on chirality. Additionally, its design is adaptable to a wide range of target analytes, as well as compact, rugged, and devised to consume minimal resources [Sch01a].

Biosensors were first developed for clinical applications and the medical applications for these biosensors are numerous. They include drug discovery and design, the monitoring of drug delivery in time, and the detection and quantification of small molecules. The first such device was an enzyme electrode developed by Leland C. Clark in 1962 and the first biosensor system to come to market was for glucose in 1975 [Set94]. More biosensor instruments were launched in the late 1980's, beginning a surge in the development of biosensor products designed for the diagnostics market and sold worldwide.

In the last decade, there has been great interest in the development of efficient and portable pathogen detection biosensors for biosecurity [Fis07] stemming from the intentional dissemination of *Bacillus anthacis* spores by contaminated U.S. Postal Service mail in the fall of 2001. This not only resulted in panic in the general public, but also a deeper awareness of the importance of rapidly and accurately detecting such events. Great strides have been made in the environmental surveillance of potential biologically threatening agents [Lim05], however, technological developments are still needed for fabrication of efficient, portable, fieldable, and highly robust sensors [Fis07].

The limitations of biosensors can be extended far beyond their current uses in medicine and biosecurity to use in space flight to monitor the health status of the crew. A biosensor can potentially be used to measure the amount of radiation damage that cellular DNA has suffered by sensing 8-hydroxy-2'deoxyguanosine, a biomarker for free-radical induced damage to DNA, or to monitor a suite of cytokines to obtain a near real-time assessment of the status of the immune system of an astronaut. A biosensor is also of interest for the search of life on planetary systems, as it may detect trace amounts of signature molecules for organic life, such as certain sets of amino acids, with high sensitivity and specificity.

1.2 Targets of Interest

There are many sensitive biological elements, or target analytes, to choose from, including amino acids, antibodies, cofactors, nucleotides and nucleobases, pathogens, and small organic or inorganic compounds.

1.2.1 Pathogens

1.2.1.1 Bacillus anthracis

Increasing attention and resources have been focused on the rapid detection and characterization of pathogens in the past decade. *B. anthracis* are soil-born bacteria endemic to several regions of the US and around the world, with at least 89 reported *B. anthracis* strains, most of which to not poses any threat. However, the *Ames* is most virulent strain, used in the postal attack, and the *Vollum* strain has been deemed most suitable for use in bioweapons [Fis07]. The bacteria reside dormant in the soil as endospores, surviving for long periods of time under varying environmental conditions. Once consumed or inhaled, the bacteria rapidly multiply, ultimately causing the death of the host.

Various biosensing techniques for *B. anthracis* have been developed, including antibody affinity reagents, calorimetric assays and DNA aptamers [Bru99, Zhe02]. Bruno and Kiel first described a biosensor with the ability to bind to the anthrax spore target with a wide dynamic range from <10 to >6 x 10^6 anthrax spores. More recently, Yang and coworkers developed a detection assay capable of detecting ~4 x 10^7 spores, with a dynamic range of 4 x 10^4 to 4 x 10^7 spores [Zhe02].

1.2.1.2 Influenza Virus

Commonly called the flu, influenza is caused by an RNA-based virus that belongs to the Orthomyxoviridae family and can easily be transmitted via bodily fluids or through the air from infected individuals. Influenza has resulted in widespread disease and considerable fatalities, with three pandemics occurring in the last century. The deadly avian influenza has recently become a great concern, though it has only resulted in ~100 fatalities and is not easily transmitted

to humans [Per05]. However, mutation of the H5N1 strain could result in a strain that is more easily transmittable to, and among, humans.

Hemagglutinin (HA) is one of the main glycoproteins present on the surface of the influenza virus envelope. It facilitates viral entry by binding to sialic acid-modified receptors on host cells. HA is capable of undergoing mutations from generation to generation, making the development if high affinity reagents and the generation of vaccines against the virus very difficult [Fis07]. Sensing techniques have been developed that can not only detect HA, but can also be modified as to also inhibit the HA-mediated membrane fusion process, which greatly underscores their potential application as an anti-influenza therapeutic [Gop06a, Gop06b].

Methods most widely used to identify influenza subtypes require approximately four days. Rowlen and coworkers from the University of Colorado at Boulder and the Centers for Disease Control and Prevention (CDC) developed a microchip-based test, termed the FluChip, that can distinguish among 72 influenza strains, including the H5N1 avian influenza strain, in less than 12 hours [Tow06], allowing health professionals to more quickly respond to an infection and potentially reduce the spread of the disease.

1.2.2 Theophylline

The target for the proposed biosensor is the small organic compound, theophylline (Figure 1.1(a)), a methylxanthine that acts as a bronchodilator. Thus, theophylline has been commonly prescribed as a long-term treatment of asthma, bronchitis and emphysema [Hen83]. Because theophylline has a very narrow therapeutic range, serum levels must be monitored closely to avoid toxicity. Optimal benefits occur at serum concentrations greater than 55 μM, while the frequency and severity of toxic effects, such as dose dumping when taken with fatty meals, increase above 110 μM [Hen85]. Therefore, the stabilization of hyperreactive airways is most likely when a 55 -110 μM therapeutic range is maintained around-the-clock [Hen85].

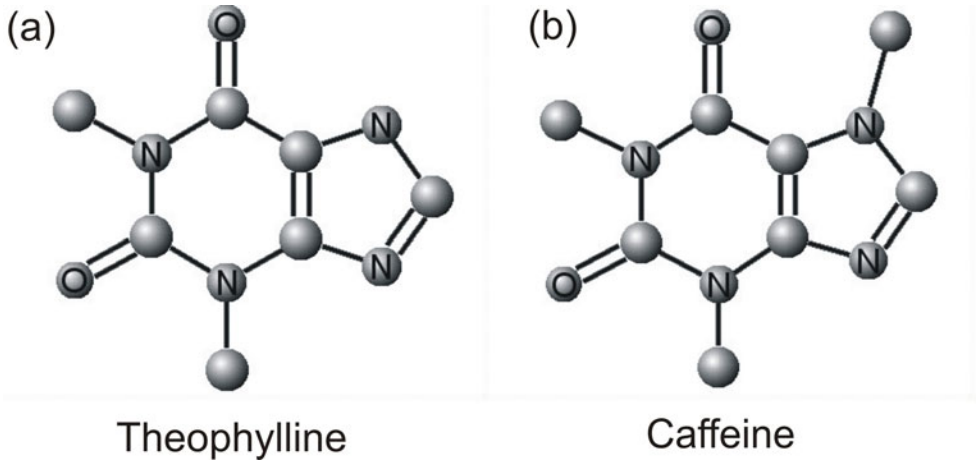

Figure 1.1 Chemical structures of (a) theophylline and (b) caffeine, which differ only by a methyl group on N7.

The development of HPLC based assays and, more recently, of antibody-based fluorescence-polarization immunoassays such as the AxSYM theophylline II assay [Abb07] made the necessary therapeutic drug monitoring in serum possible. However, theophylline detection is non-trivial due to its similar molecular structure and physicochemistry to other methylxanthines, such as theobromine and caffeine (Figure 1.1(b)), which carries a single additional methyl group on N7 of the purine ring. Theophylline, caffeine and theobromine are all found in teas, colas and other caffeinated food products, though in varying amounts. As caffeine may commonly occur in the blood stream at concentrations of about 50 – 350 μM [Foo98], theophylline detection is notoriously difficult. Therefore, a novel, more specific biosensor for theophylline is therefore highly desirable and can be evaluated compared to existing detection technologies.

1.2.3 Biological Markers of Interest in Space Flight

1.2.3.1 8-hydroxyl-2'-deoxyguanosine

Some of the largest risks of long-duration human space flights are associated with the acute and long-term effects of radiation exposure. The low to moderate doses of ionizing radiation typically absorbed during space flight damage cellular DNA by creating reactive oxygen species [Rob94]. These free radicals are extremely reactive and can damage the DNA in a number of ways,

such as creating or breaking bonds in the phosphate backbone of the DNA, or by modifying the purine or pyrimidine bases.

8-hydroxy-2'-deoxyguanosine is a product of the reaction between reactive oxygen species and the guanosine base in DNA that is generally considered a reliable biomarker for reactive-oxygen-species mediated DNA damage [Sch01b]. As current assay techniques for 8-hydroxy-2'-deoxyguanosine cannot be carried out in space flight due too their cumbersome nature [Ans00, Hua01], biosensor technology can be applied to this end.

1.2.3.2 Cytokines

Monitoring the immune system during long-duration space flight is necessary, as data suggests that some factors involved in immunologic functions may be altered during space flight [Hun94], and continuous monitoring of these changes is necessary to determine if pharmacological or other countermeasures must be used to maintain a healthy immune system. Also, continuous monitoring of the immune system can provide an early indication of a developing health problem, such as an infection or inflammation.

Cytokines, such as interleukins and interferons, modulate the immune response, and can provide a great deal of information about the status of the immune system. These substances, however, have very low concentrations in the human body, and their detection and quantification is non-trivial. As the analysis of blood samples of astronauts with respect to these compounds is usually done upon return to earth, this facilitates the need for biosensors that can detect a suit of cytokines from a very small sample volume. Such a device would provide for easy monitoring of the immune status of astronauts during long space flights.

1.3 Biosensor Recognition Elements

1.3.1 Antibody-Based Sensor Technology

The traditional recognition elements for detection of analytes in the sub-nanomolar concentration region are antibodies, in combination with optical or

electrochemical sensors. These immunosensors register the concentration of an analyte in real time without auxiliary reagents. Currently, antibodies are used for small-sized devices to target a single defined analyte or for the simultaneous detection of a very large number of different proteins with protein chips for proteomics [Sch01a]. Most immunosensors are based on enzyme-linked immunosorbent assay (ELISA) principles, with sensor-immobilized antibodies or antigens where the enzyme label such as peroxidase, alkaline phosphatase or glucose oxidase, is detected by measuring the produced iodine [Ris97], *p*-aminophenol [Duc97] or hydrogen peroxide [Ben00].

Reliable measurements using antibodies are only possible if the antibody layer is renewed after each measurement or if an indirect competitive assay is applied with a stable derivative of the antigen bound to the sensor surface [Bie94]. Antibodies are also limited, by their structural robustness under varying temperatures and humidity levels [Fis07].

1.3.2 Aptamers and Aptasensors

It is widely known that RNA can carry genetic information encoded in its linear sequence. Due to the high thermodynamic stability of the secondary structure (Watson-Crick base pairing), RNA provides for a stable scaffold that allows it to acquire diverse tertiary structures, or aptamers. These aptamers can have catalytic functions and can recognize specific analytes with extremely high specificity and sensitivity, in some cases even surpassing those of antibodies [Osu02].

Although aptamers were only discovered in 1990, they are already being developed as analytical agents [Tom05] and for clinical treatments [Cer02]. They have also been proposed as alternatives to antibodies for biosensing applications [Kir04, Pot98, McC03, Sil03, Sek02]. Aptamers often retain their ligand-binding properties when incorporated into larger RNA, allowing for the engineering of allosteric ribozymes comprised of a specific aptamer motif, hammerhead catalytic core, and a structurally responsive communication domain between the two [Koi99, Sou99a Sou99b, Sou00, Sou01].

There are several advantages of using RNA molecules as components of biosensors. The first advantage is the simplicity of generating high quality molecular recognition elements for analytes by implementing the systematic evolution of ligands by exponential enrichment (SELEX) [Klu94]. Additionally, the ease of designing aptazymes from the aptamer, ribozyme, and a substrate strand [Bre97, Bre02, Sek02] and the relative ease of the use of optical techniques, such as TIRF microscopy [Zhu02] for single-molecule detection.

1.4 Thesis Outline

1.4.1 Design and Characterization of Aptazyme

As further described in Chapter 2*, in vitro*-evolved RNA molecules, or aptamers, act as receptors that recognize a wide variety of target molecules with specificity higher than that of antibodies. An aptamer of high affinity for theophylline is chemically synthesized and coupled through a communication domain to an RNA enzyme, generating an aptazyme that is bound to an immobilized fluorescent substrate. The design and synthesis of the aptamer, aptazyme and other oligonucleotides used is discussed in Chapter 3.

Upon analyte binding, the aptazyme becomes activated and cleaves surface immobilized RNA substrate molecules between a site-specifically attached Cy3/Cy5 donor-acceptor pair. As a result, the products, which individually bind only weakly to the aptazyme, dissociate and FRET between the fluorophores breaks down; thus, the signal changes from one that is acceptor dominated to one that is donor dominated. The aptazyme is then free to bind and cleave other immobilized substrates. This amplified signal change is easily detected by the various optical methods described in Chapter 4, including prism based TIRF or confocal microscopy. Fluorescence techniques are used to detect this signal with high sensitivity.

Chapter 5 includes characterization of the RNA using bulk method techniques, single molecule studies and microarray techniques.

1.4.2 Multiplexing in a Microarray Format

Experimentation in solution, as well as on the single-molecule level, shows the feasibility of the system for biosensing. Adapting microarray technologies allows for compact optical detection methodology and grants us the adaptability to detect multiple targets on a single chip.

DNA microarrays are typically used for rapid detection of gene mutations [Shu97], as well as for gene expression [DeR96, DeS98, Sch96], though their potential applications in biosensor technology have become more apparent in recent years [Ben05, Che06]. For example, McCauley and coworkers utilized immobilized DNA and RNA aptamers to develop a biosensor for muliplex analysis of protein analytes [McC03]. More recently, Collet and coworkers immobilized biotinylated RNA aptamers onto streptavidin coated slides in a microarray to develop a protein biosensor [Cho06, Col05].

CHAPTER 2
STRUCTURE AND FUNCTION OF CATALYTIC RNA

DNA and RNA are typically described as carriers of genetic information, where DNA stores the genetic information until recruiting specific protein enzymes to guide its own replication as well as transcription to yield RNA. In turn, RNA directs the biosynthesis of proteins through translation. However, in spite of more than half a century of study, new roles for DNA and RNA are still being discovered. These discoveries subsequently lead to new ways in which nucleic acids can be manipulated to study their biological function, physical properties, or use as a material to create devices and surface patterns [Fei04].

DNA is a double stranded helix which is stabilized via Watson-Crick pairing, while RNA is single stranded. However, most biologically active RNAs including transfer RNA (tRNA), ribosomal RNA (rRNA), small nuclear RNAs (snRNAs) and other non-coding RNAs (such as the signal recognition particle, or SRP, RNAs) are highly structured in that they are extensively base paired to form short regions of double stranded helices formed by the same Watson-Crick base pairing as in DNA. The high thermodynamic stability of these secondary structures provides for a stable scaffold that allows it to acquire diverse tertiary structures [Ges99]. These structures are not limited to long double-stranded helices, as in DNA, but rather collections of short helices packed together into structures analogous to proteins.

This information has led to the discovery that RNA can catalyze chemical reactions, like enzymes, based on its ability to fold into complex three-dimensional structures [Dou02, Ges99]. In 1986, Gilbert coined the phrase “The RNA World”, in reference to the hypothesis that RNA could have once combined the roles of genetic material and biocatalyst in living systems [Gil86]. During this

hypothetical evolutionary stage, proteins were not yet engaged in biochemical reactions and RNA solely carried out both the information storage task of genetic information and the full range of catalytic roles necessary in a very primitive self-replicating system. Gilbert pointed out that neither DNA, nor proteins, was required in such a primitive system if RNA could perform as a catalyst [Gil86]. While protein enzymes are now the dominate catalysts in cells, RNA still contains the necessary elements to aid catalysis in an effective manner. For example, in translation, genetic information is coded and decoded via RNA secondary structure interactions that allow formation of intricate tertiary structures that contain catalytically active components of the gene processing machinery [Moo02]. While forming discrete secondary and tertiary structures, RNA can also undergo substantial conformational changes in the course of a reaction pathway. Therefore, numerous structural and biochemical studies of RNA enzymes or ribozymes have revealed that catalysis is inherently coupled to their three-dimensional structure and conformational dynamics [Tin05].

2.1 Catalytic RNAs

The belief that all known enzymes were proteins was demolished over two decades ago with the discovery that some RNA can exhibit catalytic activity or behave in an enzyme-like manner to catalyze a reaction [Cec81, Cec92]. The discovery of these fairly large catalytic RNAs, or ribozymes, fuelled the growth of the RNA field.

Although some of these reactions are facilitated by proteins *in vivo*, their reactions can be simulated *in vitro* without the aid of proteins, supporting the view that the RNA itself can do the job. With the exception of RNase P RNA and the ribosome, the RNAs undergo an intramolecular, or in *cis*, transesterification in these transformations [Gil86]. These reactions are sequence specific, and more importantly, occur with rates orders of magnitude faster than expected from the background reactivity of RNA. Thus there must be a catalytic element involved, and therefore these active RNAs are called ribozymes, in analogy to the classical protein enzymes.

There are four classes of naturally occurring ribozyme motifs (Figure 2.1) that exhibit self-cleavage [Sco07]. Each motif can accelerate the divalent-metal-dependent cleavage of RNA via a cyclizing transesterification mechanism shown in Figure 2.2. The different motifs are defined by characteristic secondary structure folds and by regions of conserved nucleotides and can fold into a defined tertiary structure that properly orients the phosphate for attack by the adjacent 2'-hydroxyl [Bre97, Wal98, Wil92].

Of these four motifs, the hammerhead is the smallest, affording the advantageous arrangement that contains only Helix II, resulting in a complex where the conserved residues reside in a short domain of approximately 30 nucleotides (nt) [Sta98]. Therefore, to study the mechanism of these ribozyme-catalyzed reactions and their structural requirements, the ribozymes were redesigned for intermolecular, or in *trans*, reactions [Sek02]. Thus the substrate and ribozyme are localized on different RNA strands.

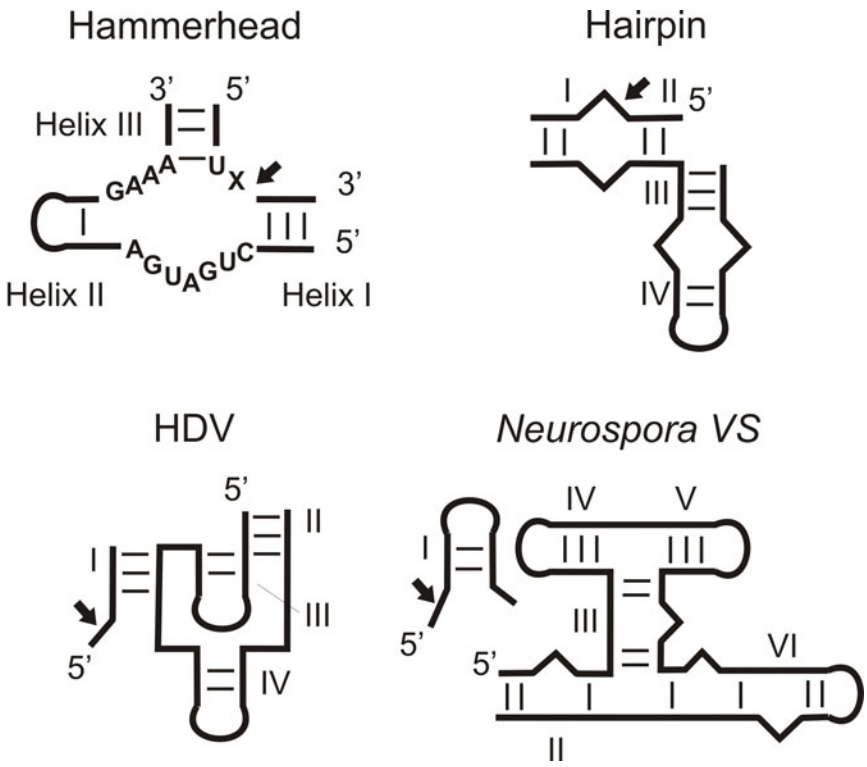

Figure 2.1. The generalized secondary structures of the four natural self-cleaving ribozyme motifs. The sequences and lengths of the helices may vary. X represents A, U, or C.

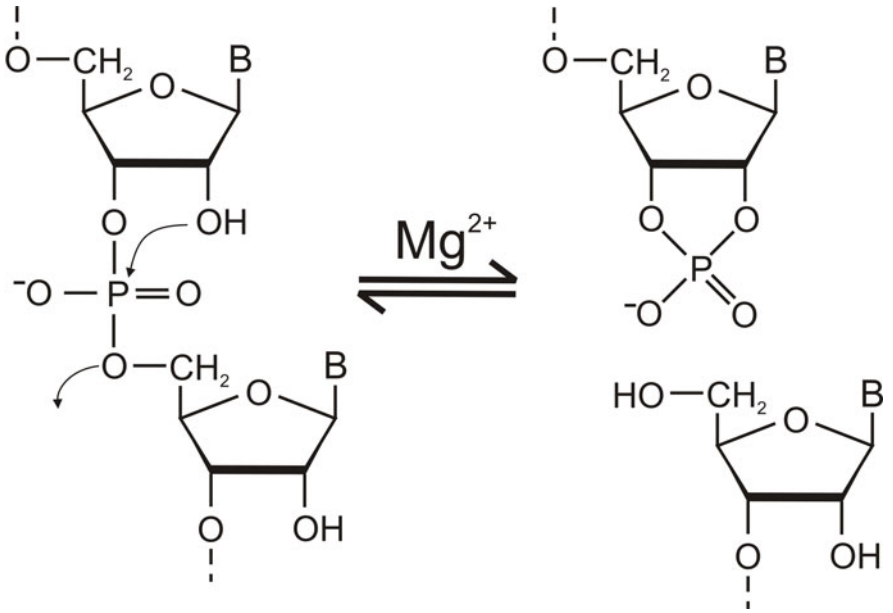

Figure 2.2. In the RNA self-cleavage reaction the RNA folds into a tertiary structure that orients the phosphate for attack by the adjacent 2'-hydroxyl. A simple modification of the RNA where the 2'-hydroxyl group is replaced with a 2'-methoxy group will prevent this RNA from self-cleaving.

2.2 RNA Aptamer

2.2.1 Aptamer Selection Using SELEX

The highly repetitive nature of RNA and DNA molecules makes them relatively simple to synthesize and manipulate *in vitro*, using the SELEX (systematic evolution of ligands by exponential amplification) method. This *in vitro* selection method isolates catalytic molecules from random sequence pools of RNA or DNA. This approach relies on the probability that in a given pool of random sequences, molecules which can perform the function of interest, such as binding to a specific target molecule, will exist. A rigorous mathematical analysis of SELEX has been recently described by Levine and Nilsen-Hamilton [Lev07].

The process begins with a large (~10^{15}) random pool of nucleic acid sequences, where approximately 15 million molecules are expected to carry the hammerhead catalytic core, and some are expected to efficiently catalyze RNA cleavage [Bre97]. Each molecule in the pool is of the same length, between 40-80 bases long, but varies in its internal sequence. These molecules are subject to a negative selection by incubation in the absence of the desired target. RNA

molecules that do not self-cleave are then isolated and subject to a positive selection. The target of interest is attached to a solid support, such as a column or gel, to select molecules with sequences that promote folding into structures that bind to the target. These allosterically controlled ribozymes are then RT-PCR amplified and transcribed to produce material for a new round of selection. In each round of SELEX, the goal is to select the nucleic acid sequences with the highest affinity for the target molecule while eliminating background sequences that may bind to the support. Successive rounds (typically 10-15) lead to an optimization of the molecule to the desired sensitivity and selectivity [Wil99].

The molecules that emerge from *in vitro* selections are hence termed "aptamers". These aptamers can be selected for very high affinity and specificity, even chiral specificity, for targets of interest. The affinities are often comparable to those observed for antibodies, with most of the calculated K_D values in the low nanomolar to micromolar range, depending on the measuring principle [Pat97]. Some of these targets and their respective K_D values are listed in Table 2.1.

Table 2.1 Examples of targets with known aptamers and their respective K_D values (n.r. = not reported). Compiled from various sources. [Ber01, Fei96, Fer04, Fis07, Lor94, Pan05, Sto07, Wil99]

Target		Aptamer Type	K_D
Amino acids			
	l-Arginine	RNA	330 nM
		DNA	2.5 mM
	l-Citrulline	RNA	62–68 µM
	d-Tryptophan	RNA	18 µM
	l-Valine	RNA	12 mM
Antibiotics			
	Chloramphenicol	RNA	25–65 µM
	Kanamycin A	RNA	≤300 nM
	Kanamycin B	RNA	180 nM
	Lividomycin	RNA	≤300 nM
	Neomycin	RNA	100 nM
	Streptomycin	RNA	n.r.
	Tetracycline	RNA	1 µM
	Tobramycin	RNA	2–3 nM
Cofactors			
	Cyanocobalamin (Vitamin B12)	RNA	320 +/- 90 nM
	NAD	RNA	2.5 µM
	Riboflavin	RNA	1–5 µM
	RMP-botin	RNA	2 µM
Inorganic components			
	Ni^{2+}	RNA	0.8–29 µM
	Zn^{2+}	RNA	1.2 mM
Nucleotides and nucleobases			
	Adenine	RNA	10 µM
	ATP	RNA	4.8–11 µM
	ATP/adenosine	DNA	6 µM
	Guanosine	RNA	32 µM
	7-methyl-GTP	RNA	~0.5 µM
	Xanthine	RNA	3.3 µM
Pathogens			
	Anthrax spores	DNA	n.r.
	Salmonella typhi	RNA	7 nM
	Tularemia	DNA	n.r.
Small organic molecules			
	Caffeine	RNA	1 mM
	Dopamine	RNA	2.8 µM
	Ricin toxin	DNA	58–105 nM
	Theophylline	RNA	100 nM

2.2.2 HHT5 Aptamer Specific to Theophylline

Although aptamers were only discovered in 1990, they are already being developed as analytical agents [Tom05] and for clinical treatments [Cer02]. Aptamers often retain their ligand-binding properties when incorporated into larger RNA, allowing for the engineering of allosteric ribozymes comprised of a specific aptamer motif, hammerhead catalytic core, and a structurally responsive communication domain between the two [Koi99, Sou99a Sou99b, Sou00a, Sou00b, Sou01]. By incorporating the aptamer motif and the communication domain into Helix 2 of a hammerhead ribozyme, catalytic activity becomes responsive to the binding of the aptamer to the target molecule [Sek02]. This catalytic RNA complex is sometimes described as an “aptazyme” [Nav06].

Breaker and coworkers have engineered such a hammerhead ribozyme to be activated in the presence of theophylline (Figure 1.1(a)), a bronchodilator commonly used for the treatment of respiratory diseases such as asthma. It is a member of the xanthine family and bears structural and pharmacological similarities to caffeine (Figure 1.1(b)) [Bre97]. Therefore, caffeine is used as an experimental control for this biosensor.

The theophylline ribozyme designed by Breaker, HHT, is 77 nucleotides long and cleaves intramolecularly (in *cis*) with a rate constant of ~0.1 min^{-1} in 1 mM theophylline, which is ~100-fold faster than background cleavage in the absence of cognate ligand [Bre97, Bre02]. There has been significant interest in this aptamer and, consequently, its potential incorporation into a biosensor [Sou00, Zim98, Zim00]. Sekella, *et al* [Sek02] subsequently utilized a modified construct, HHT1, for the development of a fluorescence-based biosensor. The original HHT *cis*-acting construct was disintegrated into a ribozyme and its complementary external substrate strand as shown in Figure 2.3. This allows for efficient chemical synthesis of the substrate and the creation of a rechargeable biosensor, capable of multiple turnover.

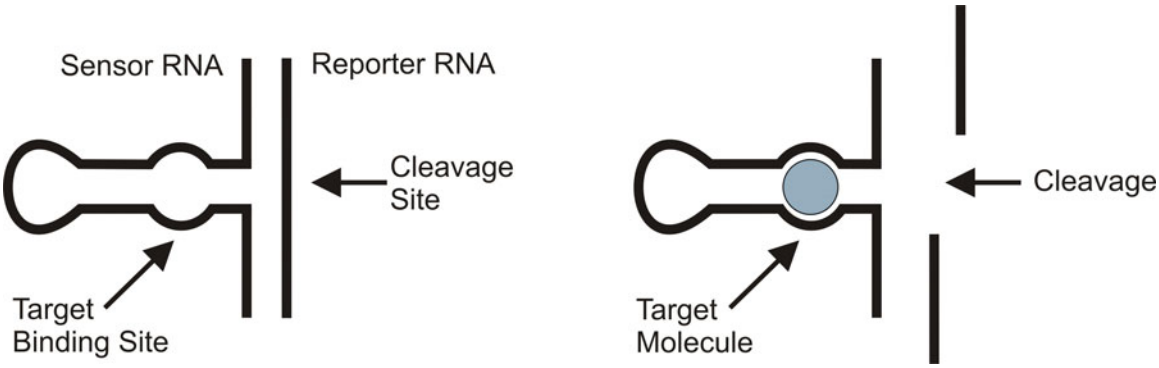

Figure 2.3 Schematic showing a cis-acting construct disintegrated into a ribozyme and its complementary external substrate strand, or reporter RNA. After cleavage of the reporter RNA, the sensor RNA retains its catalytic activity and is free to bind and cleave a new, uncut reporter RNA.

We have redesigned the HHT1 construct with several modifications to improve the biosensing capabilities of the ribozyme. The sequences of the substrate and the substrate-binding arms of the ribozyme were changed to those of a previously characterized hammerhead ribozyme [Mic00] to avoid self-complementarities of the original substrate strand. Additionally, an A:U base pair is placed downstream of the cleavage site to accelerate hammerhead ribozyme cleavage [Clo97], so that the detection time for biosensing is decreased.

This modified construct is a result of several experiments that have led to a better understanding of the theophylline-specific aptamer-ribozyme complex, including the work by Sekella, *et al* [Sek02]. This newest generation, labeled HHT5, is shown in Figure 2.4(a). A G:C pair has been removed from the hairpin region for some reason. Additionally, the 3' end has been extended with the sequence AUAUAUA and the GG on the 5' end has been replaced with AUAG. These modifications were made so that when the ribozyme is incorporated into the substrate, any labels on the substrate will be a sufficient distance away from Guanine. The importance of this redesign will become more apparent in Chapter 4, as fluorescent labels are used for the detection mechanism and fluorophore quenching due to stacking interactions must be prevented.

The theophylline binding reaction of this newest construct generation, HHT5, is shown in Figure 2.4(b). In the absence of theophylline, the communication module region (indicated by rounded light boxes) is misaligned in a base-pairing pattern that is stabilized by the formation of a G:U wobble pair.

Once the aptamer binds to theophylline, the communication module is correctly aligned, which allows formation of the catalytically active conformation.

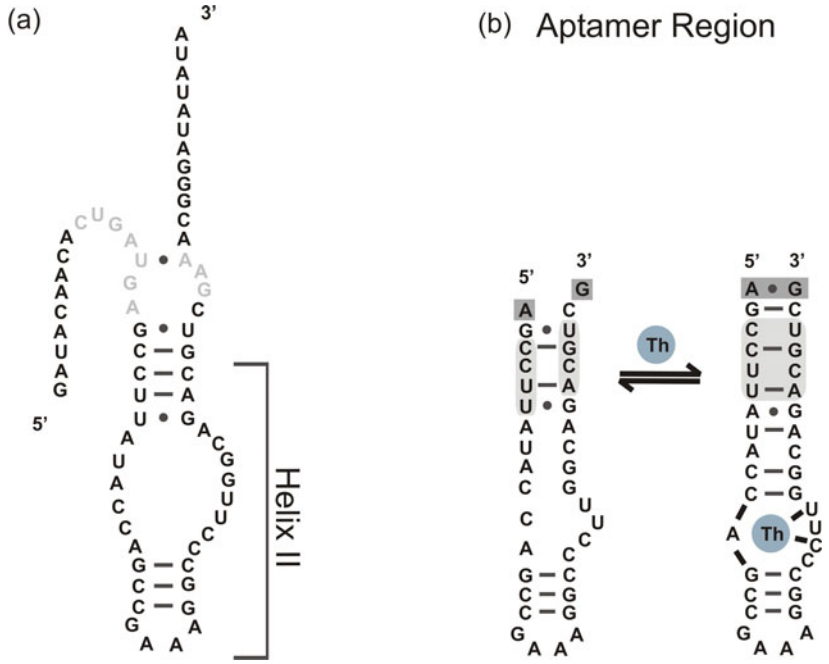

Figure 2.4 The hammerhead ribozyme for theophylline. (a) The HHT5 construct. (b) Details of the conformational change in Helix II. In the absence of theophylline, the communication module (rounded light boxes) is misaligned in a base-pairing pattern that is stabilized by the formation of a G:U wobble pair. With theophylline bound, the communication module is correctly aligned (rounded light box), which allows formation of the catalytically active conformation.

2.3 RNA Aptamers as Biosensor Component

In recent years, the promise of aptamers as biosensing components has been recognized and extensive research is being done in this field. Aptamers have been generated against a large range of targets and adapted for numerous chemical or biological sensing systems [Fis07], several of which are listed in Table 2.1. For example, Bruno and Kiel derived DNA aptamers against the Stern strain of *bacillus anthracis* in 1999 [Bru99]. These aptamers were incorporated into an aptamer-magnetic bead-electrochemiluminescence sandwich assay as well as into a calorimetric assay to demonstrate binding to the target with a dynamic range from less than10 to >6 $\times$ 10^6 anthrax spores. Extensive studies have also been done on the development of aptamers against the glycoproteins found on the surface of the influenza virus envelope. One of these studies led to

the isolation of RNA aptamers against the purified HA of human A influenza virus, subtype H3N2 [Mis05, Gop06a, Gop06b].

Several different techniques have been employed, including SELEX, for the development of aptamers with very high specificity for targets of interest. These aptamers can then be incorporated into a variety of sensing platforms and detection assays, such as microarrays, microbead platform, nanoparticle-based platforms, or various electronic platforms [Fis07]. For this biosensor, we have incorporated various optical techniques to measure fluorescence signals due to fluorescence resonance energy transfer (FRET) [For48, Rue06, Vog06], which will be discussed in detail in Chapter 4. In short, excitation energy of a donor fluorophore is transferred to the acceptor fluorophore via an induced dipole-dipole interaction without the involvement of an intermediate photon as shown in Figure 2.5. FRET will occur if the emission spectrum of the donor overlaps with the absorption spectrum of the acceptor.

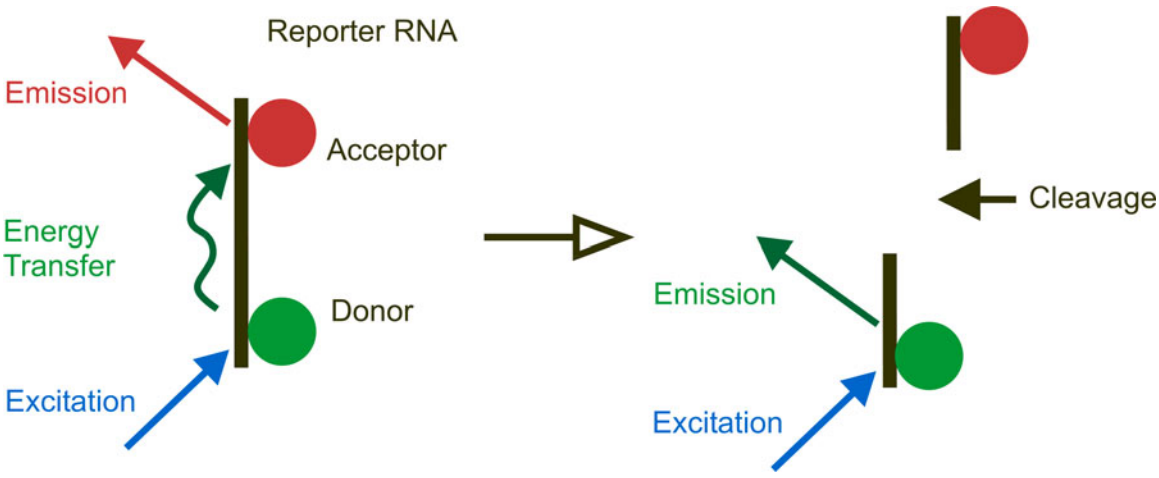

Figure 2.5 Schematic showing FRET between a donor and acceptor fluorophore placed on either end of a catalytically active site. Upon cleavage of the reporter RNA, or substrate, the FRET signal is lost.

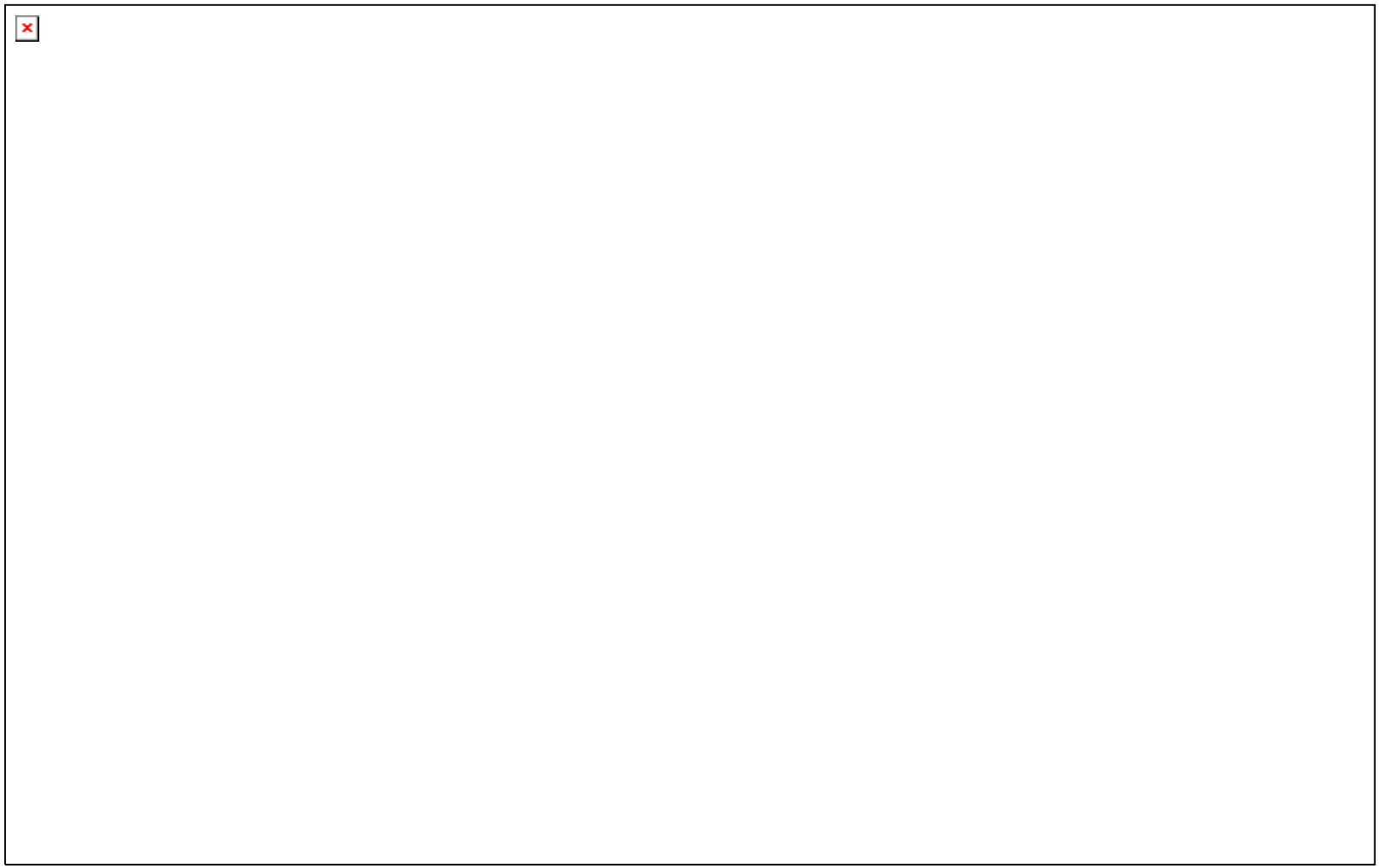

Figure 2.6 The HHT5 reaction pathway. The aptamer domain, Helix II, specifically binds to theophylline, at which point the sensor molecule becomes catalytically active and cleaves the substrate. A unique fluorescence signal can be detected with a Cy3/Cy5 fluorophore pair.

Therefore, we have incorporated the theophylline-specific aptamer into a ribozyme with a complementary structurally responsive substrate domain that permits structural changes and allows for tethering to a solid surface for experimentation. Site-specific labeling of the substrate with a Cyanine 3 donor fluorophore and Cyanine 5 acceptor fluorophore (Cy3/Cy5, respectively) on either end of the catalytically active site will allow for direct detection of target-binding induced cleavage of the substrate RNA (Figure 2.5). The loss of FRET signal due to substrate cleavage leads to a unique fluorescent signal that can be detected using a variety of optical techniques, such as total internal reflection microscopy (TIRF) or confocal fluorescence imaging, on the single molecule level (see Chapter 4 for further discussion). This gives the detector its high fidelity.

Figure 2.6 shows the reaction pathway of the RNA complex designed for the theophylline specific biosensor. Upon binding to theophylline, the HHT5 complex will rearrange and undergo substrate cleavage. The cleavage will then cause disassociation of the labeled substrate reporter, allowing the fluorophores to proliferate, hindering FRET between them. The 3' end of the RNA substrate has been extended to allow for a "tail" region that can bind to a complementary DNA primer, allowing the HHT5 complex to be secured to a glass surface for experimentation.

CHAPTER 3
DESIGN AND PREPARATION OF OLIGONUCLEOTIDES

3.1 Design of RNA Oligonucleotides

As previously described, the RNA substrate strand (RC) was designed with a region complementary to the HHT5 ribozyme and a 24 nt tail on the 3' end. For structural and kinetic studies, a non-cleavable (NC) substrate analog with a distinguishable tail region was synthesized with the nucleotide 5' to the cleavage site modified with a 2'-methoxy group to chemically block cleavage. The detailed substrate cleavage mechanism has been described in Figure 2.2. Using Michael Zuker's *mfold* secondary structure predictor, *mfold* program version 3.0 [Zuk03, Zuk99], RNA sequences were tested for sufficient distinguishability between the NC and RC species as well as their complementary primers.

To find and test possible sequences, a computational evolution method was implemented and the generated sequences were checked for dimerization (the hybridization of two identical molecules), RNA cross-hybridization (the hybridization of the substrates or primers to one another), and binding specificity (where the RNA substrate binds only to its primer). A more detailed description of this process is given in Appendix A. In short, 1000 random starter sequences of 23 bases long were generated. Each random sequence, and its corresponding 19 nt primers, were tested for dimerization, cross-hybridization, and binding specificity. The sequences then underwent twenty iterations of mutation and recombination using a simple crossover technique before the "best" sequences were chosen from the final results. These sequences were then tested for secondary structure at 22 ˚C with a 0.6 mM Na concentration. This process was repeated several times before two new sequences were eventually chosen for the RC and NC RNA substrate. The secondary structures for these

sequences and corresponding DNA primers, pRC and pNC, are shown in Figure 3.1 and the dG values for these sequences and each test case are given in Table 3.1, showing a low thermodynamic stability of each non-ideal case. The secondary structures and dG values for the various test cases are given in Appendix A.

All oligonucleotides were thus designed based on these sequences. For simplicity in referencing, the oligonucleotides used and their respective sequences are listed in Table 3.2.

Table 3.1 dG values for sequences.

Sequences	dG (kcal/mole)	Dimerization	dG (kcal/mole)	Cross-hybridization and binding specificity	dG (kcal/mole)
RC sequence	-1.8	RC + RC	-6.2	RC + pNC	-1.9
NC sequence	-2.8	NC + NC	-5.5	NC + pRC	-3.57
pRC (primer)	-1.2	pRC + pRC	-2.6	RC + NC	-5.3
pNC (primer)	-1.6	pNC + pNC	0.53		

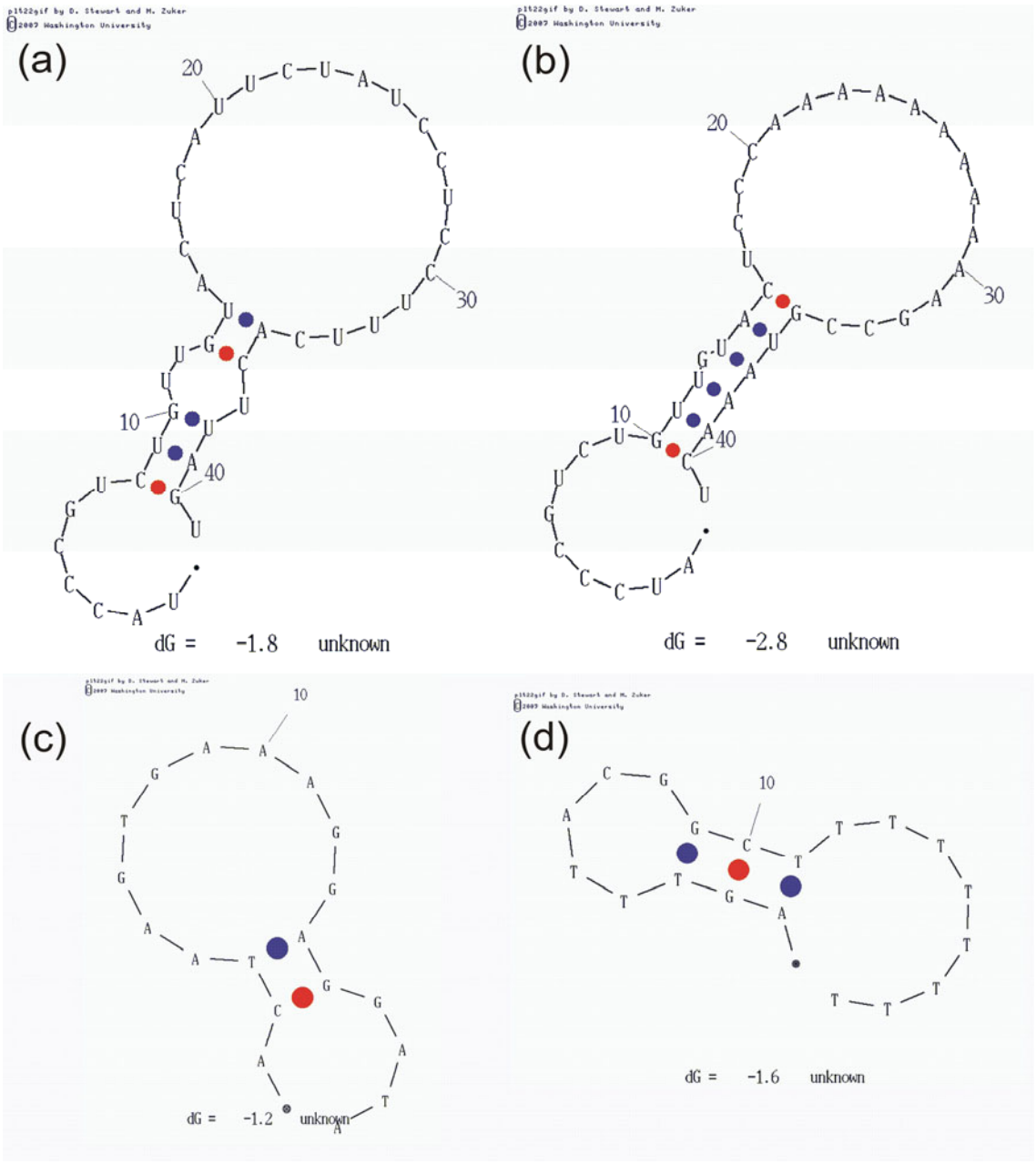

Figure 3.1 Secondary structures and corresponding dG values predicted using *mfold* for (a) RC (b) NC (c) the DNA primer complementary to RC and (d) the DNA primer complementary to NC.

3.2 Preparation of synthetic substrate RNA oligonucleotides

RNA oligonucleotides were purchased from the Y. M. Keck Foundation Biotechnology Resource Laboratory at the Yale University School of Medicine. The following RNA substrate and primer sequences were purchased: cleavable RNA substrate 5'- [Cy5] UAC CCG UCU GUU GUA [dt_NH2] UC AUU CUA UCC UCC UUU CAC UUA GU -3' and its corresponding primer 5'- ACT AAG TGA

AAG GAG GAT A -3' and non-cleavable RNA substrate 5'- [Cy5] AUC CCG U [C 2'-methoxy] U GUU GUA [dT_NH2] UC CCA AAA AAA AAA AGC CGU AAA CU -3' and its corresponding primer 5'- AGT TTA CGG CTT TTT TTT T -3'. [Cy5] indicates a Cy5 label, while [dT_NH2] indicates the presence of an amino linker for labeling with Cy3 post synthesis. In the [C 2'-methoxy] modification, the hydroxyl group on the 2' position of the ribose is replaced with an O-methyl group, inhibiting the RNA self-cleavage reaction described previously (Figure 2.2).

Oligonucleotides were deprotected by a two-step protocol as suggested by the manufacturer and previously described (see Appendix B for detailed protocol) [Per02]. Deprotected RNA was purified by denaturing 15% polyacrylamide, 8 M urea gel electrophoresis. Bands of interest were diffusion eluted into 1 mM EDTA overnight at 4˚C, chloroform extracted and ethanol precipitated. Pure RNA was isolated using either C8 or C18 reverse-phase HPLC with a linear acetonitrile gradient in triethylamonium acetate as describe previously [Per02]. The RNA concentration was qualified by UV absorption at 260 nm with a correction background at 320 nm. For fluorescence measurements, substrate oligonucleotides were labeled with Cy5 presynthetically and with Cy3 postsynthetically, as previously described (see Appendix B for detailed protocol) [Per02, Zhu02].

Table 3.2 All oligonucleotide sequences used in various experiments.

Name	Type	Sequence (5' – 3')
RC	Cleavable RNA substrate	[Cy5] UAC CCG UCU GUU GUA [dt_NH2] UC AUU CUA UCC UCC UUU CAC UUA GU
NC	Non-cleavable RNA substrate	[Cy5] AUC CCG U [C 2'-methoxy] U GUU GUA [dT_NH2] UC CCA AAA AAA AAA AGC CGU AAA CU
pRC	19 nt DNA primer specific to RC tail region	ACT AAG TGA AAG GAG GAT A
pNC	19 nt DNA primer specific to NC tail region	AGT TTA CGG CTT TTT TTT T
mRC	DNA sequence based on pRC printed on microarray	ACT AAG TGA AAG CAG GAT AAC TAA CTA ACT AAC TAA GTG AAA CGA GGA TA
mNC	DNA sequence based on pRC printed on microarray	AGT TTA CGG CTT TTT TTT TTT GGA GTT TAC GGA GTT TAC GGC TTT TTT TT
mpRC-C3	DNA probe specific to mRC	[Cy3] TAT CCT CCT TTC ACT TAG T
mpNC-C5	DNA probe specific to mNC	[Cy5] AAA AAA AAA GCC GTA AAC T

3.3 In Vitro Transcription of HHT5 Hammerhead

Upstream and downstream single-stranded DNA primers for the transcription of the HHT5 construct was purchased from Invitrogen with the following sequences: HHT5 5' primer: 5'- TAT ATA TCC CGT TTC GAC GTC TGC CAA GGG CCT TTC GGC TGG TAT AAG GCT CAT CAG TGT TGT ATC TAT AGT GAG TCG TAT TAC TG – 3'; T7 promoter sequence: 5' - CAG TAA TAC GAC TCA CTA TAG - 3'.

The HHT5 hammerhead was generated by in vitro transcription in a reaction containing 3 micromolar of each primer, PEG, and 4X Reaction Buffer (HEPES-KOH pH 7.5, $MgCl_2$, Spermidine, DTT, 1% Triton X-100) and is described in further detail in Appendix B. The reaction is heated in a 90˚C heat bath for 3min then cooled on ice. After the addition of ATP, UTP, CTP, GTP, PPi 0.1 u/μl (Pyrophosphatase inorganic) and T7 Polymerase, the reaction is incubated for at least 3 hours at 37 ˚C. The reaction is then stopped and the RNA is phenol/chloroform extracted, concentrated, and gel purified to extract the final HHT5 product.

3.4 DNA Primers Designed for Microarray Printing

DNA primers for microarray printing were designed based on the 19 nt primers complementary to the RNA substrate sequences. Hybridization to printed DNA oligonucleotides occurs at higher rates for longer sequences, with a minimum length of 50 nt for printing, as suggested by the Microarray Core at the University of Michigan Comprehensive Cancer Center (UMCCC) . Therefore, the 19 nt primers were extended by repeating the sequences, resulting in the design of the following sequences: for cleavable version, mRC: 5'- ACT AAG TGA AAG CAG GAT AAC TAA CTA ACT AAC TAA GTG AAA CGA GGA TA -3'; and for non-cleavable version, mNC: 5'- AGT TTA CGG CTT TTT TTT TTT GGA GTT TAC GGA GTT TAC GGC TTT TTT TT -3'.

CHAPTER 4
OPTICAL MEASUREMENT TECHNIQUES

4.1 FRET as a Measurement Technique

Equation Chapter 4 Section 1Fluorescence (or Förster) resonance energy transfer (FRET) is a non-radiative process transferring the excited state energy between two fluorophores, a donor and acceptor. This has proven to be a powerful tool for single molecule experiments [Ha01, Kri01, Wal01] and allows for the measurement of distances in the 10 – 75 Å range, well below the resolution limit of the optical microscope [Vog06, Rue06]. In this process, excitation energy of the donor is transferred to the acceptor via an induced dipole-dipole interaction without the involvement of an intermediate photon. FRET can occur if the emission spectrum of the donor overlaps sufficiently with the absorption spectrum of the acceptor.

The rate of the energy transfer between the donor and acceptor, $k_T(r)$, is given by

$$k_T(r) = \frac{1}{\tau_D}\left(\frac{R_0}{r}\right)^6 \tag{4.1}$$

where r is the distance between the donor and acceptor, τ_D is the lifetime of the donor in the absence of energy transfer and R_0 is the Förster distance [For48]. The Förster distance is defined as the distance at which 50% of the energy is transferred and is a function of the absorption and emission spectrum of the fluorophores, as well as their relative orientation [Ha01]. The typical range for R_0 is between 20 – 60 Å, which translates to approximately 6 – 18 nt. This value of R_0 (nm) can be calculated using

$$R_0 = 2.11\times10^{-2}[\kappa^2 J(\lambda)\eta^{-4}Q_D]^{1/6} \tag{4.2}$$

where κ^2 is the orientation factor describing the relative spatial orientation between the transition dipoles of the donor and acceptor, $J(\lambda)$ is the overlap integral of the donor emission and acceptor absorption spectra, η is the refractive index of the medium, and Q_D is the quantum yield of the donor [Oly07].

The orientation factor, κ^2 is typically assumed to be 2/3 if the geometry of the fluorophore is not rigid or limited by steric effects. This assumed value results from the randomization of the orientation of the donor and acceptor by rotational diffusion prior to energy transfer [Lak99]. The orientation factor can range from zero to 4, depending upon the relative orientations in space of the donor emission dipole and the acceptor absorption dipole. A value of 1 corresponds to parallel transition dipoles, while a value of 4 results from dipoles that are both parallel and collinear [Oly07]. For a two-fluorophore system, κ^2 is given by

$$\begin{aligned}\kappa^2 &= (\cos\theta_T - 3\cos\theta_D \cos\theta_A)^2 \\ &= (\sin\theta_D \sin\theta_A \sin\phi - 2\cos\theta_D \cos\theta_A)^2\end{aligned} \tag{4.3}$$

where, θ_T is the angle between the emission transition dipole of the donor and the absorption transition dipole of the acceptor, θ_D and θ_A are the angles between these dipoles and the vector joining the donor and acceptor, and ϕ is the angle between the planes containing the two transition dipoles. For a completely fixed relative fluorophore orientation, κ^2 would be known; however, for a solution-based system, the value is difficult to determine [Wal01].

The efficiency of energy transfer, E, is a measure of the fraction of photons absorbed by the donor that are transferred to the acceptor. This value is related to the separation between the donor and acceptor and is given by

$$E = \frac{1}{1+\left(\frac{r}{R_0}\right)^6}. \tag{4.4}$$

FRET efficiency can also be written in terms of the donor and acceptor intensities, or I_D and I_A, respectively, as

$$E = \frac{I_A}{(I_A + \gamma I_D)} \tag{1.5}$$

where γ is the acceptor-to-donor ratio of the products of fluorescence quantum yield and the instrument detection efficiency in the respective channel [Ela03, Rue05]. Typically, this factor is close to unity, so equation (1.5) is often simplified to

$$E \approx \left[1 + I_D/I_A\right]^{-1}. \tag{4.6}$$

Since single-molecule studies concern mostly relative changes in the FRET signal, the approximation does not affect most of the data interpretation [Ha01].

The FRET pair commonly used in single molecule FRET, and therefore used in this experiment is Cyanine 3/Cyanine 5, or Cy3/Cy5, developed by Amersham Biosciences [Ame07]. The Jablonski energy diagram for this pair is given in Figure 4.1(a). The donor fluorophore, Cy3, is excited maximally at 550 nm and emits maximally at 570 nm, in the yellow/orange spectrum, while the acceptor, Cy5, is excited maximally at 649 nm and emits maximally at 670 nm, in the red spectrum. Figure 4.1(b) shows the absorption (blue peaks) and emission (red peaks) scans of a Cy3 donor (left peaks) and Cy5 acceptor (right peaks) pair [Ame07]. The spectrum has been normalized to give an indication of the degree of spectral overlap (green region), allowing the donor to fluoresce in the acceptor channel. Figure 4.2 shows a plot of the energy transfer efficiency for a Cy3 donor and Cy5 acceptor pair. The strong distance dependence on the energy transfer efficiency can be clearly seen, indicating that both cleavage and conformational changes of the aptazyme can be quantified.

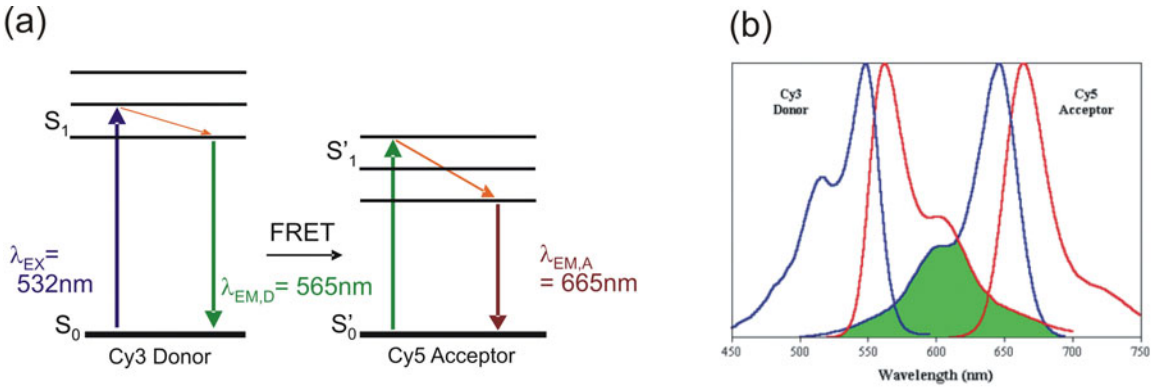

Figure 4.1 (a) A simplified Jabłonski diagram for a FRET pair. The values included are the excitation and emission wavelengths for a Cy3/Cy5 FRET. (b) Normalized absorption (blue) and emission (red) spectra for Cy3/Cy5. The green area indicates the region of spectral overlap for FRET. Image reproduced from Amersham Biosciences.

Cy5 is widely used as an acceptor fluorophore because its high extinction coefficient allows it to be paired with a donor with a large spectral separation while maintaining a relatively large Förster distance [Ras06]. However, Cy5 is sensitive to the electronic environment it resides in and conformational changes of the substrate may produce an enhancement or quenching of the fluorophore emission. Additionally, Cy5 shows extensive blinking that is greatly affected by the presence of oxygen, which may require the use of an oxygen scavenger system. This indicates that triplet states are a possible source of fluctuations as well as radical cation and *cis–trans* isomerizations [Hua06].

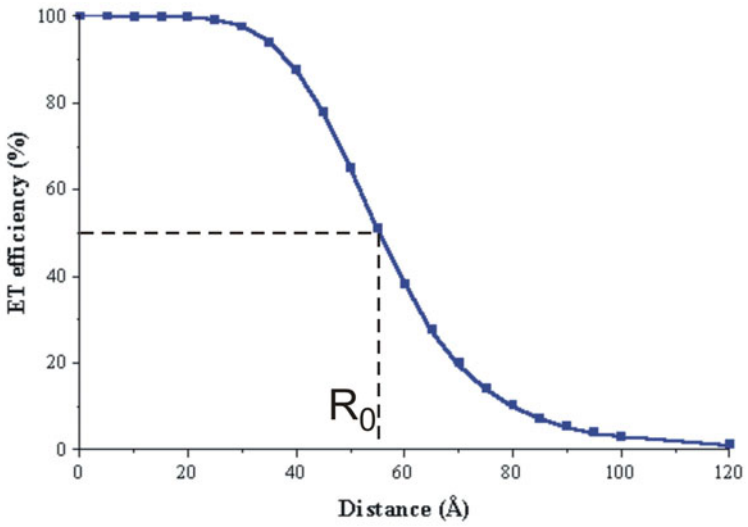

Figure 4.2 Energy transfer efficiency plot for a Cy3/Cy5 pair. Image reproduced from [Ame07].

4.2 Fluorophore Photobleaching

Photobleaching is an inherent property of organic dyes and effectively limits the number of meaningful FRET measurements on a single molecule. Therefore, in single-molecule experiments, a tradeoff is made between the signal strength (photon-emission rate), photobleaching rate, and saturation; all dependant on laser excitation power. Photobleaching is the result of an increased reactivity of the fluorophore in its excited states, leading to irreversible loss of emission, or fluorophore destruction. This is usually due to a photochemical reaction [Kon07].

Photobleaching is a major impediment in single-molecule spectroscopy. Antioxidant additives have been shown to reduce photobleaching [Ras06, Ha03] by preventing oxidation when in the triplet state, though this is only a partial solution.

4.3 TIRF Microscopy for Single-Molecule Measurements

In total internal reflection fluorescence microscopy, or TIRF microscopy, has been previously used in the Walter Lab for single molecule FRET detection [Wal02a, Wal02b, Zua02]. TIRF microscopy employs the unique properties of an induced evanescent wave to selectively illuminate and excite fluorophores in a region immediately adjacent to a glass-buffer interface. An excitation light beam travels through a prism or objective, to reach the solid glass or quartz slide at a high incident angle, θ, greater than the critical angle, θ_c. The critical angle, given by Snell's law as

$$\sin\theta_c = n_1/n_2 \tag{4.7}$$

the beam of light is totally reflected from the slide/buffer interface. Here, n_1 and n_2 are the indices of refraction of the slide and buffer, respectively. The reflection generates a very thin electromagnetic field, usually less than 200 nanometers, in the aqueous medium, which has an identical frequency to that of the incident light. This evanescent field undergoes exponential intensity decay with increasing distance from the surface according to the equation:

$$I_z = I_0 e^{-z/d} \tag{4.8}$$

where I_z represents the intensity at a perpendicular distance z from the interface and I_0 is the intensity at the interface. The characteristic penetration depth, d, at λ_0, the wavelength of incident light in a vacuum, is given by:

$$d = \frac{\lambda_0}{4\pi\sqrt{n_1^2 \sin^2\theta - n_2^2}}, \quad (\theta > \theta_c) \tag{4.9}$$

The penetration depth, which usually ranges between 30 and 300 nm, is independent of the incident light polarization direction, and decreases as the reflection angle grows larger. This value is also dependent upon the refractive

indices of the media present at the interface and the illumination wavelength, 532 nm.

4.3.1 Single Molecule FRET Using TIRF

The evanescent field produced in TIRF can be used to excite the donor fluorophore, and therefore allowing FRET to occur between the donor and acceptor, as seen in Figure 4.3. The FRET between the donor and acceptor fluorophores can then be detected. However, once the RNA substrate is cleaved, only the donor fluorescence can be detected as the acceptor will leave the evanescent field. As the penetration depth of the evanescent field is on the order of ~200nm, molecules farther away from the slide surface are not exposed to excitation light, and therefore do not give rise to a background signal.

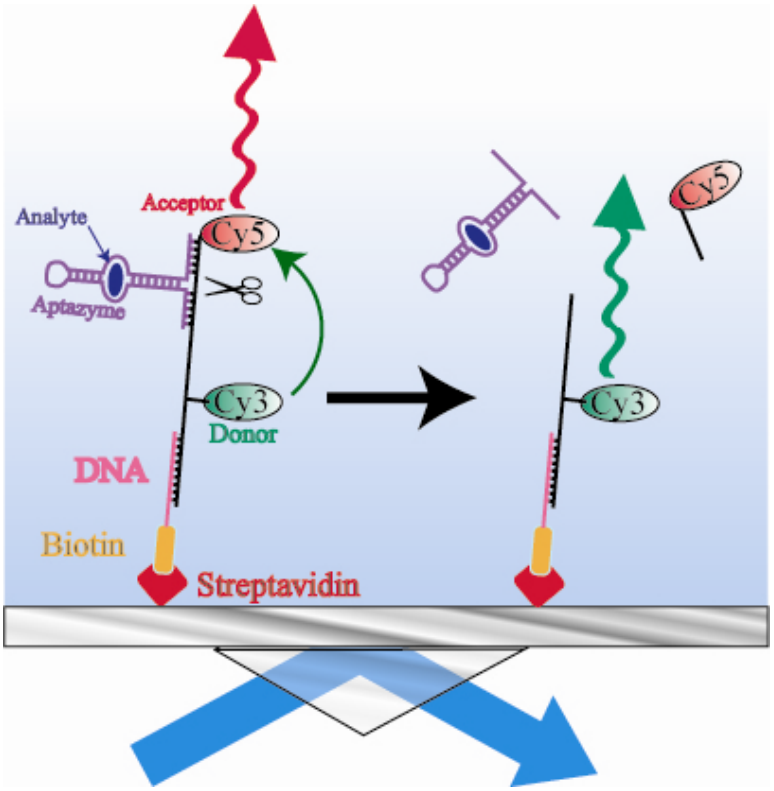

Figure 4.3 Cy3/Cy5 donor-acceptor labeled RNA substrates are bound to specific DNA oligonucleotides that are immobilized on a quartz coverslip through a biotin-streptavidin interaction. Once the aptazyme binds an analyte molecule, it is catalytically and cleaves the substrate molecule. Upon cleavage, FRET between a donor-acceptor fluorophore pair breaks down, leading to a change from a donor to an acceptor dominated fluorescence signal. Prism-based TIRF microscopy excites the donor with an evanescent light field and detects the fluorescence signal.

4.3.2 Optical Setup

Figure 4.4 shows a schematic of the TIRF microscopy setup used for single molecule studies. Prism-based TIRF, as opposed to objective-based TIRF, is used because of the wider excitation area, flatter illumination field, superior contrast and greater signal-to-noise ratio [Axe01, Oly07]. A 535 nm beam from a picosecond-pulsed Spectra Physics Titanium:Sapphire laser passes through an electronic shutter, filter, λ/2 plate and polarizer before passing through a quartz prism at a high incidence angle to create the excitation field. The resulting fluorescence beam passes through the Olympus IX71 inverted fluorescence microscope to a 630 nm dichroic to separate the Cy3 and Cy5 fluorescence beams. Each beam is then focused adjacent to one another onto a Roper Scientific I-PentaMAX intensified CCD for imaging. This allows both fluorescent channels to be measured simultaneously, as shown in false color in Figure 4.5.

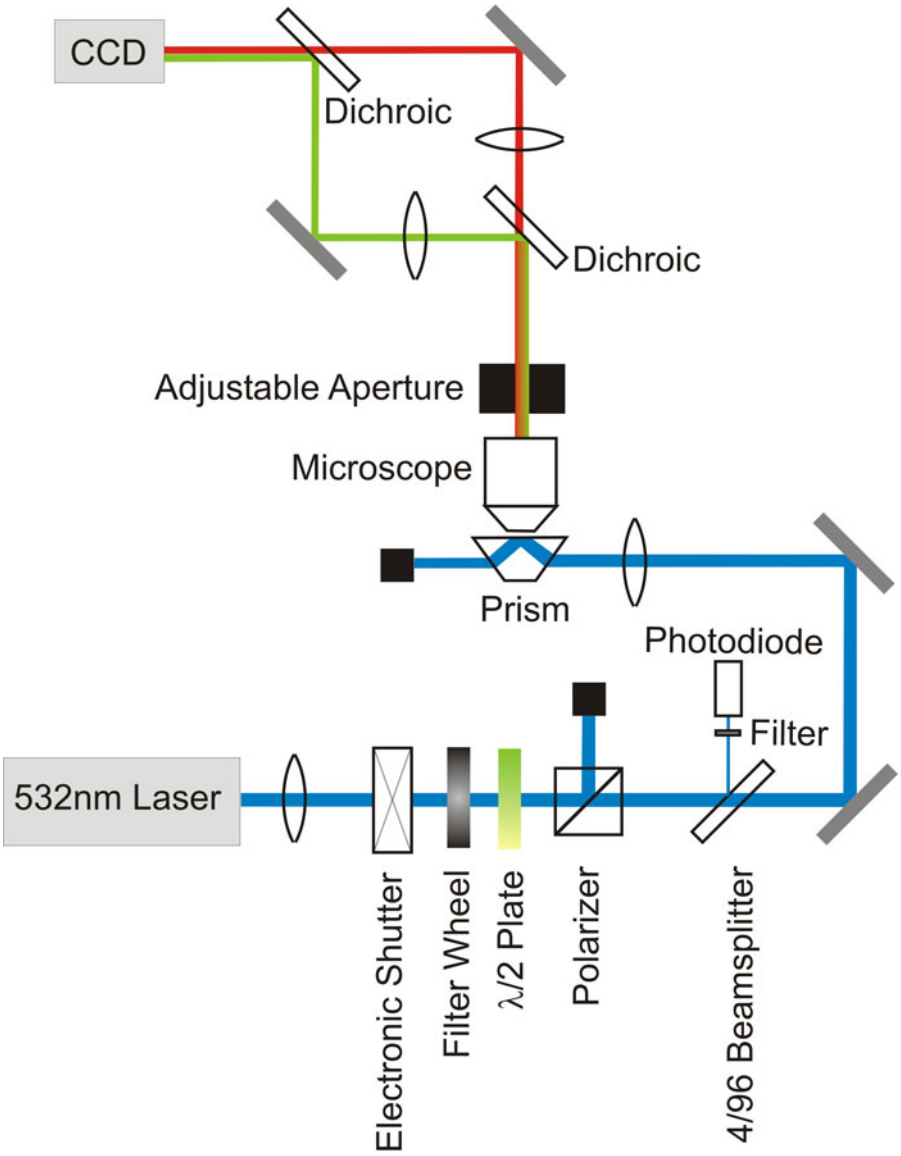

Figure 4.4 Schematic of the TIRF microscopy set-up used for single-molecule studies. The setup involves prism-based total internal reflection excitation at 532nm on an Olympus IX71 inverted fluorescence microscope. The resulting donor/acceptor emission is separated using a 630nm dichroic mirror (transmitting wavelengths <630nm and reflecting wavelengths >630nm) and one arm is spatially shifted so that the resulting two images will be projected side-by-side onto the Roper Scientific I-PentaMAX intensified CCD camera.

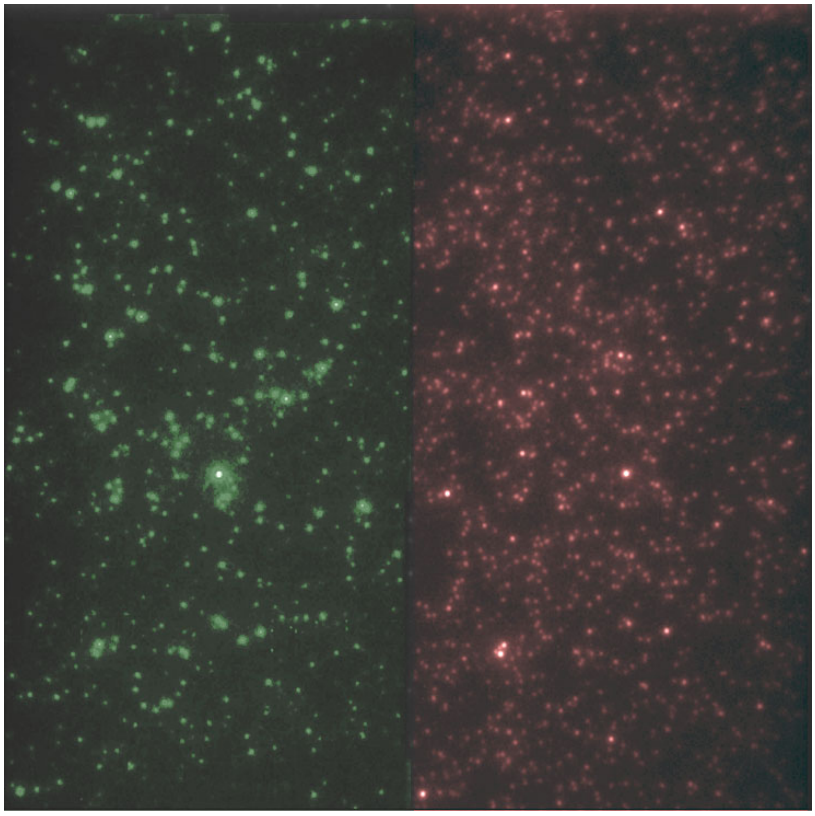

Figure 4.5 False color image of the Cy3 (left) and Cy5 (right) channels focused onto the imaging CCD.

4.3.3 Flow Cell Preparation

The platform on which single molecule experiments are conducted is a flow cell made using an ultra-clean quartz slide, ensuring the index of refraction the excitation beam encounters upon entering the prism does not change. As quartz slides are not as readily available as their glass counterparts, these slides are reused. Therefore, to ensure no RNases are present, as well as to limit any background fluorescence, an extensive cleaning and preparation process is used.

If the slides have been used previously, they are boiled in water with a stir bar for about 20 min to soften any epoxy glue. When the epoxy turns yellow, it is carefully scraped away, along with the coverslip, with a razor blade. The slides are then cleaned with a very thick paste of Alconox and water mixture by rubbing them thoroughly and rinsing with water to ensure all of the detergent is removed.

Finally, the slides are rubbed with ethanol, rinsed with ethanol, and rinsed with water, resulting in perfectly clean slides.

The slides are then placed in a pre-wash solution of 100ml autoclaved water, 20ml of 30% Ammonium Hydroxide, and 20ml of 30% Hydrogen Peroxide. This solution is then placed on a hot plate and heated, covered, on a hot plate, in the hood for 20 min while being slowly mixed with a stir bar. The slides are then rinsed with water and dried by passing each side at least 10 times slowly over a flame. Immediately after cooling, a coverslip is adhered to each slide to limit the amount of air that the measurement surface is exposed to. This will minimize contamination.

To adhere a coverslip, two strips of double-sided tape are first placed diagonally on the slide and parallel to the line defined by the previously drilled holes. The tapes are placed such that there is a hole in the upper left and lower right corners and the separation between them is approximately 4 – 6 mm. A second layer of tapes is applied and a fresh cover slip is centered on top. The excess tape is then removed with a razor blade and all sides are sealed using a quick-setting epoxy glue. The slides can now be stored for several months if covered.

To fill the flow-cells with a pipette, about 2 – 3 mm of the cone end of the pipette tip must be cut off with a razor blade and the tip snugly fits into the injection hole. The liquid injected into the slide should flush the channel and just flow out of the second injection hole. If the tip flows well, it is kept for all injections.

4.4 Confocal Fluorescence Imaging

Confocal imaging microscopy was pioneered in 1955 by Marvin Minsky while he was a junior fellow at Harvard University [Min88]. Modern confocal imaging has preserved the essence of Minsky's design while incorporating new advances in optics and electronics to provide improvements in speed, image quality, and data acquisition and storage. The typical confocal microscope images either by reflecting light off of a specimen or by stimulating a fluorophore

applied to the specimen [Sem05, Wal03a, Wal03b]. The latter is the more common technique used in biological applications, such as in scanners used for imaging microarrays.

4.4.1 Confocal Imaging System

The confocal microscope incorporates the concepts of point-by-point illumination and rejection of out-of-focus light. In Figure 4.6, laser light reflects off of a beamsplitter, or dichroic lens, and passes through an objective which focuses the light onto the sample. The longer-wavelength fluorescence beam resulting from this excitation passes through the beamsplitter to a filter wheel, which filters the wavelength of interest. This beam then travels through a pinhole which allows only focused light to pass to the detector element, usually a CCD.

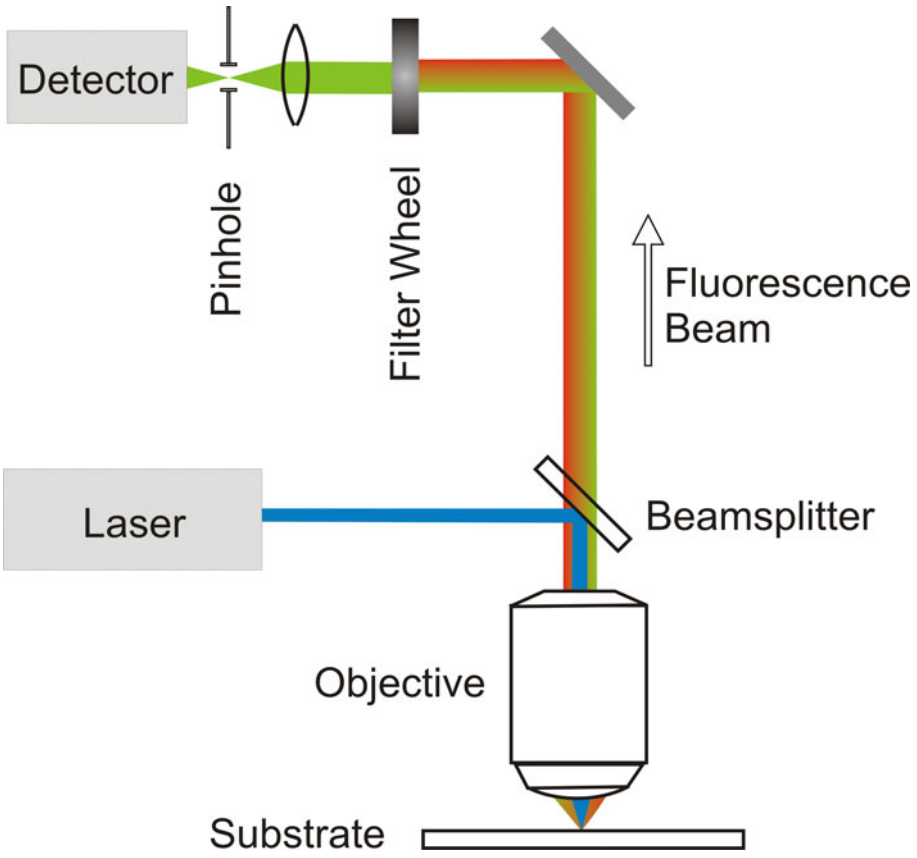

Figure 4.6 Schematic of the basic setup of a confocal imaging system utilized by a microarray scanner. Light from a laser is reflected off of a beamsplitter, or dichroic mirror, toward the sample. The returning (longer wavelength) fluorescence is allowed to pass through the dichroic, where it is filtered according to wavelength of interest, before reaching the detector element.

4.4.2 Microarray Scanner Function

The microarray scanners used for data acquisition are the PerkinElmer *ScanArray Express*, in the Richard Miller Laboratory of Gerontology, and the GSI Lumonics *ScanArray 5000*, in the Robert Thompson Laboratory at the Molecular and Behavioral Neuroscience Institute. These scanners have several pre-installed excitation lasers and emission filters, as well as software with pre-determined laser/filter combinations specific to a variety of common fluorophores. For the fluorophores of interest, the excitation lasers emit at wavelengths of 543 nm for Cy3 excitation and 633 nm for Cy5 excitation. 570 nm and 670 nm 10 nm bandwidth emission filters are used for detection of Cy3 or Cy5 fluorescence. As the scanner software allows for the customization of fluorophores, a “FRET fluorophore”, that uses the 543 nm excitation laser and 670 nm emission filter, can be defined and subsequently used to measure FRET between Cy3 and Cy5, as indicated by Figure 4.7.

The goal of confocal microscopy is to see the image at only one point, consequently making this detection method very sensitive to the focus. The sample must also be scanned to create an image of a thin planar region of the sample, an effect known as optical sectioning. The scanners used for this experiment keep the optics stationary while moving the sample back and forth in the vertical and horizontal planes. This method of scanning is slower than moving the optics, but it has two major advantages [Sem05]. First, the sample is illuminated axially, avoiding optical aberrations and illuminating the entire field of view uniformly. Second, controlling the amplitude of the stage movement allows the field of view to be made larger than that of the static objective.

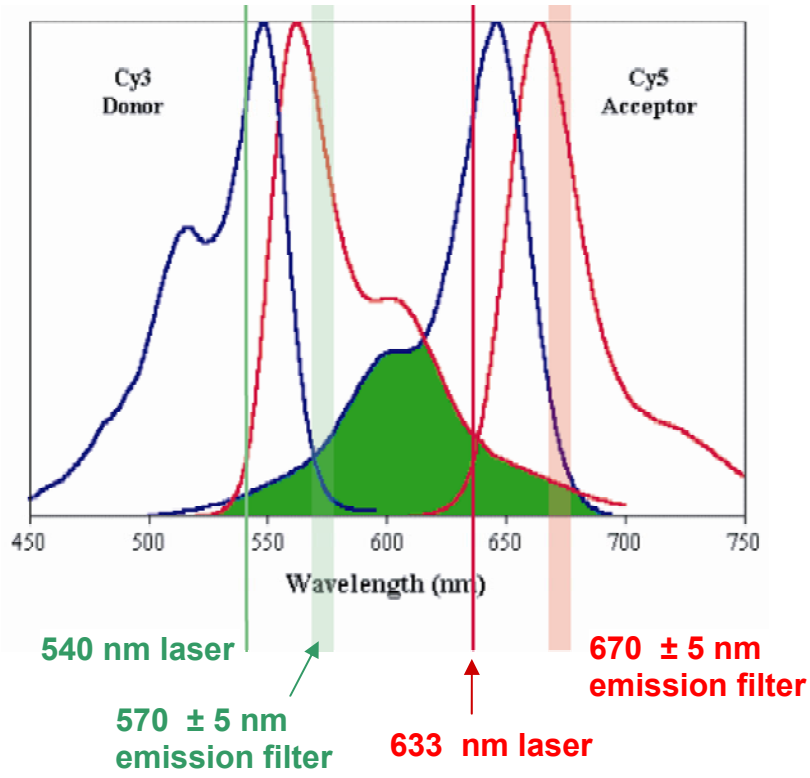

Figure 4.7 Normalized absorption (blue) and emission (red) spectra for Cy3/Cy5 showing excitation and emission using microarray scanner.

4.5 Adapting Single-Molecule Experiments onto a DNA Microarray

To develop a biosensor with the adaptability to detect multiple targets, as well as to incorporate the compact detection methodology afforded by microarray scanners, single molecule experiments were adapted onto a microarray platform.

A microarray is a general term referring to biological assays of DNA, protein, tissue, chemical compounds or antibodies. DNA microarrays are typically collections microscopic DNA spots arrayed on a solid surface by covalent attachment to a chemical matrix. These arrays are used to either measure DNA or to use DNA as part of a detection system utilizing the selective nature of DNA-DNA or DNA-RNA hybridization.

DNA microarrays are typically used for rapid detection of gene mutations [Shu97], as well as for gene expression [DeR96, DeS98, Sch96], though their potential applications in biosensor technology have become more apparent in recent years [Ben05, Che06]. For example, McCauley and coworkers utilized immobilized DNA and RNA aptamers to develop a biosensor for muliplex

analysis of protein analytes [McC03]. More recently, Collet and coworkers immobilized biotynolated RNA aptamers onto streptavidin coated slides in a microarray to develop a protein biosensor [Cho06, Col05].

Utilizing the DNA-RNA hybridization techniques previously described [Lee05], we can adapt the single molecule experiments onto a DNA microarray, where the DNA primers, mRC and mNC, are printed in an array such that spots of labeled RC and NC can be detected using a microarray scanner post DNA-RNA hybridization. As shown in Figure 4.8, upon introduction of the aptazyme and analyte, there will be a detectable signal change due to a cleavage reaction.

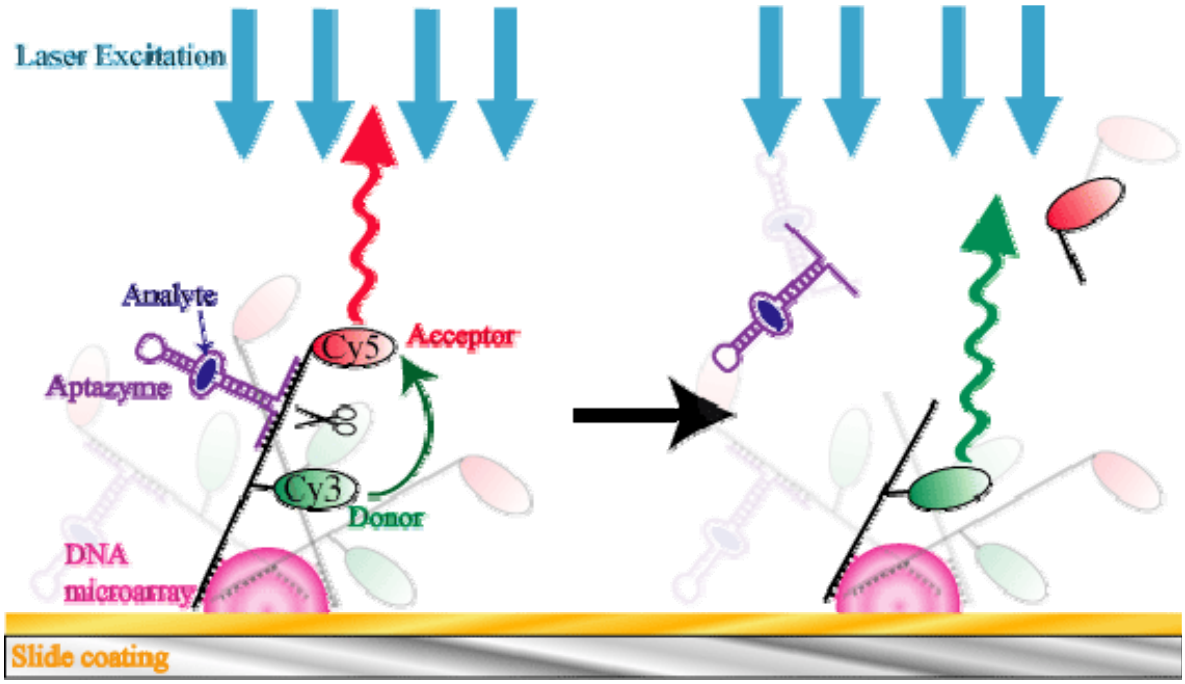

Figure 4.8 Cy3/Cy5 donor-acceptor labeled RNA substrates immobilized onto a coated glass slide through hybridization to DNA oligonucleotides that are printed in a microarray. Once the aptazyme binds an analyte molecule, it is catalytically and cleaves the substrate molecule. Upon cleavage, FRET between a donor-acceptor fluorophore pair breaks down, leading to a change from a donor to an acceptor dominated fluorescence signal. A microarray scanner using a confocal imaging system is used to excite the donor fluorophore and measure the resulting fluorescence signal.

4.5.1 Microarray Chip Design

Microarrays are printed using a robot spotter with one or more quills that are dipped into solution stored in a 384-well microplate and then lightly tapped onto a slide surface, depositing a uniform amount of solution onto the slide

surface. Spots are typically deposited in a grid pattern, often called a constellation, on the slide surface. After printing, slides may be crosslinked by UV light, heat treated, or simply allowed to dry at room temperature. Slides are printed by the University of Michigan Comprehensive Cancer Center (UMCCC) Affymetrix and Microarray Core Facility using a BioAutomations MagnaSpotter equipped with up to four split quills and with no post-processing of the slides.

4.5.1.1 Surface Chemistry

Slides pre-coated for printing oligonucleotide microarrays were obtained from Erie Scientific Company. The slides used are manufactured from high quality low fluorescence glass and coated with either inorganic (amino-silane (APS), ES amino-silane (ES-APS), and epoxy-silane) and organic (poly-L-lysine (PLL) and ES poly-L-lysine (ES-PLL)) coatings.

Array spot-size is often controlled by the surface energy of the coating, where hydrophobic coatings give smaller spot sizes, while hydrophilic coatings give larger spot sizes. The surface characterization information provided by Erie Scientific, obtained using atomic force microscopy, is shown in Figure 4.9. For the enhanced surface, or ES, type of coating, acid etching is used to control the surface morphology of the glass, resulting in a surface with microscopic canyons and valleys, but still uniformly coated with functional groups. The average roughness of the coatings, defined as the arithmetic average of the absolute values of the roughness profile ordinates, is given as 0.4339 nm for the standard coating and 16.2485 nm for the ES coating, with average heights of respective surface features of 5.2893 nm and 83.8990 nm [Eri07]. The benefit of the ES surface is that it allows for spotting of smaller, more uniform spots without affecting the focusing or use of microarray spotters and scanners.

Finally, microarrays printed on slides with inorganic coatings showed no effects from degradation after six months, while those printed on organic coatings showed some degradation in this time period. However, qualitative comparisons of signal-to-noise levels conducted by staining stamped arrays with SyBr Green and DNA-DNA hybridization showed that microarrays printed on the thicker ES

slides did not show a significant improvement in spot quality. Therefore, for the current biosensor design, the surface coatings do not have a significant effect on the microarray print quality.

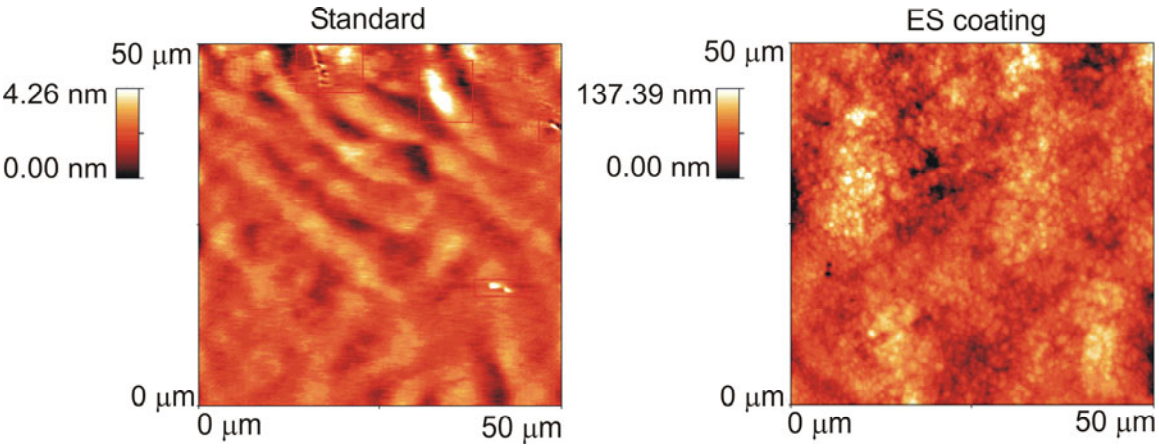

Figure 4.9 Surface characterization profiles, provided by Erie Scientific Company, for standard coatings (left) and Enhanced Surface, ES, (right) coatings. The average roughness values of the coatings are given as 0.4339 nm for the standard coating and 16.2485 nm for the ES coating, with average heights of surface features of 5.2893 nm and 83.8990 nm, respectively.

4.5.1.2 Array Design

DNA oligonucloetides for stamping were designed based on the DNA primers specific to the cleavable (RC) and non-cleavable (NC) versions of the RNA substrate described earlier. Figure 4.10 shows a schematic of a constellation design incorporating arrays of these DNA oligonucleotides, mRC and mNC, printed in rows of increasing concentration. Asymmetrically located calibration spots, composed of a mixture of mRC and mNC, were added to the array to ensure proper orientation of the array during measurement. These spots are also used to manually locate and focus the array during scanning. The mRC and mNC arrays are separated within the constellation with spots of buffer for background measurement and to prevent cross-contamination of the spots during the printing process. Spots stamped with air, rather than buffer, showed some residue even with pin cleaning. Several generations of this design, using the same concentrations of mRC and mNC were used for experimentation.

DNA for printing is prepared using the protocols required by the UMCCC [Was06]. DNA is suspended in a standard stamping buffer of 3X SSC with a

minimum concentration of 0.5 µg/µl. Therefore, aliquots of DNA primers of the following concentrations – 0.5 µg/µl, 1.5 µg/µl, 5 µg/µl, and 15 µg/µl – in standard stamping buffer were prepared, as well as the 5 µg/µl, 3X SSC primer mixture. Using a 384 well plate, appropriate wells were filled with 3 µl of solution. The printing order for the first quill is as follows: A1, A2, B1, B2, A13, A14, B13, B14, C1, C2, D1, D2, C13, C14, etc. For the remaining three quills, which were not used, the pattern can be repeated, but shifted to the right.

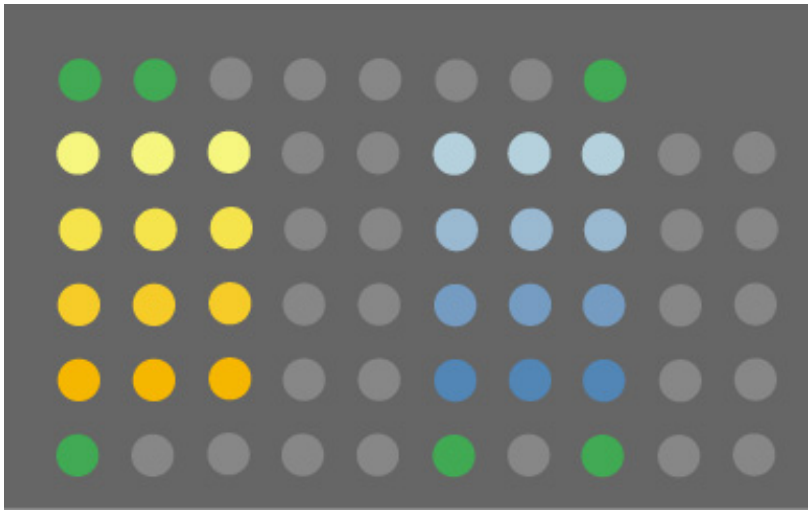

Figure 4.10 Schematic of a constellation design where arrays of the DNA oligonucleotides, RCm and NCm (yellow and blue circles), are printed in rows of increasing concentration (0.5 µg/µl, 1.5 µg/µl, 5.0 µg/µl, and 15 µg/µl). Green circles indicate calibration spots composed of a 0.5 µM mixture of RCm and NCm. Grey circles indicate buffer spots.

Variations in spot size and shape can be caused by a variety of factors, including the robot's dwell time on the slide, the slide's coating, the solution viscosity, and environmental factors, such as humidity and temperature. However, spots printed using a robot spotter typically have a diameter of approximately 120 µm.

4.5.2 Preparation and Hybridization of Microarrays

The specific protocols followed in the preparation of the printed microarray slides for hybridization and subsequent experimentation are described in more detail in Appendix B. These protocols are based on the procedures previously described in literature [Beh02, Bro99, Cos05, Loc00, Tay03, Wal00].

4.5.2.1 Blocking Strategy

To effectively inactivate reactive groups that may remain post-printing on coated microarray slides and prevent the labeled substrate from adsorbing into the surface of the printed microarray during hybridization, the exposed surfaces must be blocked using a blocking buffer. Blocking methods also wash away any unwanted DNA from the surface that might otherwise compete with the labeled substrate [Tay03]. Therefore, background noise will be reduced while maintaining full signal intensities.

Two of the most common blocking methods to address non-specific adsorption involve blocking with succinic anhydride or bovine serum albumin (BSA) [Tay03]. Both strategies are intended to block the unreacted functional groups of the printed microarray with chemistries that have a low affinity for RNA or DNA. The latter strategy, using BSA – a large, globular protein with hydrophobic regions which enable it to stick to glass – is employed here. Also included in the blocking buffer is sodium dodecyl sulfate (SDS), an anionic surfactant with a hydrophilic head and hydrophobic tail, as well as EDTA, which complexes divalent ions which cause NA's to collapse.

Therefore, the blocking buffer composed of 5X SSC pH 7.0, 0.5% SDS, 0.1 mM EDTA pH 8.0, and 1% BSA must first be incubated at 42˚ for 30 min. It is interesting to note that this blocking buffer does not lose its effectiveness when adjusted to contain 3X SSC but will not show visible precipitant when stored at RT. Approximately 40 µl of this buffer is spotted onto each constellation and covered with a coverslip. The slide is then incubated in a humid environment at 42˚C for 30 min upon which the coverslip is removed and the slide is placed in a Coplin jar filled with ddH_2O and shaken for 1-2 min to wash. The slide is washed in this manner four more times in ddH_2O and once in isopropanol before being allowed to air dry. The slide is now ready for hybridization.

4.5.2.2 Hybridization of RNA Substrate

In a hybridization reaction, labeled molecular targets, such as the doubly-labeled RNA substrate, are transported from a bulk sample volume to a

hybridization site by both diffusion and convection. At the hybridization site, the substrate will hybridize to a complementary region of the DNA primer. It is imperative to hybridize under controlled environmental conditions to ensure strong and irregular streaks of high-intensity background that is typically caused by evaporation and subsequent drying of the hybridization buffer [Cos05].

To isolate the constellations during the hybridization stage and to minimize the amount of material needed, small hybridization chambers are cut out of double-sided tape and placed around the constellations. Hybridization buffer composed of 50% formamide, 5X SSC, 0.1% SDS, 1/40 herring sperm DNA, and 1/10 RNA substrate is heat annealed at 90˚C for 2 min then cooled on ice. The hybridization chambers are then filled and covered with a glass coverslip. The slides are then incubated in a dark and humid environment at room temperature. Hybridization times is dependant on nucleotide lengths, the hybridization buffer, specifically the formamide content, as well as whether the hybridization is between DNA-DNA and RNA-DNA. For the former, we incubate for 1.5 hours; for the latter, 6 hours.

Post incubation, the coverslips and hybridization chambers are removed and the slide is washed by agitating for 5 min in each wash buffer I, II, III and finally in ddH_2O. Wash buffer I is composed of 1X SSC, 0.2% SDS; II is composed of 0.1X SSC, 0.2% SDS; and III is composed of 0.1X SSC. After washing, the slide is allowed to air dry in a dark environment and stored at 4˚C to prevent premature photobleaching of the fluorophores.

4.5.2.3 Flow Cell Preparation

To create a flow cell around the RNA-DNA hybridized constellations, a flow cell pattern is cut out of parafilm and placed around each constellation. Next, a washed and plasma-cleaned coverslip is placed atop the parafilm and the excess parafilm is cut away. A soldering iron is used to melt the parafilm, securing the coverslip to the slide and completing the flow cells shown in Figure 4.11. A soldering iron is used to melt the parafilm instead of the conventional hot

plate because the iron will apply heat to a localized area and melt the parafilm without introducing a significant amount of heat to the RNA-DNA array.

Recall that the microarray scanner moves the sample, as opposed to the optics, when imaging. As microarray slides are typically scanned when dry, this feature does not normally present any negative effects. However, my measurements are done in a fluid environment and the very quick movement of the slide causes buffer to splash out of the inlet and outlet of the flow cell. This effect results in a change in the experimental environment over time and therefore must be prevented. To this end, once the final sample solution has been introduced into the flow cell, high viscosity vacuum grease is used to seal the inlet and outlet of the flow cell. In practice, this has proven to be a very effective method to maintain the integrity of the experimental environment.

Figure 4.11 Microarray flow cells. Two microarray constellations are printed on each glass slide. The constellations are surrounded by a parafilm channel, atop which the coverslip is placed. The parafilm is melted using a soldering iron, adhering the coverslip to the slide and creating a flow channel for measurements in a fluid environment. Once fluid is introduced into the channel, the inlet and outlet are sealed using vacuum grease.

4.5.3 Controls and Calibrations

To ensure FRET measurements are feasible using microarry scanning techniques, several proof-of-principle and calibration tests were conducted on the system. Therefore, we must check for quality and specificity in hybridization of the substrates (RC or NC) between the cleavable and non-cleavable regions of the microarray constellations, ensure good signal–to–noise ratio in appropriate channels and determine the extent of signal bleed–through between channels.

Short, singly labeled DNA probes specific to the RC and NC regions, mpRC-C3 and mpNC-C5, are used for these calibration tests. Singly labeled RNA is also used to ensure hybridization specificity and quality.

Figure 4.12 shows the result of the calibration tests using DNA-DNA hybridization, where the rows of figures show the channel signals for the Cy3 singly-labeled DNA probe (top row) and Cy5 singly-labeled DNA probe (bottom row). As expected, Figure 4.12(a) shows strong signal strength in the Cy3 channel with good spotting quality, where the spots are round and evenly spaced. The intensity of the spots increases with row, with the concentration of DNA in stamping solution, but does not saturate. Also, negligible non-specific binding exists, indicating good pre-hybridization blocking. As the DNA probe is singly labeled with Cy3, there is no signal in the CY5 channel Figure 4.12(b); however, an average signal bleed-through into the FRET channel of 6.45 ± 0.75 % Figure 4.12(c) is observed. Bleed-through of about 7% is expected due to the spectral overlaps shown in Figure 4.7 indicating that the correct channel settings are used.

The results of the hybridization of the Cy5 singly-labeled DNA probe are shown in Figure 4.12(d), (e), and (f). In (d), a negligible signal is seen in the Cy3 channel. This signal is a result of the scattering of laser light off of surface artifacts left behind in the stamping process. There is a strong signal in the Cy5 channel, (e), however the spot quality is not as good on this half of the microarray constellation. This is simply due to poor printing procedure, where either the slide(s) or the 384-well microplate were not level during the printing process and should not affect future experiments. Finally, there is no signal in the FRET channel, as there is no fluorophore excitation at 543 nm or bleed-through into this channel.

NC substrate, both singly labeled with Cy5 and doubly labeled, was used to test the quality of RNA-DNA hybridization. Figure 4.13 shows the results of the hybridization of NC to a first-generation microarray constellation, where the top row of images is of singly-labeled RNA while the bottom row is of doubly-labeled RNA. As the singly-labeled RNA has only a Cy5 label, there is no signal in (a) or

(c), but a strong signal in (b), as expected. The spot quality in (b) is sufficient to extract data and the signal does not saturate. In the bottom row of images in Figure 4.13, (d) shows a relatively weak signal in the Cy3 channel, a stronger signal in the Cy5 (e), and the strongest signal in the FRET channel (f). This indicates that FRET occurs between the Cy3 and Cy5 fluorophores on the NC substrate.

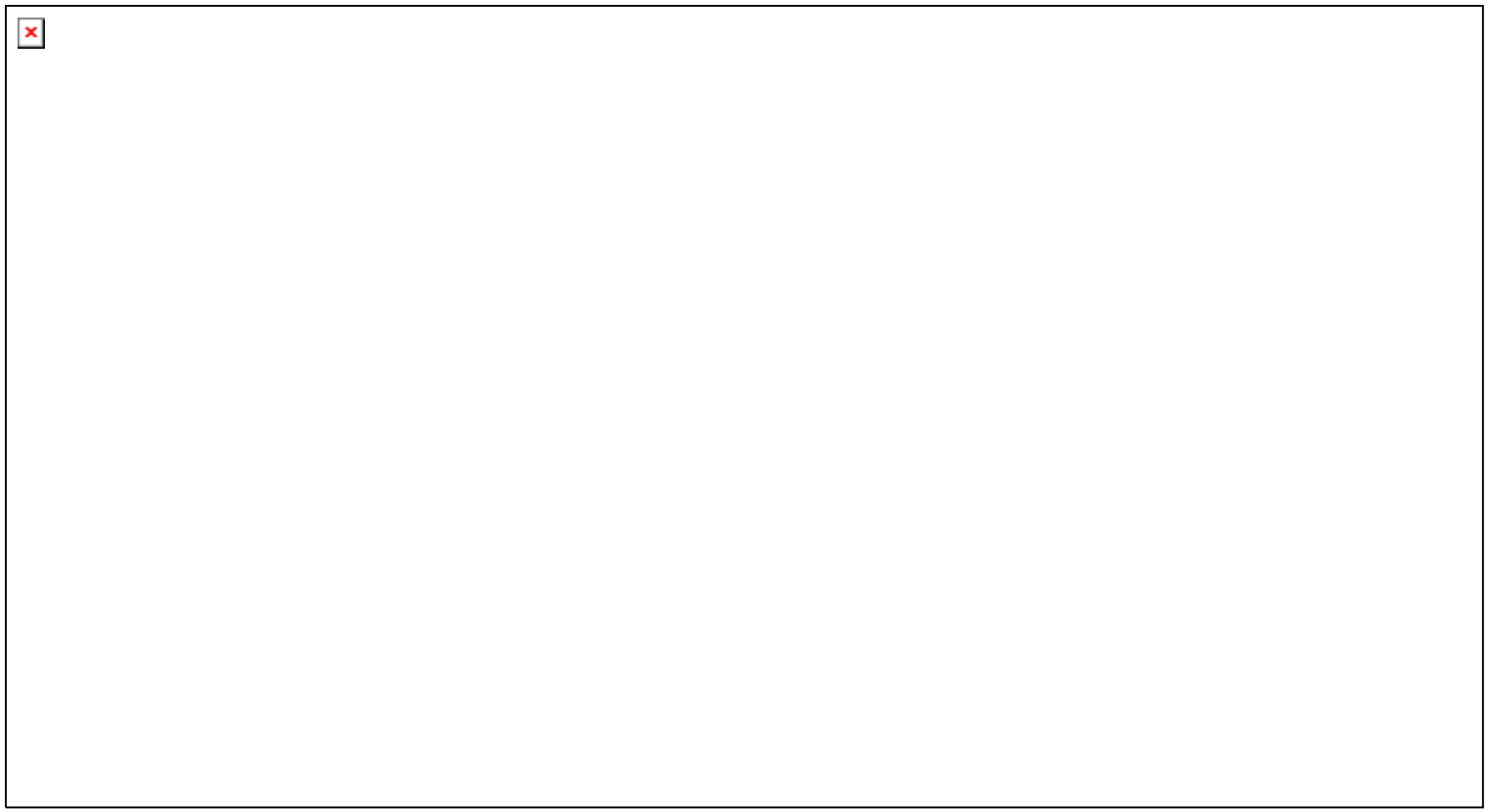

Figure 4.12 Singly labeled DNA primers hybridized to microarray to test specificity and channel quality. The signals from a Cy3 singly labeled DNA probe in all three channels are shown in (a), (b), and (c). In (a), the strong signal shows highly specific hybridization of the singly labeled probe DNA to its respective printed spots. (b) No excitation of the Cy3 fluorophore in the Cy5 channel. (c) The extent of signal bleed-through of the Cy3 fluorophore in the FRET channel resulting from the spectral overlap seen in Figure 4.7. The signals from a Cy5 singly labeled DNA probe in all three channels are shown in (d), (e), and (f). In (d), there is no signal in the Cy3 channel. The strong signal in (e) shows highly specific hybridization of the singly labeled probe DNA to its respective printed spots. (f) The extent of signal bleed-through of the Cy5 fluorophore in the FRET channel.

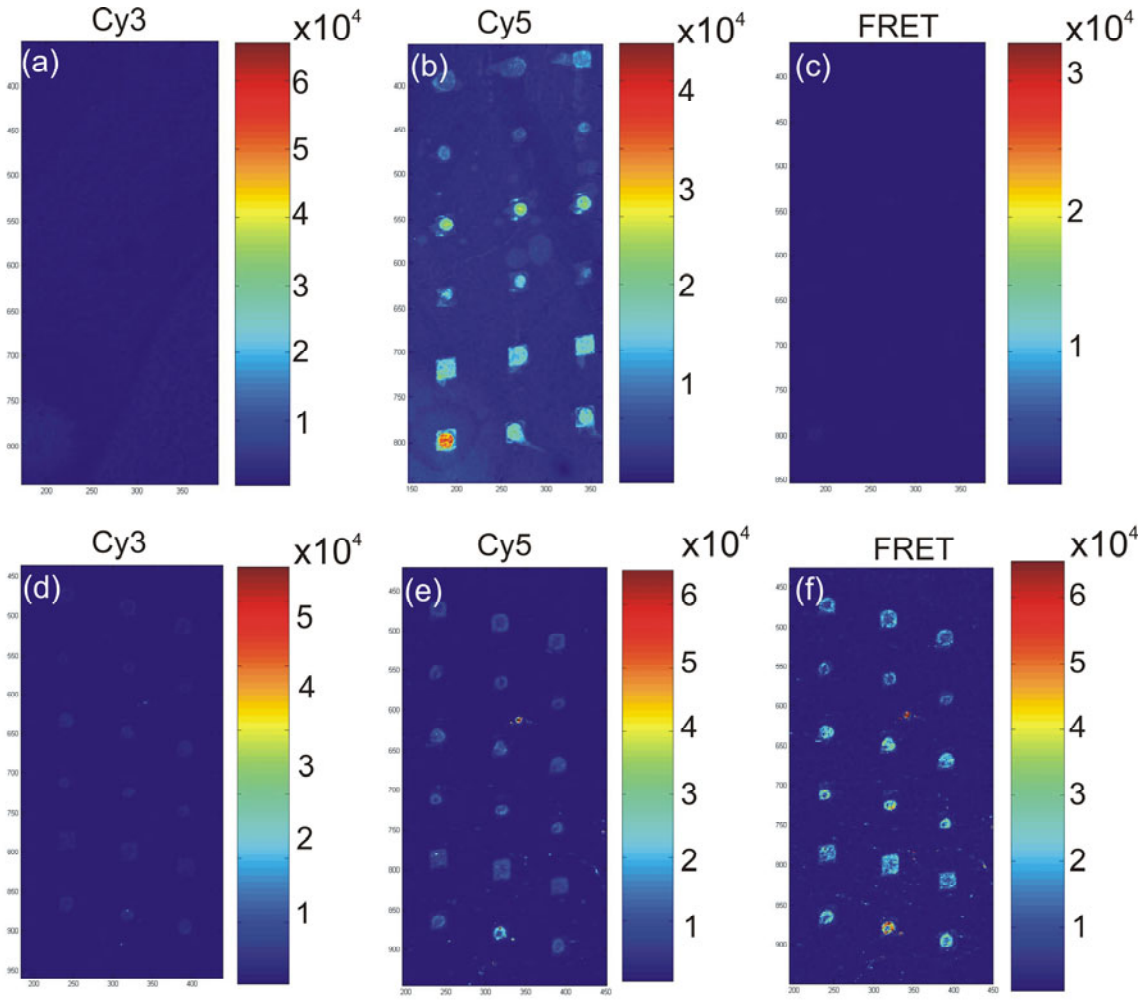

Figure 4.13 Singly (top) and doubly (bottom) labeled NC RNA hybridized onto a microarray chip to test hybridization quality as well as the three measurement channels: Cy3 (a) & (d), Cy5 (b) & (e), and FRET (c) & (f).

CHAPTER 5
APTAMER CHARACTERIZATION

5.1 Bulk Measurements

5.1.1 Steady state FRET assays

Equation Chapter 5 Section 1Steady-state FRET assays are performed to monitor the FRET breakdown that occurs upon substrate cleavage as well as to measure rates of binding and dissociation of the substrate and cleavage products. Steady-state fluorescence spectra were recorded on an Aminco-Bowman Series 2 spectrofluorometer using the HHT5 complex consisting of the HHT5 ribozyme, doubly labeled RNA substrate and biotynolated DNA primer. The annealed ribozyme (final concentration of 50 nM based on the concentration of the substrate strand; with a 4-fold (saturating) excess of both HHT5 ribozyme and DNA primer was incubated at 25 ^{o}C for at least 15 min in standard buffer (50 mM Tris-HCl, 10 mM $MgCl_2$), supplemented with 25 mM β-mercaptoethanol as a radical quencher, and was then transferred to a 150 μL cuvette. Cy3 was excited at 540 nm (4 nm bandwidth) and fluorescence emission was recorded simultaneously at the Cy5 (665 nm, 8 nm bandwidth) wavelength. The PMT voltage was set to 945V. Theophylline solution was manually added to a concentration of 500 nM. The resulting time traces, an example of which is shown in Figure 5.1, were fit to a single-exponential decrease

$$y = A_1 \exp\left(-x/t_1\right) + y_0 \tag{5.1}$$

in MicroCal Origin 7.0 to extract the rate of decay of the FRET signal, k_{obs}, as

$$k_{obs} = 1/t_1 . \tag{5.2}$$

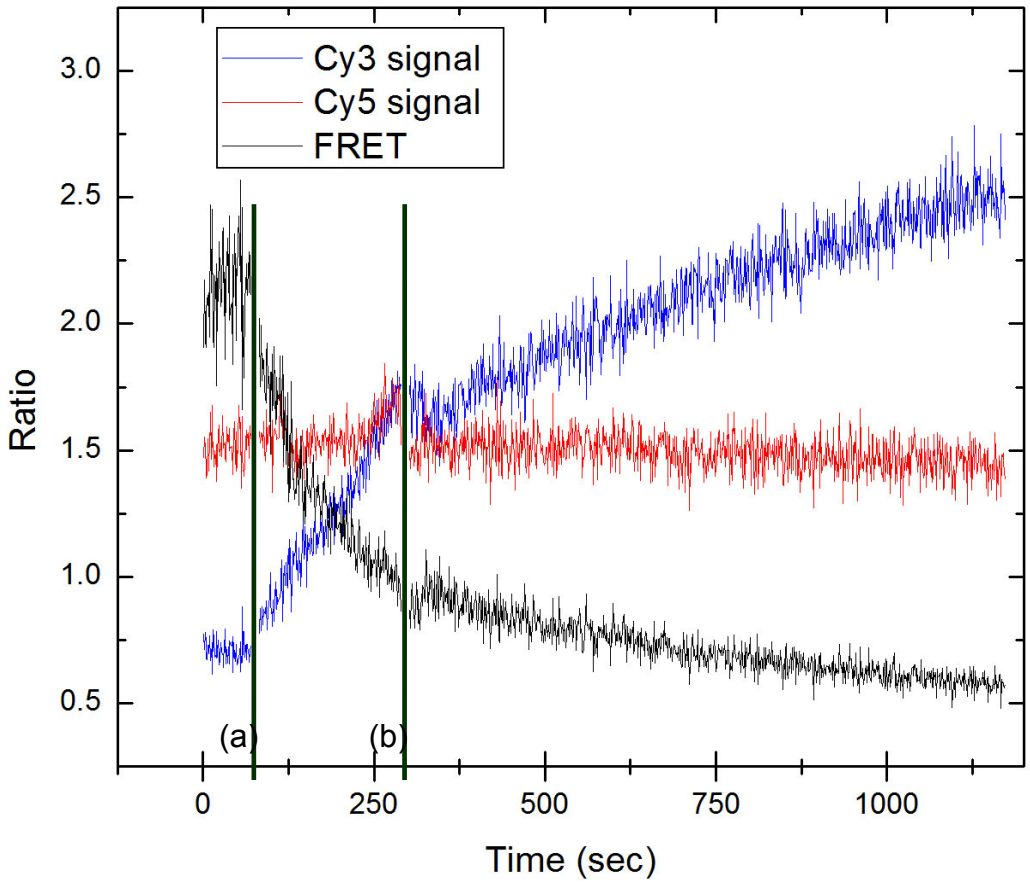

Figure 5.1 Steady state fluorescence time trace for a cleavage experiment. Initially, only 50 nM RC and 50 nM biotinolated pRC are present in 50 mM TRIS-HCl, pH 7.5, 10 mM $MgCl_2$ and the fluorescence is constant. At t = 75 sec (a), 150 nM HHT5 solution is introduced into the system and background cleavage of the substrate is observed. At approximately t = 300 sec (b) 1.5 mM theophylline is introduced into the system.

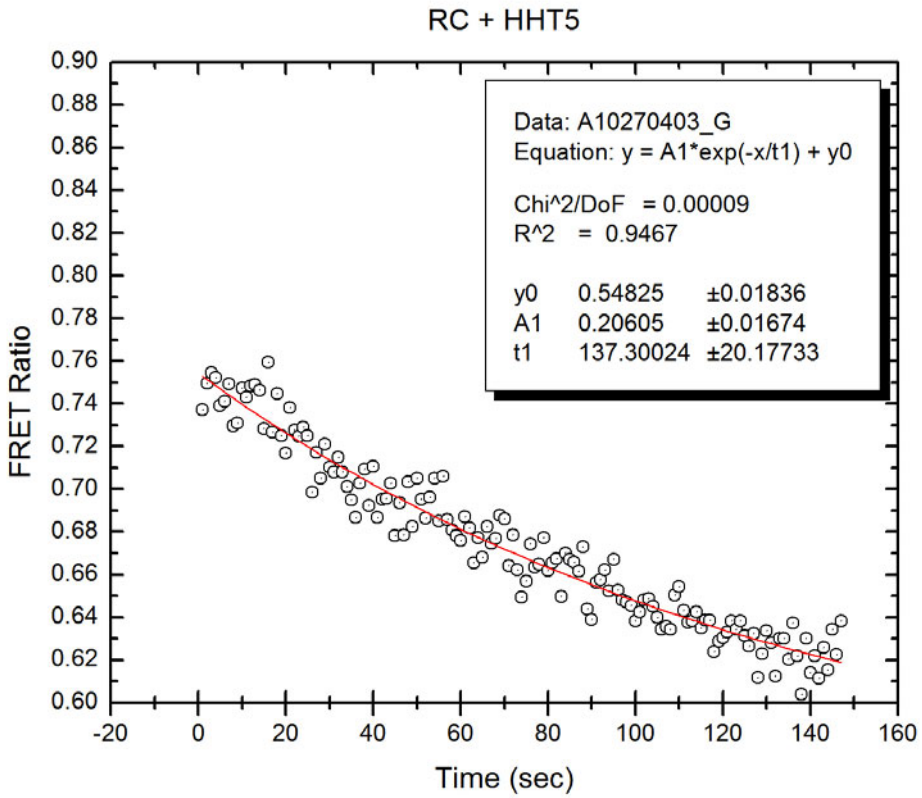

Figure 5.2 Steady state FRET assay data showing the FRET ratio as a function of time for the doubly-labeled RC substrate + HHT5 complex. This is the background cleavage.

The FRET ratio as a function of time based on the fluorescent signals of the acceptor and donor fluorophores in the presence of a three-fold concentration of HHT5 is shown in Figure 5.2. This is the background cleavage activity of the ribozyme, with a measured value of k_{obs} = 0.007418 ± 0.001086 s^{-1}. Upon the addition of some concentration of theophylline, an increase in k_{obs} is expected, indicating cleavage due to the presence of the analyte. However, a decrease in k_{obs} is consistently measured. Figure 5.3 shows the FRET ratio as a function of time for the doubly-labeled HHT5 ribozyme complex upon the addition of 50 mM theophylline. The FRET decay is expected to be due to the cleavage of the RC substrate and is faster than the decay due to photobleaching and background catalytic activity. The cleavage rate is measured to be k_{obs} = 0.00198 ± 0.00005 s^{-1}. Upon the addition of a higher concentration of theophylline, as in Figure 5.4, a faster cleavage rate is expected than for 50 mM theophylline. However, for 1.5 mM theophylline, the cleavage rate is observed to

be k_{obs} = 0.00102 ± 0.00009 s^{-1}. The results of several experiments at various theophylline concentrations are shown in Figure 5.5. A higher k_{obs} is observed in the presence of theophylline and the rate is concentration dependent, increasing with concentration, not as expected.

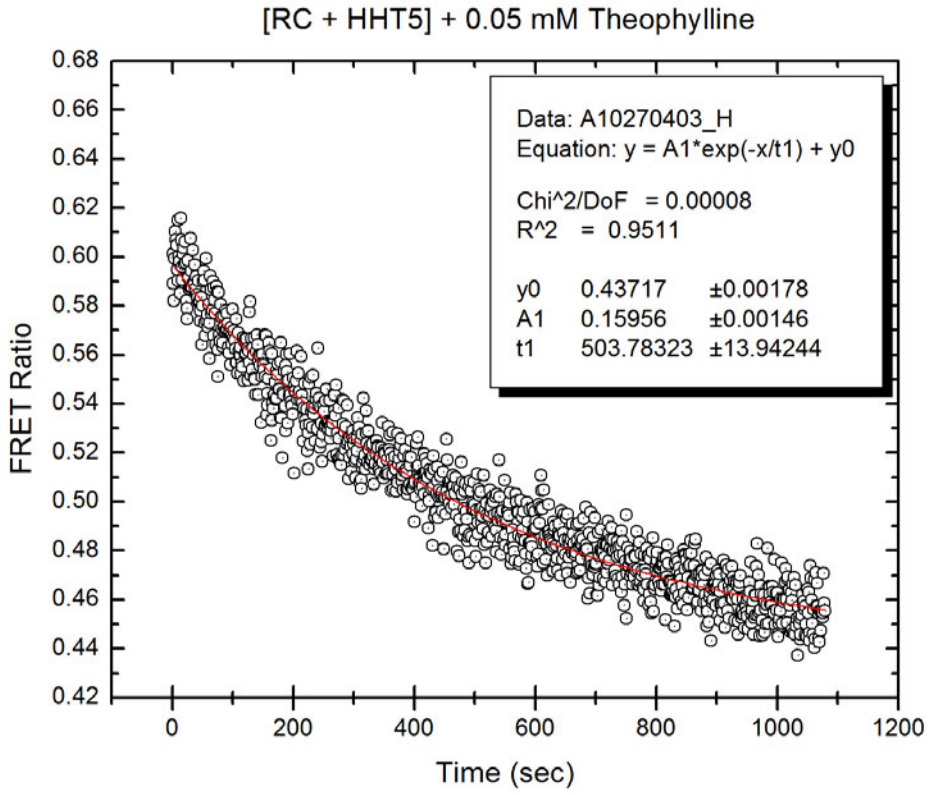

Figure 5.3 Steady state FRET assay data showing the FRET ratio as a function of time for the doubly-labeled RC substrate + HHT5 complex upon the addition of 50 μM theophylline. The FRET decay is due to the cleavage of the RC substrate and is slower than the decay due to photobleaching and background catalytic activity.

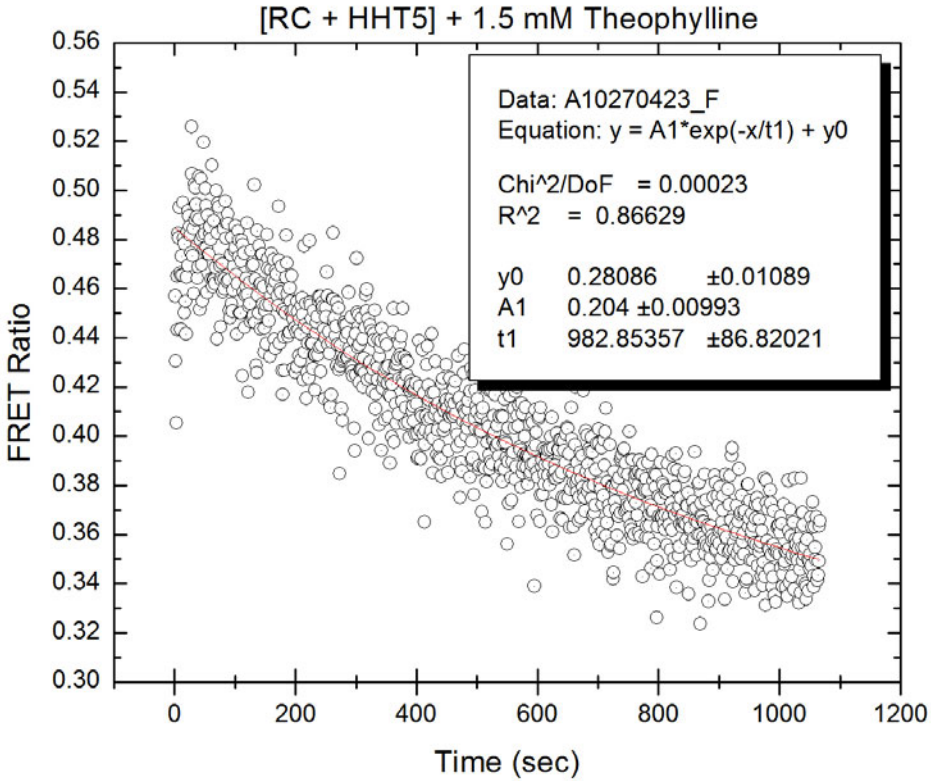

Figure 5.4 Steady state FRET assay data showing the FRET ratio as a function of time for the doubly-labeled RC substrate + HHT5 complex upon the addition of 1.5 mM theophylline. The FRET decay is due to the cleavage of the RC substrate and is slower than the decay observed for the complex in the presence of 50 μM theophylline.

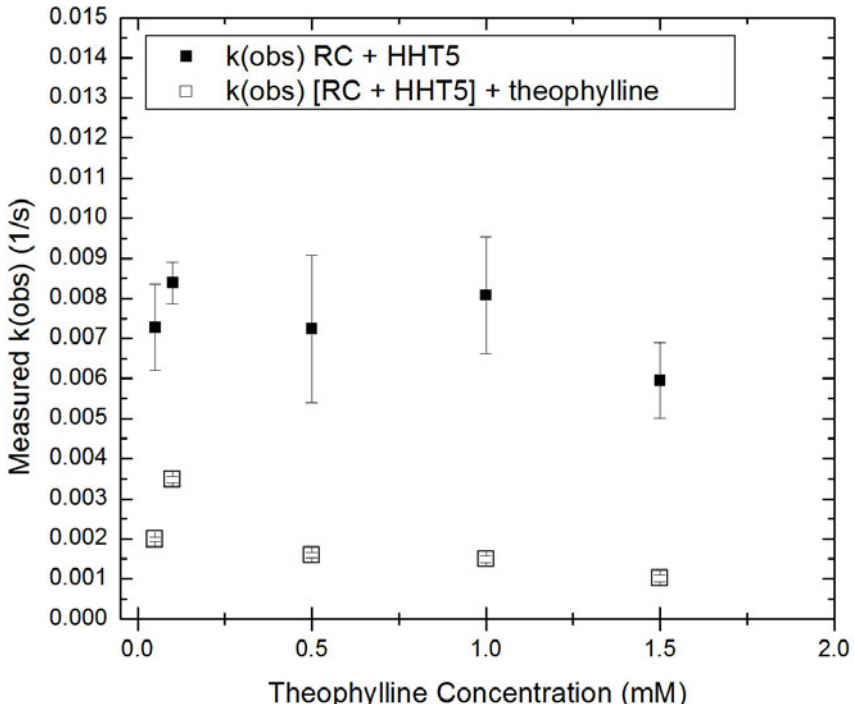

Figure 5.5 The measured rates of decay at various theophylline concentrations. A faster rate of decay is observed in the presence of theophylline.

The results of the steady state FRET assays do not show the viability of this ribosomal complex as the basis for a theophylline-specific biosensor. AThe expected difference in the rate of cleavage due to the presence of theophylline is not clearly observed in bulk solution. However, whether the expected response of the complex can be observed on the single-molecule level is yet to be determined. As the experimental environment plays an important role in the cleavage reaction, specifically the temperature and divalent ion concentration, this environment must first be studied and carefully monitored. These studies take the form of radioactive cleavage assays.

5.1.2 Radioactive cleavage assays and titrations

The (non-fluorescently) 5'^{32}P-labeled substrate was prepared by phosphorylation with T4 polynucleotide kinase and [$\tilde{\gamma}^{32}$P]ATP.

HHT5 complex was pre-annealed from <1 nM labeled substrate, 50 nM HHT5 ribozyme and 300 nM non-biotynolated DNA primer in standard buffer, by heating to 70 ^{o}C for 2 min and cooling to room temperature. After pre-incubation, theophylline buffer was added, as appropriate. Aliquots (2 μL) were taken at appropriate time intervals and the reactions quenched with 13 μL of 80% formamide, 0.025% xylene cyanol, 0.025% bromophenol blue, and 50 mM EDTA. The 5' cleavage product was separated from the uncleaved substrate by denaturing 20% polyacrylamide, 8 M urea, gel electrophoresis (Figure 5.6)and was quantified and normalized to the sum of the substrate and product bands using a Storm 840 PhosphorImager with ImageQuant software (Molecular Dynamics). Time traces of product formation (Figure 5.7) were fit to the single-exponential first-order rate equation 1.

$$y = y_0 + Ae^{-t/\tau} \tag{5.3}$$

Using Equation (5.3), we employed Marquardt-Levenberg nonlinear least-squares regression (Microcal Origin), where A is the amplitude and τ^{-1} the pseudo-first-order rate constant k_{obs}.

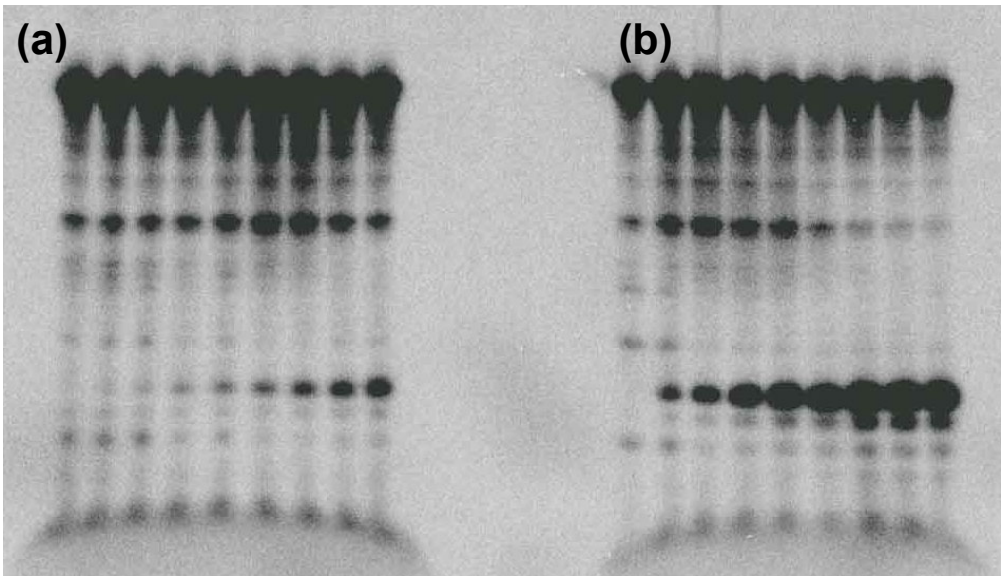

Figure 5.6 Results of a radioactive cleavage assay, showing (a) the background cleavage of the HHT5 ribozyme and (b) the enhanced cleavage due to the presence of 10 mM theophylline.

.

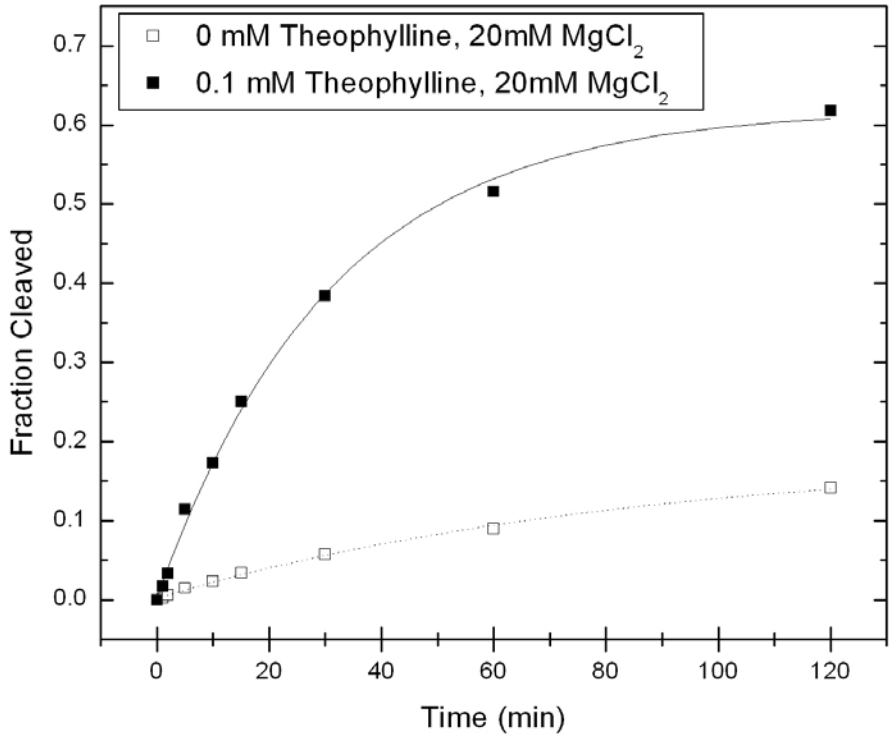

Figure 5.7 Radioactive cleavage assay results showing an enhancement of the catalytic activity of the HHT5 ribozyme in the presence of 0.1 mM theophylline. The cleavage rates found for 0.0mM and 0.1mM theophylline are k_{obs} = 0.01 min^{-1} and k_{obs} = 0.03 min^{-1}, respectively.

Metal ions neutralize the negatively charged phosphate backbone, significantly contributing to the folding of RNA molecules [Pyl02]. Furthermore, active tertiary conformation and catalytic function in RNA is often sensitive to the type and concentration of present cation(s) [Han00, Mur98]. Therefore, as the catalytic activity of the hammerhead ribozyme is enhanced with the concentration of divalent ions, several magnesium and theophylline titrations were conducted to determine the appropriate buffer conditions for single-molecule (and later - microarray) experiments. Figure 5.8 shows the results of the magnesium titration conducted at a 0.1 mM theophylline concentration. Here, we see a marked enhancement of catalytic activity for magnesium concentrations greater than 10 mM, the concentration typically used for standard reaction buffer. Subsequent titrations (Figure 5.9) over theophylline concentrations of interest were taken at 10 mM and 20 mM $MgCl_2$, showing an enhancement of catalytic activity at the greater magnesium concentration. Standard experiment buffer was subsequently adjusted to include 20 mM $MgCl_2$.

Figure 5.9 shows the results of a cleavage assay performed under the adjusted buffer conditions. The background cleavage rate that can be expected from the conformational changes of the HHT5 ribozyme, causing the ribozyme to undergo catalysis, was determined from the 0.0 mM theophylline data. Thus a background cleavage rate of $k_{obs} = 0.0118 \pm 0.0013$ min^{-1} is expected. For a concentration of 0.1 mM theophylline, the $k_{obs} = 0.0323 \pm 0.0020$ min^{-1}, showing a 65% cleavage enhancement over the background cleavage.

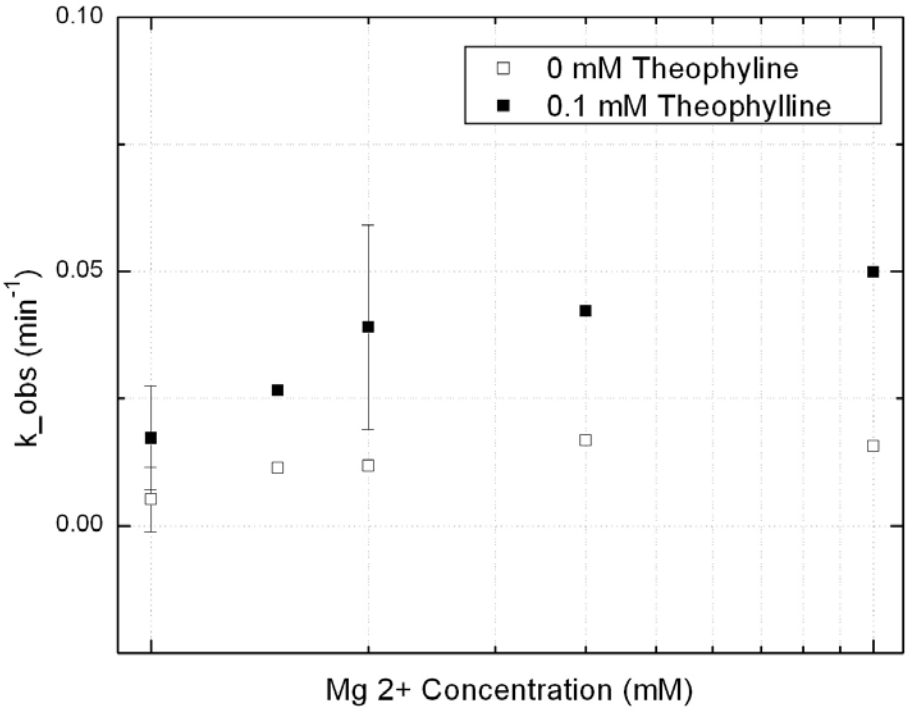

Figure 5.8 Magnesium titration showing an increase in the rate of cleavage of the HHT5 ribozyme with magnesium concentration.

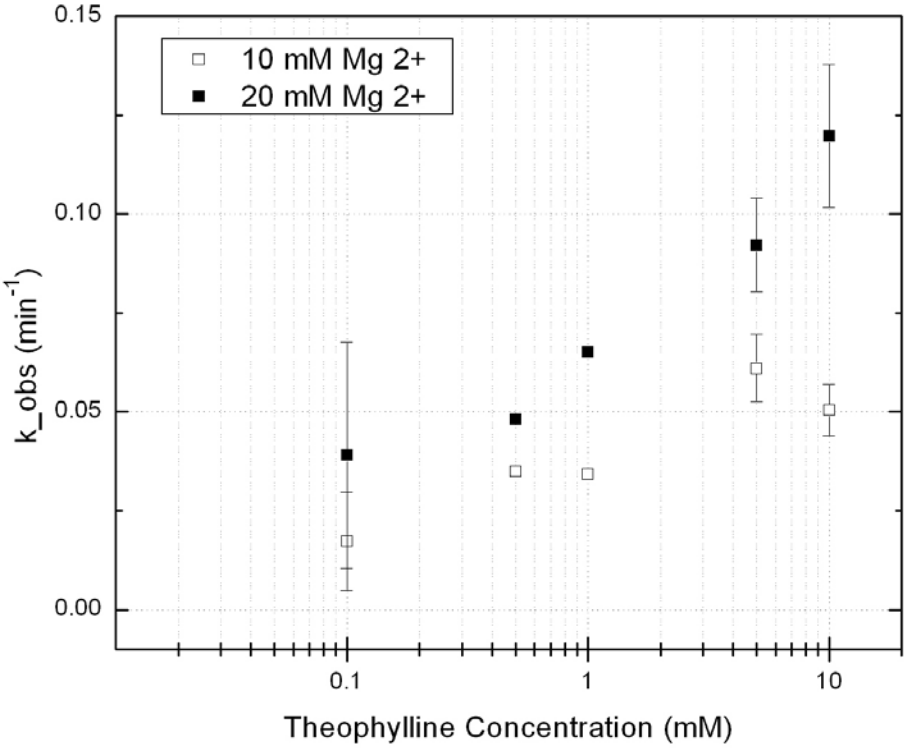

Figure 5.9 Theophylline titration data showing an increase in the rate of cleavage of the HHT5 ribozyme with magnesium concentration.

5.2 Single Molecule Measurements

5.2.1 Sample Preparation

Samples for single molecule experimentation are prepared using the specific protocol described in Appendix B. In short, previously prepared flow cells (see Chapter 4.3) were injected with 60 µl of biotinylated BSA and left to incubate at RT for 10 min. The channels were then flushed with 80 µl of a 50 mM Tris pH 7.5, 50 mM NaCl buffer to remove excess BSA and injected with 80 µl streptavidin. After flushing the channels with 80 µl of Standard Buffer (50 mM Tris-HCl pH 7.5, 20 mM MgCl2), and injection with approximately 80 µl Sodium buffer and approximately 80 µl streptavidin, the flow cells are ready for sample.

To prepare the 100 pM sample solution (Solution C), combine 4 µl of 5 nM solution (Solution B), 4 µl βME (Beta-mercapto-ethanol), and 192 µl Standard Buffer (50 mM Tris-HCl pH 7.5, 20 mM $MgCl_2$). Solution B is prepared by diluting 2 µl Solution A and 4 µl βME in 194 µl Standard Buffer. Solution A consists of 1 µl doubly labeled RC substrate, 0.411 µl biotynolated pRC primer, 7.60 µl Standard Buffer and 1 µl βME. Solution A is heat annealed at 90°C and allowed to cool to RT before dissolution into Solution C. Finally, a 250 nM HHT5 ribozyme buffer is prepared in oxygen scavenger system (OSS) buffer. The OSS buffer, composed of 192 µl Glucose Buffer, 2 µl OSS, and 4 µl βME, is prepared from the OSS composed of 12.5 µl Catalase, 50 µl equivalent volume glucose oxydase, and 100µl of buffer containing 50 mM Tris-HCl and 50 mM NaCl, pH 7.5.

5.2.2 Single molecule FRET events

Single molecule events are detected using the TIRF microscopy techniques previously described. In Figure 5.10 through Figure 5.13, examples of typical single-molecule event data are shown. Figure 5.10 shows a single molecule FRET event. Here, the Cy3 donor fluorophore (blue line) transfers energy to the Cy5 acceptor fluorophore (red line) for approximately t = 750 sec,

at which point the Cy5 disappears. This acceptor disappearance is either due to photobleaching or cleavage of the RNA substrate molecule. At approximately t = 1400 sec, the Cy3 disappears in a single step, indicating detection of a single molecule. Both Figure 5.11 and Figure 5.12 show single molecule events where FRET cannot be conclusively determined. In Figure 5.11, the Cy5 disappears in a single step at t = 350 sec, but as there is no Cy3 signal, FRET between Cy3 and Cy5 on the same molecule cannot be ascertained and this event type is of no interest. Similarly, Figure 5.12 shows an event where the Cy3 does not efficiently transfer energy to the Cy5. At t = 150 sec, the donor undergoes photobleaching and no information is gleaned regarding the nature of the event and is therefore not of interest. However, the event shown in Figure 5.13 is of interest as this event may indicate conformational changes of the RNA complex in solution. As the complex undergoes molecular dynamics, the locations of the donor and acceptor fluorophores change, also changing the FRET efficiency. At approximately t = 6600 sec, at which point the Cy5 disappears due to either a photobleaching or cleavage event. At approximately t = 7250 sec, the Cy3 disappears in a single step, indicating the detection of a single molecule.

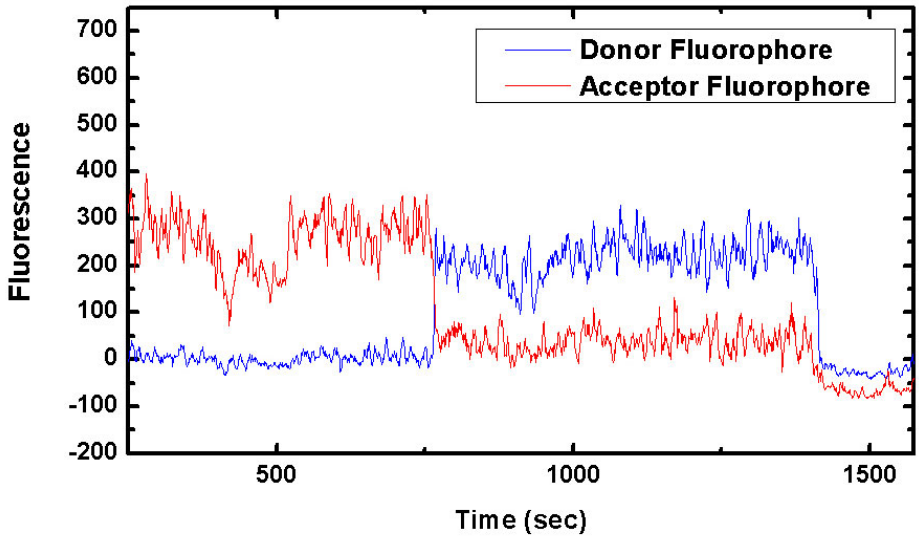

Figure 5.10 A typical single-molecule FRET event. The donor fluorophore transfers energy to the acceptor fluorophore for approximately t = 750 sec, at which point the acceptor disappears either due to photobleaching or cleavage of the RNA substrate molecule. At approximately t = 1400 sec, the donor fluorophore disappears in a single step, indicating detection of a single molecule.

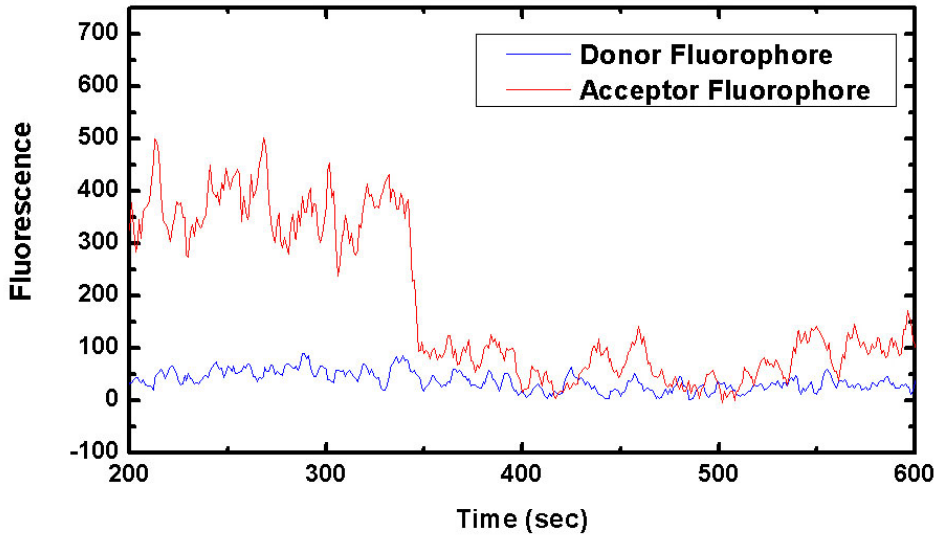

Figure 5.11 A single-molecule event where the acceptor fluorophore disappears in a single step at t = 350 sec. FRET between fluorophores on the same molecule cannot be conclusively asserted in this case.

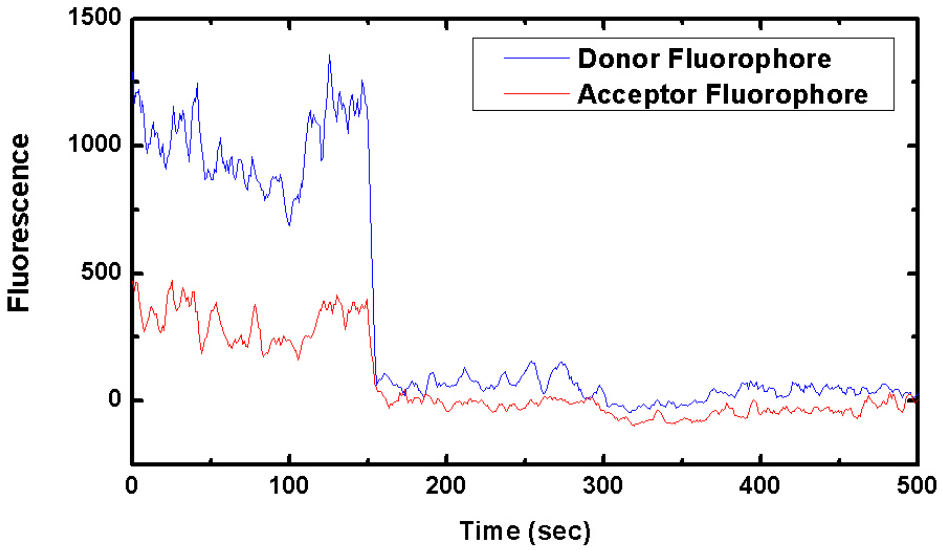

Figure 5.12 A single-molecule event where the donor fluorophore does not efficiently transfer energy to the acceptor fluorophore. At t = 150 sec, the donor undergoes photobleaching.

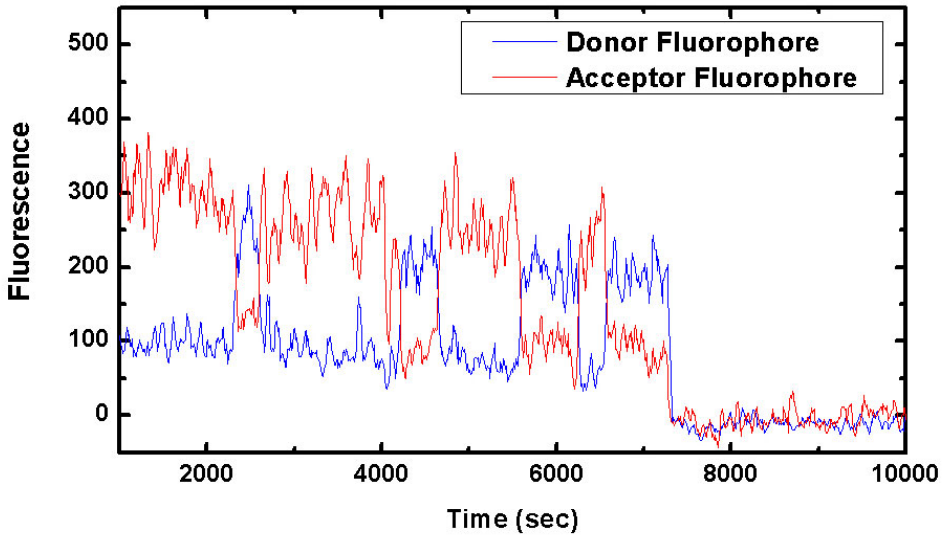

Figure 5.13 A single-molecule event which indicates conformational changes of the RNA complex in solution. As the complex undergoes molecular dynamics, the locations of the donor and acceptor fluorophores change, also changing the FRET efficiency.

5.2.3 Single Molecule Measurement Results

Preliminary single molecule experiments were conducted using the cleavable (RC) substrate to determine the time scales of the expected background effects due to photobleaching and background cleavage. The exposure time, from full frame to 0.192, was adjusted to determine the rate of background effects under these experimental conditions. The results are shown in Figure 5.14 and in Figure 5.15. At full frame exposure, the substrate is expected to photobleach in approximately 150 seconds, while at the shorter exposure, an expected photobleaching time of approximately 760 seconds was determined. According to my radioactive cleavage experiment results, cleavage due to the presence of 0.1mM theophylline in the presence of 20mM magnesium concentration is expected on a time scale of approximately 1000 seconds. Therefore, the exposure time of the fluorophores must be decreased even more for single molecule studies.

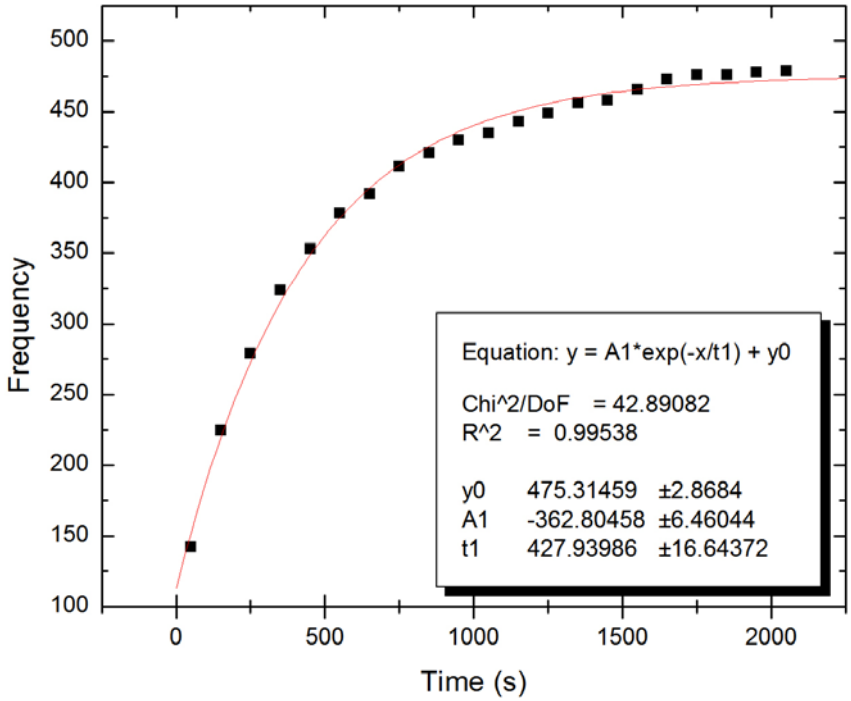

Figure 5.14 Single molecule cleavage event data to determine the photobleaching rate using cleavable (RC) substrate. Full frame data taken at 10.12 fps shows the fluorophore exposure rate must be decreased.

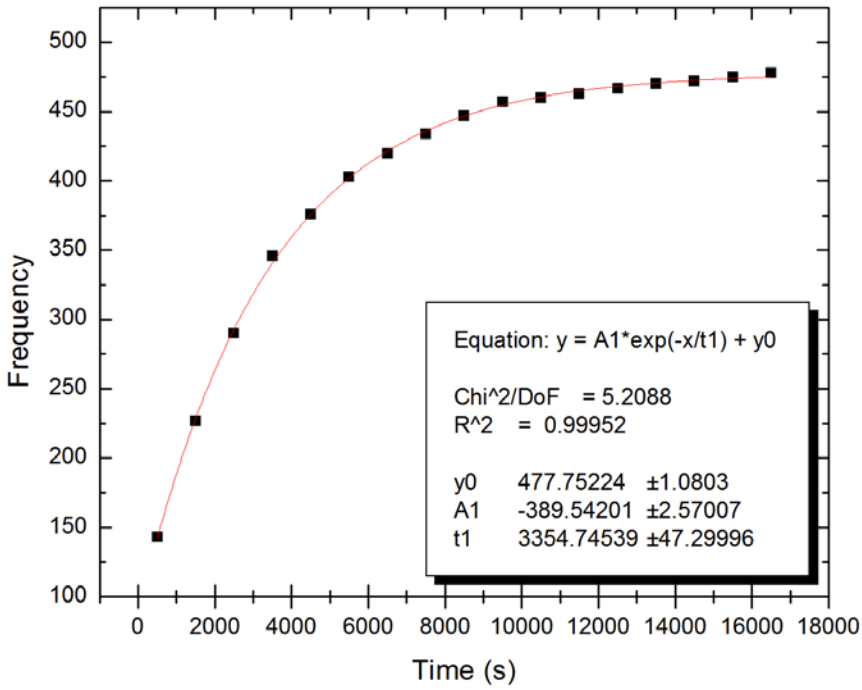

Figure 5.15 Single molecule cleavage event data to determine the photobleaching rate using cleavable (RC) substrate. Data taken at 10.12 fps with a 0.192 exposure shows photobleaching and background cleavage to be slower than the expected theophylline-enhanced cleavage based on cleavage assay results.

5.3 Microarray Measurements

5.3.1 Sample Preparation

Samples for microarray experimentation are prepared based on the protocols for bulk and single-molecule experiments and is described in more detail in Appendix B. As the microarray is printed on the surface of the glass slide, the preparation of the flow cell is modified. Also, as data measurement is done off-site, all materials and reagents must be transported, in a light and temperature controlled environment.

As the concentration of hybridized RNA substrate on the microarray is unknown, and can only be estimated based on the concentration of the DNA printed on each spot, the sample solution is prepared with an excess of HHT5. This solution of heat annealed 5 μM HHT5 in standard buffer (50 mM Tris-HCl, 20 mM $MgCl_2$) is allowed to cool on ice during transport. Theophylline or caffeine may be added to the sample solution once at the microarray scanner.

5.3.2 Experimental Results

Various experiments were conducted to measure the cleavage rate of the doubly-labeled HHT5 ribozyme in the presence and absence of theophylline. Each microarray was repeatedly scanned to obtain time traces in the Cy3, Cy5, and FRET channels. A laser power setting of 75%, PMT gain of 80% and focal length of approximately -50 was used for each experiment, however the values were adjusted for each measurement area to ensure proper focus and prevent signal saturation when necessary.

5.3.2.1 Preliminary data

Initial data taken of RC substrate hybridized onto the DNA microarray is shown in Figure 5.16. Each figure represents the average fluorescent signal intensity over time in the Cy3 and Cy5 channels for each row of printed DNA primer.

Recall that different concentrations of primer were used in the constellation design, 0.5 μg/μl, 1.5 μg/μl, 5 μg/μl, and 15 μg/μl, implying that each

row will allow the hybridization of a different RNA substrate concentration. Therefore, the fluorescence concentration is expected to increase with primer concentration. However, the signal intensity range does not change appreciably over all concentrations, and each row of the microarray will contribute cleavage data. Each plot also shows an increase in the Cy3 signal over time, corresponding to the decrease in the Cy5 channel, and indicating the occurrence of a FRET event. Therefore, we conclude that FRET can be measured indirectly by treating the microarray scanner data similarly to steady state assay data. However, we fist turn to using the capability of the microarray scanner to directly measuring the FRET signal.

Figure 5.17 shows a data set for RC substrate hybridized to the microarray where the signal was measured in the Cy3, Cy5 and FRET channels. This data shows a decrease in the Cy5 channel and a slight increase in the Cy3 channel over time due to disappearance of the acceptor fluorophore. However, no change in the FRET channel is observed and any observed intensity is attributed to the expected 10% bleed-through of the Cy3 channel into the FRET channel. It remains uncertain whether this effect is due to poor focusing or a malfunction of the microarray scanning equipment. Therefore, FRET is indirectly measured by calculating the FRET ratio based on the Cy3 and Cy5 channel signals.

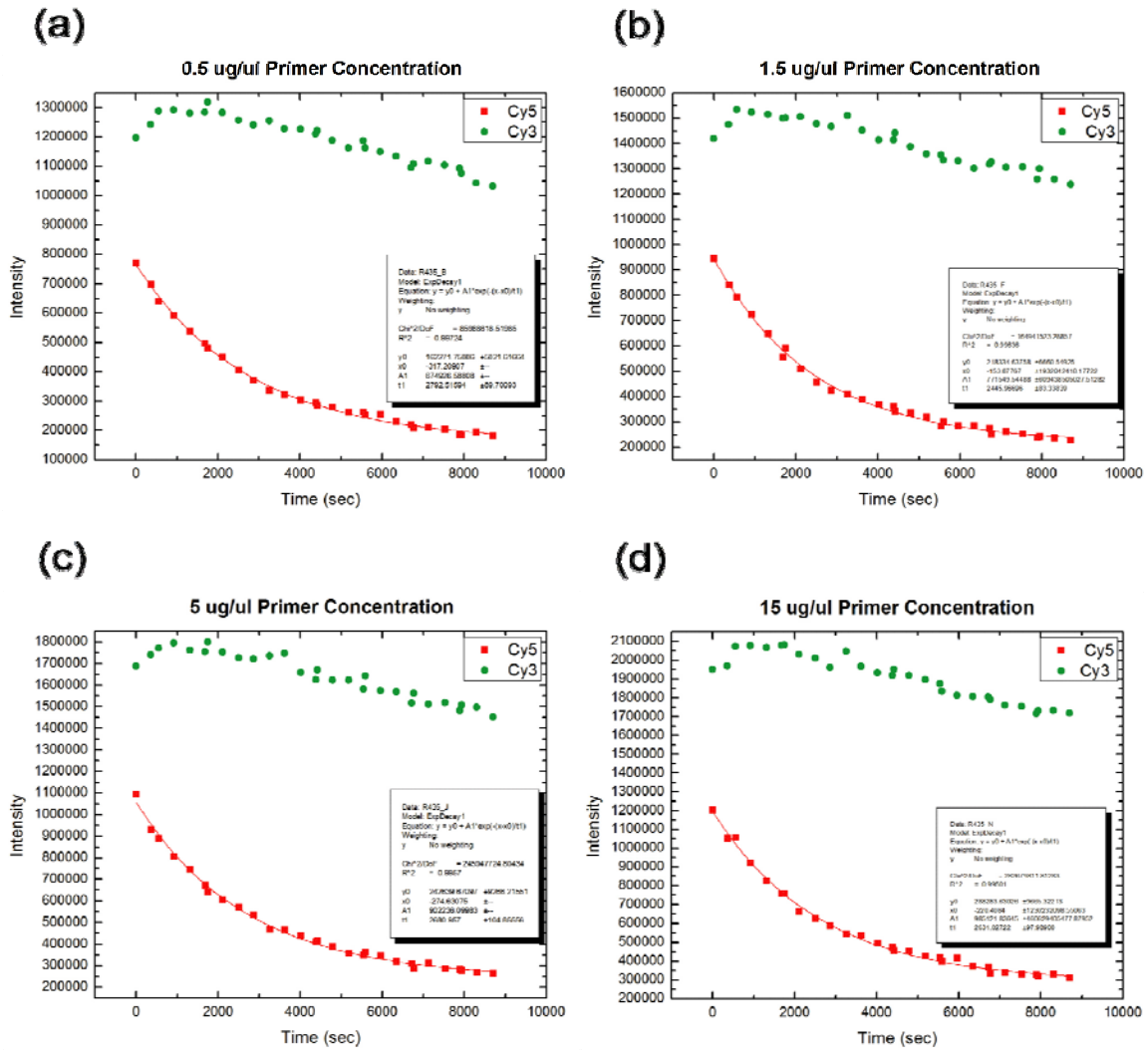

Figure 5.16 Microarray data showing the Cy3 and Cy5 signal over time for the RC substrate hybridized to the spots of (a) 0.5 µg/µl, (b) 1.5 µg/µl, (c) 5.0 µg/µl, (d) 15.0 µg/µl, mRC primer. An increase in the Cy3 signal is observed, corresponding to the decrease in the Cy5 channel, and indicating the occurrence of a FRET event. The signal intensities slightly increase with primer concentration indicating that the saturation level for hybridization has not been reached.

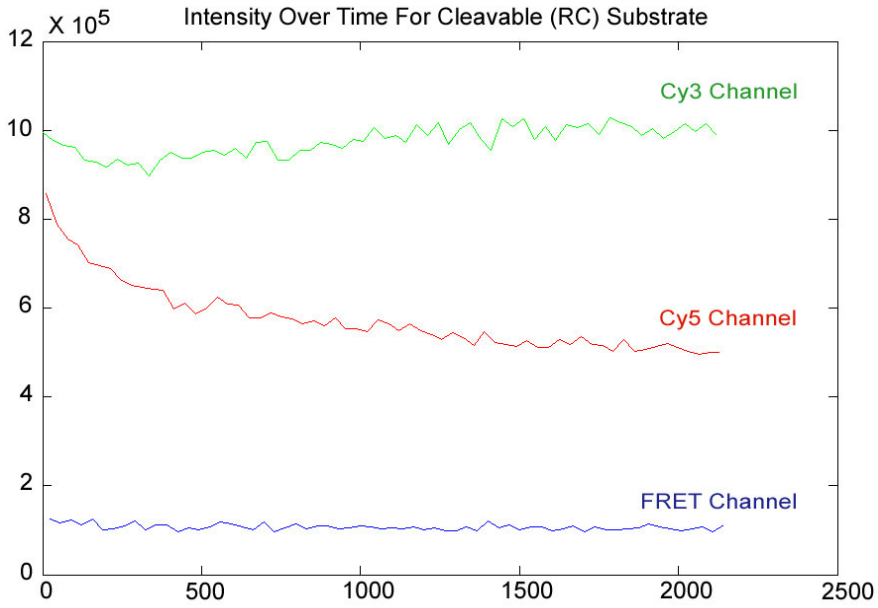

Figure 5.17 Fluorescence signal intensity over time, measured in the Cy3 (green), Cy5 (red), and FRET (blue) channels. The Cy5 signal decay is accompanied by a slight increase in the Cy5 signal. However, the signal in the FRET channel is constant and can be attributed to the expected 10% bleed-through of the Cy3 signal.

5.3.2.2 Cleavable (RC) microarray data

Cleavable RNA microarrays are incubated with an excess of HHT5 and either theophylline or caffeine. The FRET ratio as a function of time is averaged over all spots in the microarray. Error bars on the data are calculated based on the standard deviation of the FRET ratio values determined for each row of array data and may therefore be inflated.

HHT5 is first incubated with 10mM theophylline and a cleavage rate of k_{obs} = 1.6x10^{-3} ± 0.2x10^{-3} s^{-1} is calculated for this event, shown in Figure 5.18. As a control, HHT5 is incubated with 10mM caffeine and a cleavage rate of k_{obs} = 1.1x10^{-3} ± 0.10x10^{-3} sec^{-1} is calculated from the single exponential fit in Figure 5.19. It can be argued that the control data does not follow a single exponential fit but rather a linear decay. However some background effects are observed due to either photobleaching or background cleavage. However, a clear enhancement in the cleavage rate is observed for the target analyte over that of the control at high target concentrations.

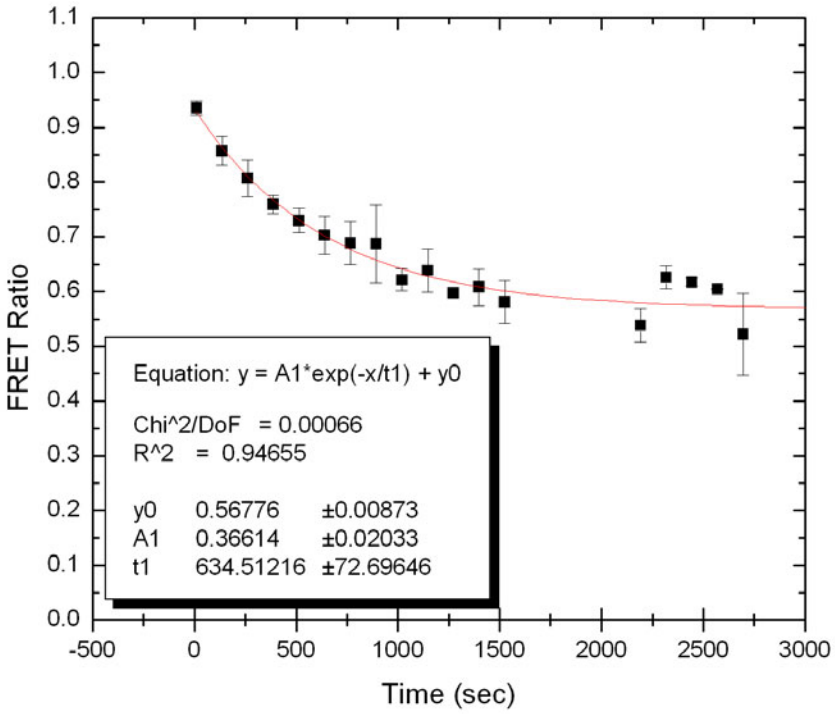

Figure 5.18 The average FRET ratio as a function of time calculated for hybridized cleavable RNA incubated with HHT5 and 10mM theophylline. A cleavage rate of k_{obs} = 1.6x10^{-3} ± 0.2x10^{-3} s^{-1} is calculated from the single-exponential fit.

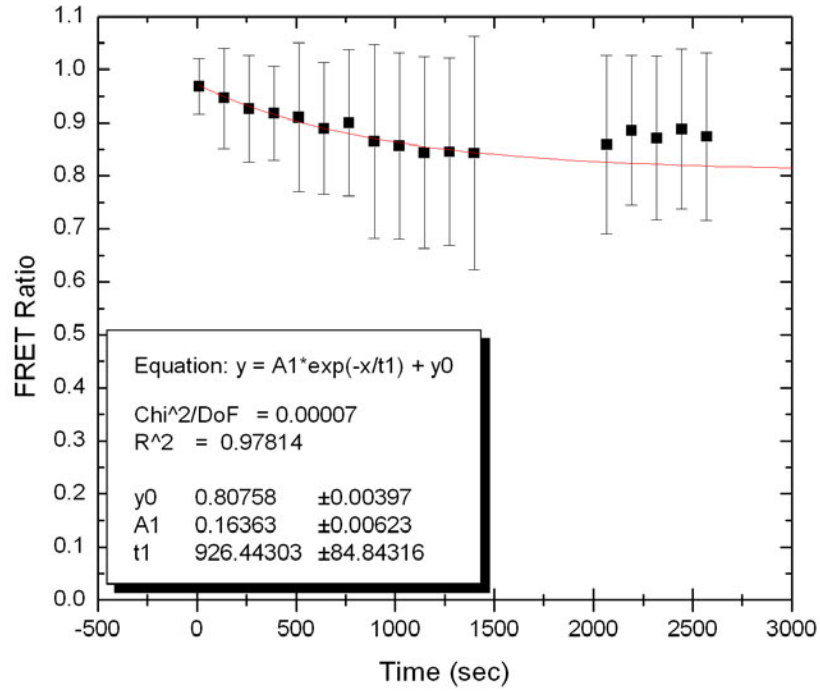

Figure 5.19 The average FRET ratio as a function of time calculated for hybridized cleavable RNA. As a control, HHT5 is incubated with 10mM caffeine and a cleavage rate of k_{obs} = 1.1x10^{-3} ± 0.1x10^{-3} s^{-1} is calculated.

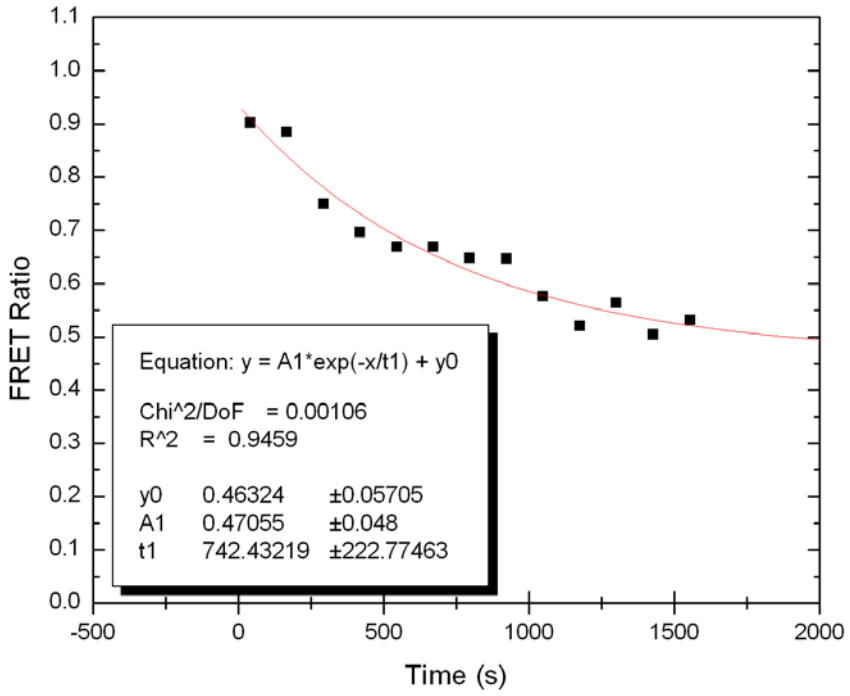

Figure 5.20 The FRET ratio as a function of time calculated based on one spot of hybridized cleavable RNA. HHT5 is incubated with 1mM theophylline and a cleavage rate of k_{obs} = 1.3 x10^{-3} ± 0.4 x10^{-3} s^{-1} is calculated.

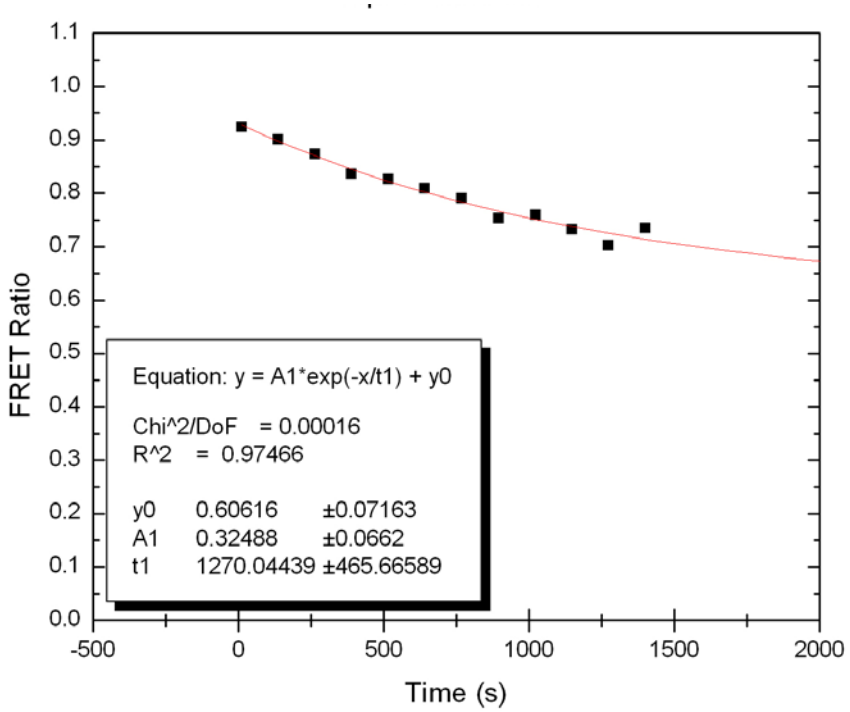

Figure 5.21 The FRET ratio as a function of time calculated based on one spot of hybridized cleavable RNA. HHT5 is incubated with 1mM caffeine and a cleavage rate of k_{obs} = 0.8x10^{-3} ± 0.3 x10^{-3} s^{-1} is calculated.

The experiment was repeated for a lower concentration (1mM) of both theophylline and caffeine. The FRET ratio as a function of time calculated based on one spot of hybridized cleavable RNA is shown in Figure 5.20. Here, HHT5 is incubated with 1mM theophylline and a cleavage rate of k_{obs} = 1.3 x10^{-3} ± 0.4 x10^{-3} s^{-1} is calculated for this event. As a control, HHT5 is incubated with 1mM caffeine and a cleavage rate of k_{obs} = 0.8 x10^{-3} ± 0.3 x10^{-3} s^{-1} is calculated, resulting in a strikingly different k_{obs}. Therefore, at lower concentrations of theophylline, a clear increase in the cleavage rate is observed for the target analyte over that of the control.

5.3.2.3 Non-cleavable (NC) microarray data

To ensure the above trends are due to cleavage of the substrate, a control experiment is conducted using a single slide with non-cleavable RNA hybridized to both constellations. The microarrays are incubated with either an excess of HHT5 or an excess of HHT5 plus theophylline. Measurements are conducted by imaging the fluorescent signal in each channel for each constellation then alternating the constellation imaged. The first constellation, shown in Figure 5.22, is incubated with the excess HHT5 and 10mM theophylline solution. No change in the average FRET ratio over time is observed. Similarly, Figure 5.23 also shows no change in the average FRET ratio over time for the non-cleavable RNA incubated with only HHT5. The two figures, however, show an odd, almost direct, correlation between the FRET ratios. This odd correlation is attributed to the equipment and may be due to inconsistent laser power or de-focusing over time. Defocusing was observed later, in the GSI Lumonics ScanArray 5000, which allows the user to focus in each of the three measurement channels, as opposed to the PerkinElmer ScanArray Express model, which only allowed focus in a single channel.

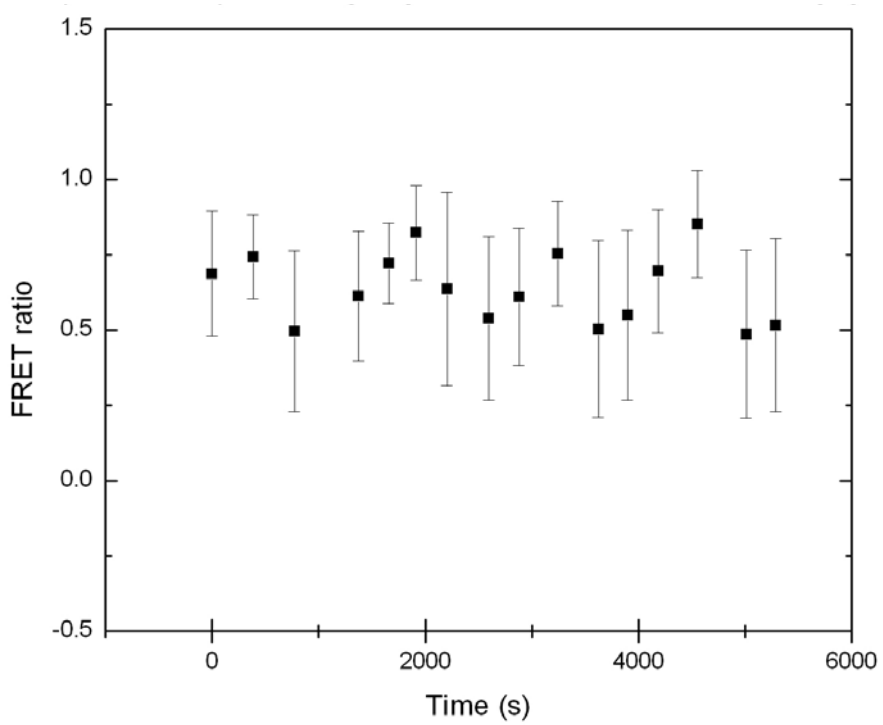

Figure 5.22 The average FRET ratio as a function of time calculated for hybridized non-cleavable RNA incubated with HHT5 and 10mM theophylline. No change in the FRET ratio is observed.

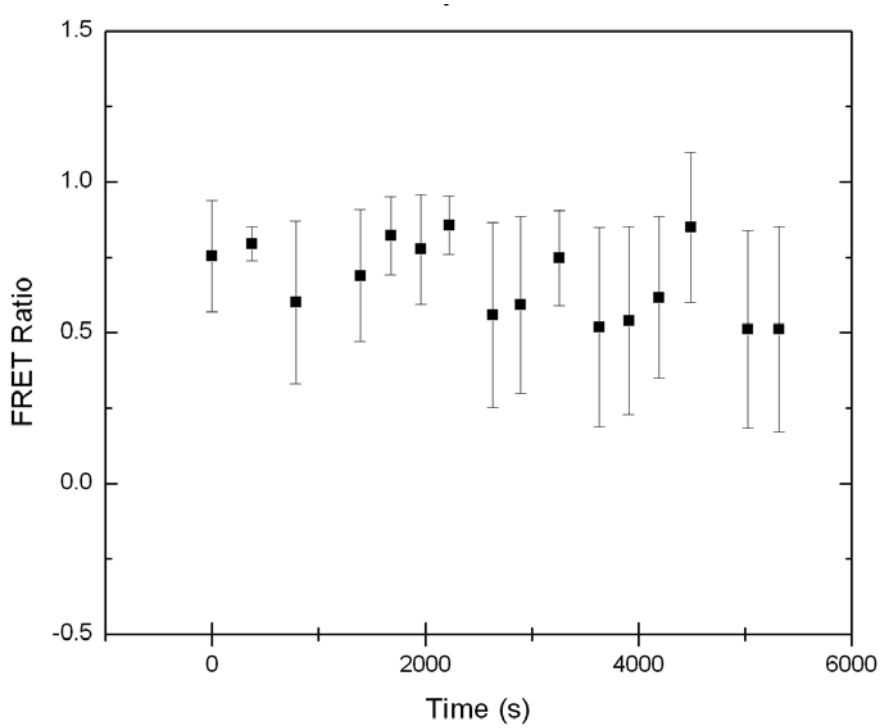

Figure 5.23 The average FRET ratio as a function of time calculated for hybridized cleavable RNA incubated only with HHT5. No change in the FRET ratio is observed.

5.3.2.4 Microarray experiment conclusions

In conclusion, signal trends show that the biosensor is sensitive to theophylline concentrations down to 1 mM. High specificity of the biosensor between theophylline and caffeine is also observed, indicating this is a feasible technology for the detection of theophylline.

However, microarray scanner function and software is not designed to accommodate repeated, alternating measurements of multiple constellations. The inability for the scanner to maintain its focus after only a few minutes of measurement was not discovered until fairly recently. This discovery forces us to refocus before each scan, a process that cannot be automated with the current software provided by the manufacturer. The resulting loss of time resolution is also significant, as a data point can be acquired only every 90 sec, as opposed to every 20 sec if no refocusing is attempted between scans.

CHAPTER 6
OUTLOOK

6.1 Microfluidics for Single-Molecule Experiments

The eventual aim of this project is to incorporate the biosensor onto a stable and compact microfluidic platform that will allow for the analysis of extremely small sample volumes and the realization of an array of different sensor molecules that can detect a suite of target molecules of interest. For single-molecule experiments, the chips can be fabricated using techniques currently in development by Meiners and coworkers [Che03, Che04a, Che04b] which closely follow those described by Unger, et al [Ung99] and Duffy, et. al. [Duf98]. The platform will take the form of a chip, manufactured in a multilayer soft lithography technique from a silicon elastomer and packaged in an epoxy casing to provide the mechanical stability for the chip to be plugged into a socket like an electronic chip Figure 6.1(d).

The microfluidic chip will feature a hybridization spot to which the sensor molecules can be attached in-situ as well as reservoirs for sensor and reporter molecules Figure 6.1(a). Microfabricated valves and pumps, created by overlapping channels separated by a thin membrane, will be incorporated into the chip to pneumatically control the flow of reagent and sample. These channels work in such a way that when the control channel is not pressurized, the valve is open and flow through the flow channel is not impeded Figure 6.1(b). However, when the control channel is pneumatically pressurized, it expands and closed the valve by pinching off the flow through the flow channel underneath Figure 6.1(c).

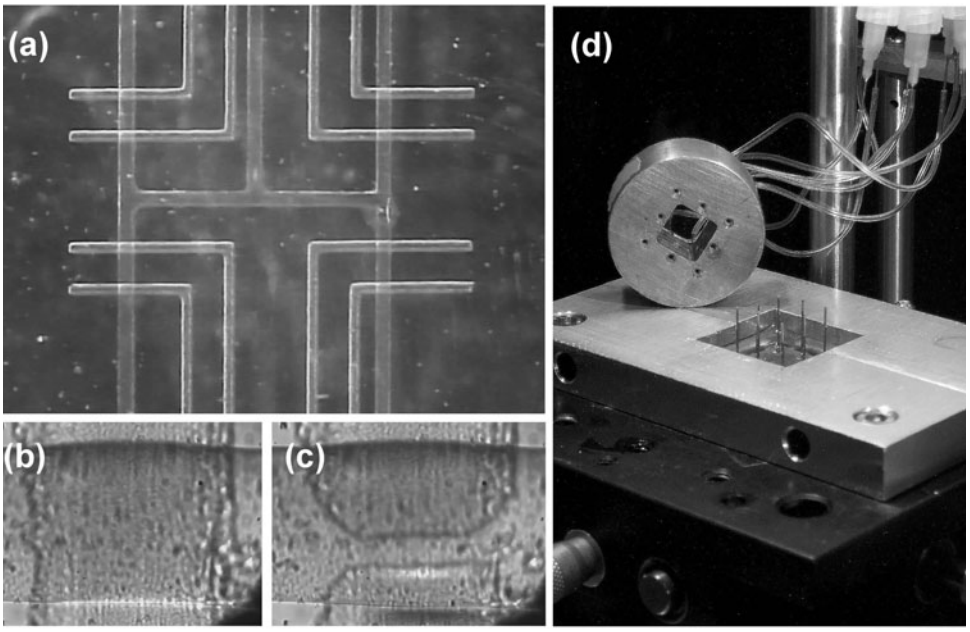

Figure 6.1 Microfabricated flow channels and pneumatically actuated valves. (a) Overview of a device with four supply and one exit channel converging in a reaction/detection area in the middle of the chip. Two pressure lines control the flow in each of the supply channels through a thin membrane. (b) Shows a close-up of an open valve, i.e., the intersection between pressure line and supply channel. In (c), the control line is pressurized and pinches the flow in the supply line off; the valve is closed. (d) Shows the assembled and packaged chip together with the external reagent delivery and pressure control system.

More recently, a topologic structure was developed for microfluidic mixing [Che04a, Che04b]. This mixer exploits the laminarity of the flow to repeatedly fold the flow and exponentially increase the concentration gradients. Helical flow channels with opposite chiralities split, rotate, and recombine the fluid stream for fast and efficient mixing by diffusion. The arrows in Figure 6.2(a) indicate the fluid flow split, rotation and recombination as two different solutions are combined in a *T*-junction. This junction is created by overlapping and fusing together the two principal elastomer layers and anchoring with a third elastomer layer on a glass cover slip (Figure 6.2(b)). The chip is then embedded in a block of epoxy resin for additional mechanical stability; steel tubes provide the inlets and outlet. Figure 6.2(c) shows the mixing of two fluorescently labeled protein solutions in a six-stage mixer at different flow rates.

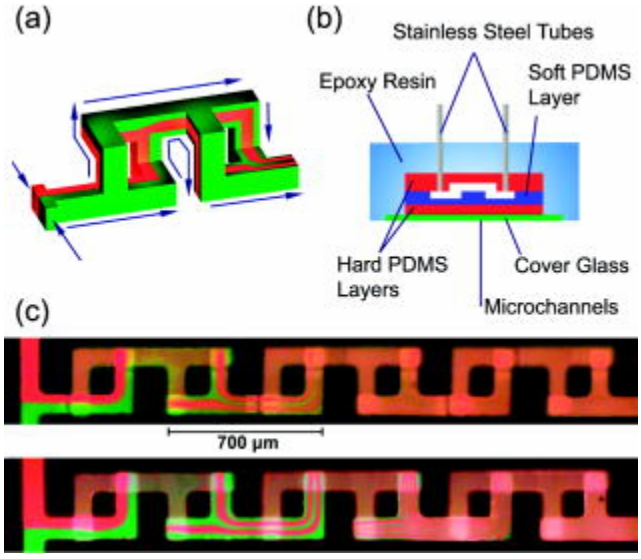

Figure 6.2 (a) Topologic structure for microfluidic mixing. Two different solutions are combined in a *T*-junction. The fluid flow is repeatedly split, rotated, and recombined as indicated by the arrows. (b) Schematic cross-section of an assembled mixing chip. The two principal elastomer layers are fused together and anchored with a third elastomer layer on a glass cover slip. The chip is embedded in a block of epoxy resin for additional mechanical stability; steel tubes provide the inlets and outlet. (c) Mixing of two fluorescently labeled protein solutions in a six-stage mixer at different flow rates. Figure reproduced with permission [Che04b].

Microfluidic systems utilizing channels, mixers and various other components have become more popular in industry and academia in the past several years. The ultimate goal of these devices is a lab-on-a-chip (LOC) that incorporates multiple aspects of laboratory work on a single microchip [Bee02].

6.2 Lab-on-a-chip prototypes

The development of lab-on-a-chip (LOC) technologies are currently of significant interest in the scientific community as these devices integrate multiple laboratory functions on a small chip (of only a few square centimeters) and are capable of handling fluid volumes down to less than pico liters. The discovery and development of microfluidic devices and their subsequent adaptability in various fields, ranging from Micro Electro Mechanical Systems (MEMS) to genomics and biological warfare defense, has fueled significant research in this area [Edw03].

LOC technologies, such as microfluidic biosensors are the focus of several research groups around the world. Most notably, Zaytseva and

coworkers have developed microfluidic biosensors for the detection of pathogens, including the dengue virus [Zay05a, Zay05b].

LOC devices provide several advantages, in addition to their compactness and low fabrication costs. Their low fluid volume consumption, due to the low internal chip volumes, lowers costs of expensive reagents as less sample fluid is used for diagnostics. Short mixing times, as a result of the short diffusion distances, and fast heating due to high wall surface to fluid volume ratios and small heat capacities allow for higher analysis and control speeds. LOCs afford better process control because of a faster response of the system and they are a safer platform for chemical, radioactive or biological studies because of the large integration of functionality and low stored fluid volumes and energies.

These devices do possess several disadvantages due to their compactness. For example, physical effects like capillary forces and chemical effects of channel surfaces become more dominant, making LOC systems behave differently and sometimes in more complex ways than conventional lab equipment. Also, detection principles may not always scale down in a positive way, leading to low signal-to-noise ratios. As these technologies are novel, there is a considerable amount of research that can be done on the viability of this technology for various applications, such as in biosensors.

APPENDICES

APPENDIX A
MFOLD SECONDARY STRUCTURE PREDICTION

A.1 RNA Sequence Generation Techniques

The following is a detailed description of the method used to generate two appropriate RNA substrate sequences for use in the biosensor experiment. An appropriate sequence contains the sequence complementary to the HHT5 hammerhead (5'- AUC CCG UCU GUU GUA C-3') followed by a random "tail" sequence of 23 bases. A primer for each substrate, complementary to the tail and composed of the random 23 base pair sequence, is also determined. Both sequences and their primers must not dimerize (the hybridization of two identical molecules) or cross-hybridize (the hybridization of the substrates or primers to one another). Therefore, once sequences for RNA A and RNA B are generated, with primers DNA A and DNA B, respectively, they are tested for structure formation under the interaction conditions listed in Table A.1.

Table A.1 Various interaction conditions tested to generate two suitable RNA sequences, A and B. The sequences and their primers must not dimerize or cross-hybridize and show appropriate binding specificities. "+" implies a non-binding spacer written as QQQ QQQ QQQ QQQ QQQ QQQ QQQ QQQ QQQ QQQ.

+	RNA A	RNA B	DNA primer A	DNA primer B
RNA A	RNA dimerization	RNA cross-hybridization	N/A	Binding specificity
RNA B		RNA dimerization	Binding specificity	N/A
DNA primer A			DNA dimerization	DNA cross-hybridization
DNA pimer B				DNA dimerization

To run the method, first download *mfold* onto an appropriate system [Zuk03]. Next, a series of files for testing in *mfold* must be generated by running evoltest.m in MatLab after changing any necessary parameters in the program. This program will call the function generate_sequences and analyze_data. Programs are compatible with MatLab version 6.5.

As written, evoltest begins by generating 100 (this was increased to 1000 later) random sequences containing 23 bases for the tail region of the RNA substate. To check for interactions, its calls generate_sequences which will generate a batch of test sequences for each random sequence. For each test sequence, *mfold* is run using analyze_data script, which collects relevant *mfold* output into a results file. The simulation is run at at 22°C with a 0.6 Na^{+2}

concentration. *mfold* generates a .ct file for each sequence it analyzes, from which the dG value and the number of bases involved in secondary structure formation (Nbases) can be extracted. A matrix is then generated including the sequence number, dG of most stable secondary structure generated for each test case, and Nbases. For each sequence, search the matrix for the test case with the smallest dG (worst loop) and sort using this parameter. The best 15 sequences (parent sequences) are chosen and considered "ok".

The parent sequences are then evolved by introducing a 2% probability for a base to undergo mutation. Sequences with a higher number of bases involved in loop formation are subsequently given a high chance for mutation. Each sequence is checked for uniqueness and a random sequence is generated for each non-unique sequence. The sequences are then allowed to breed equally; Nbreed = 6 times. This is done using a simple crossover technique where the first part of one sequence is joined to the second part of another sequence. Thus 105 new sequences are generated. Of these, we take all unique sequences, adding random sequences to ensure there are at least 100 offspring. These offspring undergo the same analysis as their parent sequences.

The parent sequences undergo 20 iterations of evolution and breeding before the best sequences are manually chosen from the final results. These sequences are manually tested using *mfold* and the process is repeated as necessary. The *mfold* results for the test cases of the two sequences that have been selected for the RC and NC substrate sequence after five batch jobs were run starting with 999 random sequences are given in Table A.2. Figure A.1 shows the expected extent of dimerization of the two substrates, while Figure A.2 shows the expected extent of dimerization of their corresponding DNA primers. Figure A.3 (a) and (b) show the predicted lack of binding specificity of the RNA substrates to their non-corresponding DNA primer and Figure A.4 shows the expected cross-hybridization of the two substrates.

Table A.2 Sequences chosen for the RC and NC substrate and primer sequences.

RC sequence	UAC CCG UCU GUU GUA C UC AUU CUA UCC UCC UUU CAC UUA GU
RC primer	ACT AAG TGA AAG GAG GAT A
NC sequence	AUC CCG UCU GUU GUA C UC CCA AAA AAA AAA AGC CGU AAA CU
NC primer	AGT TTA CGG CTT TTT TTT T

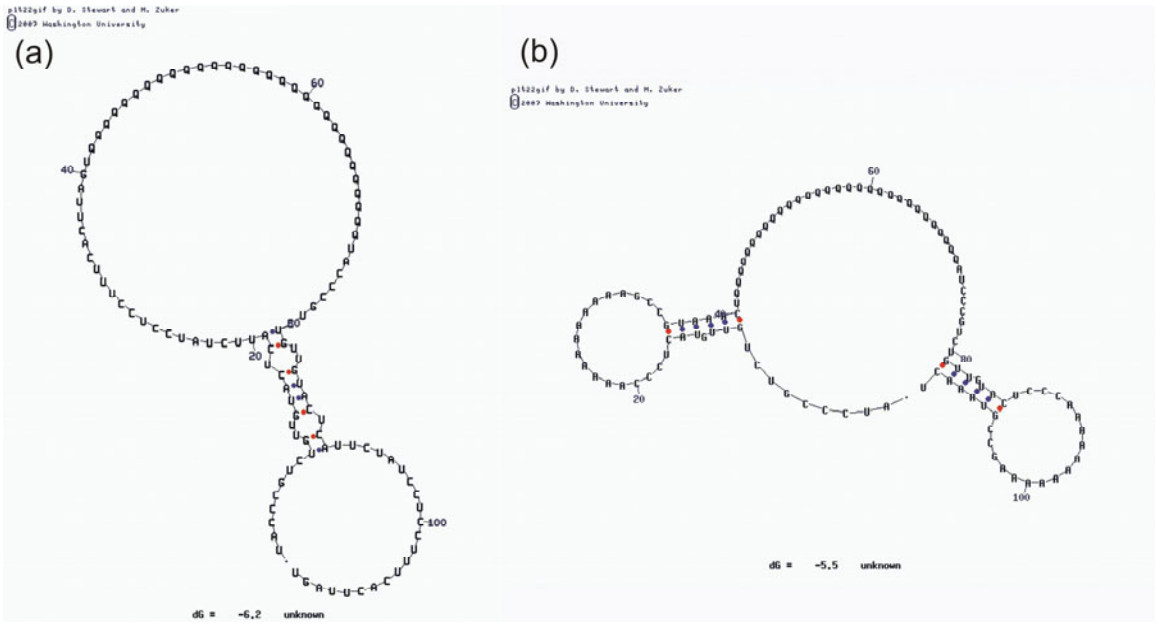

Figure A.1 Secondary structure prediction generated by *mfold* showing the potential of self-dimerization for (a) RC and (b) NC.

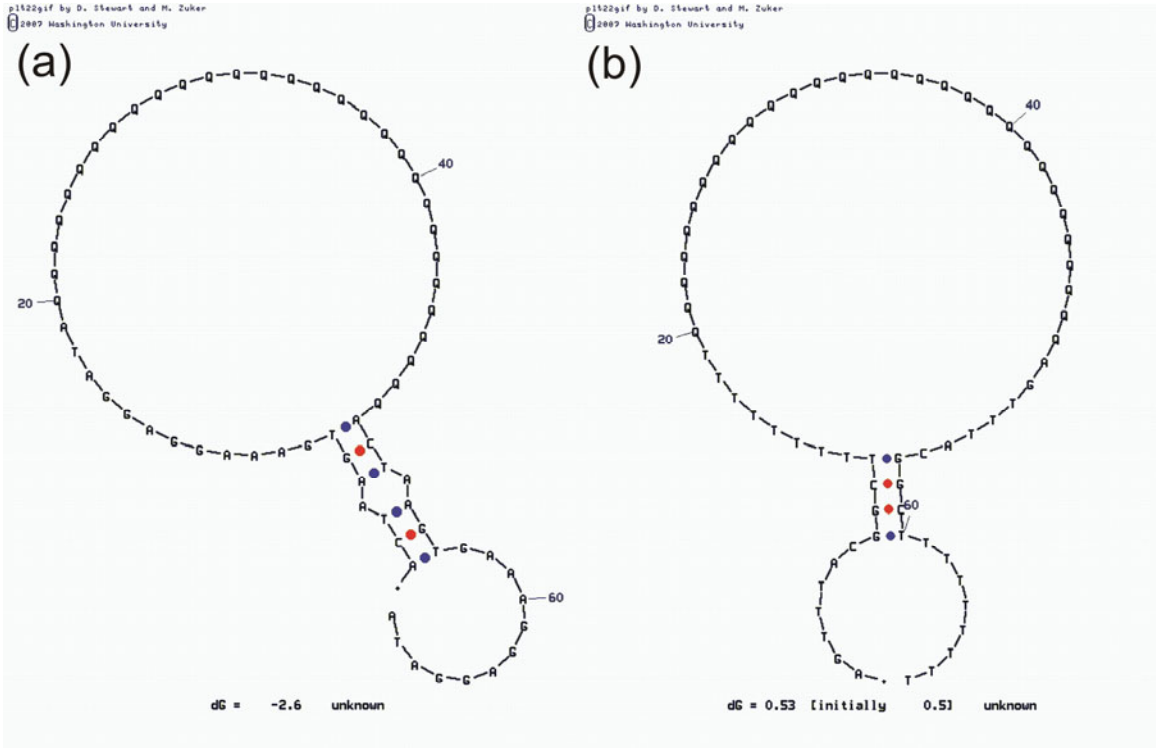

Figure A.2 Secondary structure prediction generated by *mfold* showing the potential of self-dimerization for the 19 nt DNA primers complementary to (a) RC and (b) NC.

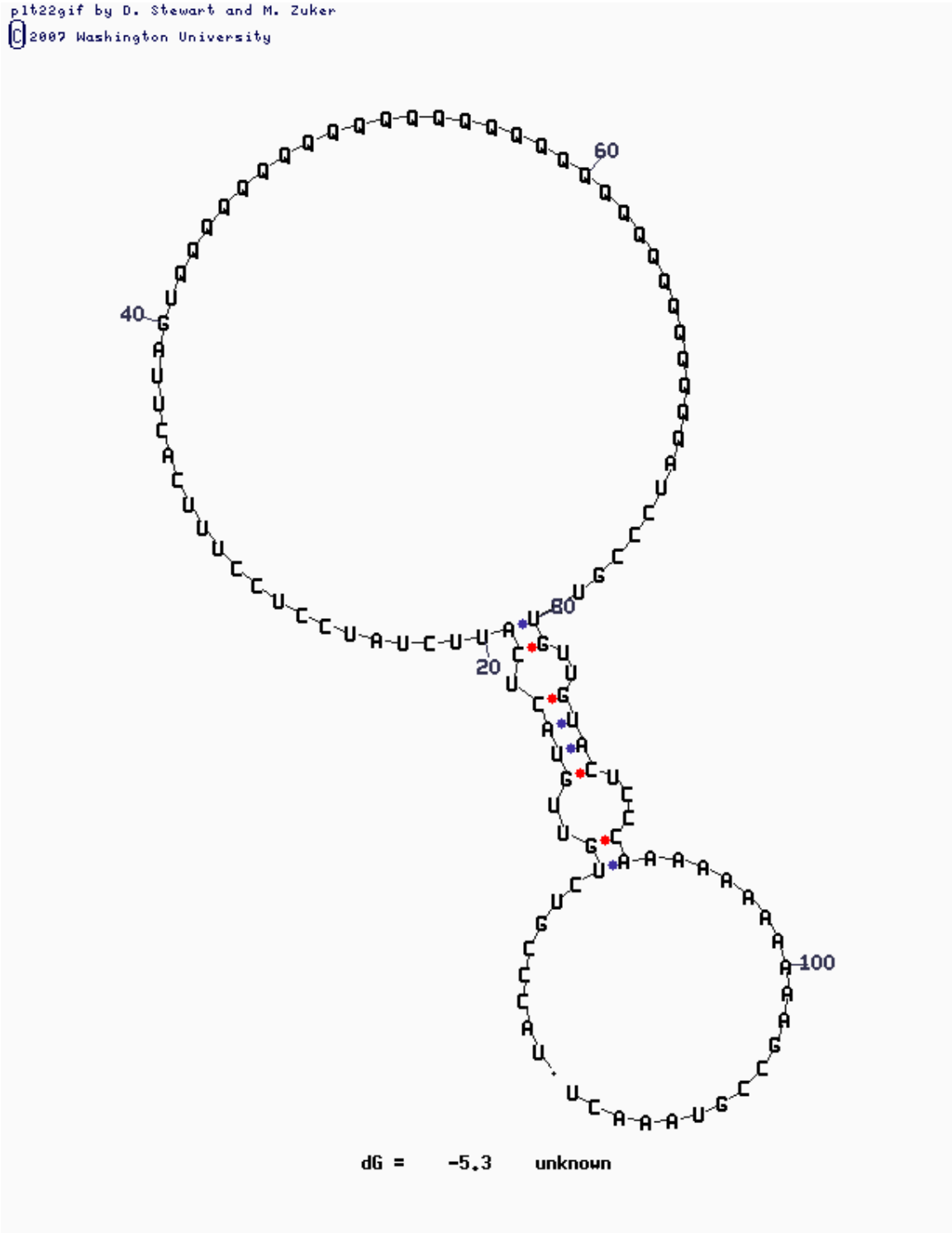

Figure A.3 Predicted cross-hybridization between RC and NC.

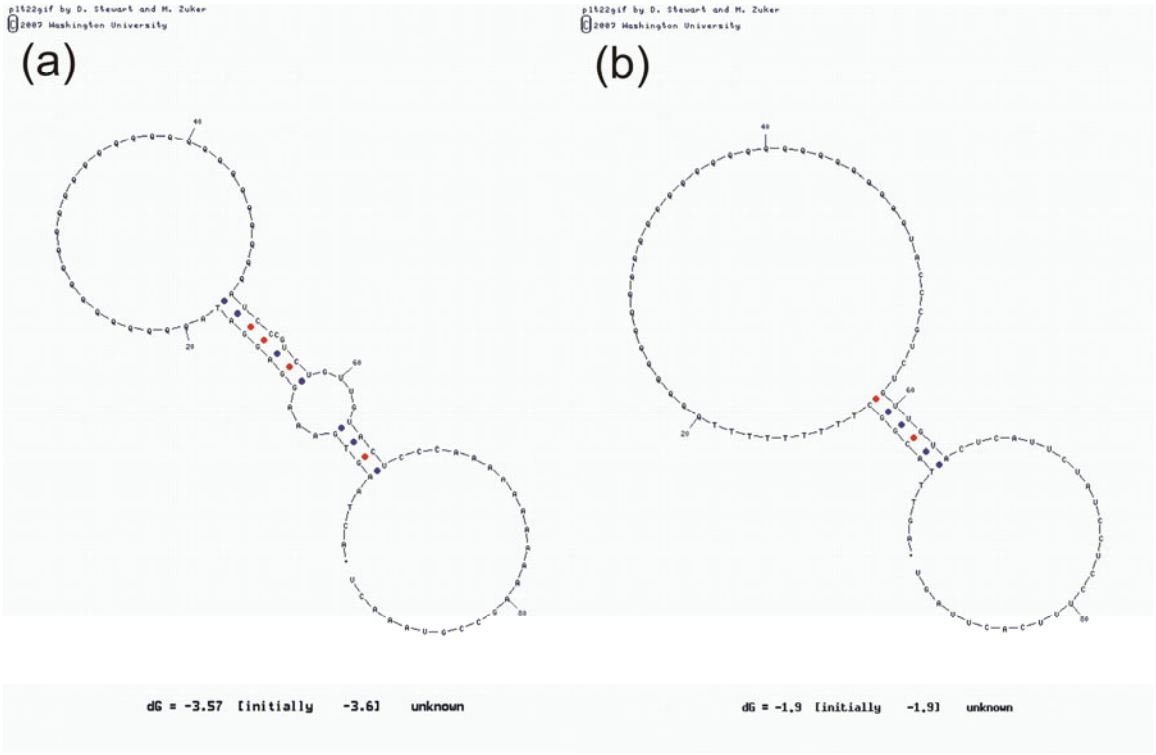

Figure A.4 Predicted cross-hybridization between (a) the RC DNA primer and NC RNA and (b) the NC DNA primer and RC RNA.

A.2 Scripts and Functions

A.2.1 Evolutionary Sequence Script evoltest.m

```
%========================================================================
% Written by Gerhard A Blab
%========================================================================

page_output_immediately=1;
page_screen_output=0;

rna_bases='AUCG';
seqlen=23; % sequence length
Nseq=100; % number of sequences to start with
Nbest=15; % number of sequences to keep in each iteration
Niter=20; % number of iterations to run
Nbreed=6; % number of offsprings of each sequence
Pmutate=0.02; % mutation likelihood (per base)
Pnomut=(1-Pmutate)^seqlen; % chance of no mutation
Ntests=5; % how many tests per sequence   NOTE: determined by generate_sequences!

no_loop_value=+42; % energy assigned if there is no looping at all

dna_complement('A')='T';dna_complement('U')='A'; dna_complement('Q')='Q';
dna_complement('C')='G';dna_complement('G')='C';

system('rm -rf batch??/*'); % clear last results
system('rm results*');

clear curr_SEQ;

for i1=1:Nseq
    seq_b=rna_bases(ceil(4*rand(1,seqlen)));
    curr_SEQ{i1}=seq_b; % generate random sequence for attachment
```

```
    sequences=generate_sequences(seq_b);
    Ntests=length(sequences);

    for i2=1:Ntests
        mkdir(sprintf('batch%02d',i2));
        fid=fopen(sprintf('batch%02d/seq_%04d_%c.seq', i2, i1, '@'+i2),'wt');
        fprintf(fid,'%s',sequences{i2});
        fclose(fid);
    end % for i2
end % for i1

clear pid;

%% run analysis
for i1=1:Ntests
    [in, out, thispid]=popen2('./analyze_data',sprintf('batch%02d',i1));
    pid(i1)=thispid;
    % start parallel analysis, only works in linux (octave)
end % for i1
for i1=1:Ntests
    waitpid(pid(i1)); % wait for analysis to finish
%   pclose(pid(i1));
end % for i1

clear run_best;

run_results=zeros(length(curr_SEQ),Ntests);
bound_res=zeros(length(curr_SEQ),seqlen);

for i1=1:Ntests
    fid=fopen(sprintf('batch%02d/results',i1));
    fid2=fopen(sprintf('batch%02d/results_bound',i1));
    res=[]; file_no=[]; b_res=[]
    while ~feof(fid)
        s=fgetl(fid); s2=fgetl(fid2);
        if length(s)>1
            res=[res;str2double(s(12:22))];
            file_no=[file_no;str2double(s(27:30))];
            b_res=[b_res; (s2((end-seqlen+1):end)=='X')];

            % read dG and file number (4 digits)
            % as well as which bases were involved in a structure
        end % if length
    end % while not EOF
    fclose(fid); fclose(fid2);

    for i2=1:length(curr_SEQ)
        ind=find(file_no==i2);
        if (length(ind))
            run_results(i2,i1)=min(res(ind));
            % the smaller, the better binding
            % so we are selecting the 'worst' case
            bound_res(i2,:)=sum(b_res(ind,:));
        else
            run_results(i2,i1)=no_loop_value;
        end % if length
    end % for i2
end % for i1

total_results=min(run_results')';   % the 'worst' of all tests

fid_res=fopen('results','wt');
fprintf(fid_res,'** results of sequence evolution\n\n');
fprintf(fid_res,'Run:   0\n\tsequences:\t%d\n',length(curr_SEQ));

[total_results,ind]=sort(total_results,'descend');
cutoff_val=total_results(Nbest);
ind2=(total_results>=cutoff_val);

fprintf(fid_res,'\t surviving sequences (%d, dG >= %5.2f)\n',sum(ind2),cutoff_val);
```

```
old_SEQ = curr_SEQ(ind(ind2));
bound_res=bound_res(ind(ind2),:);

for i1=1:sum(ind2)
    fprintf(fid_res,'\t\t%3d: %s (%.2f)\n',i1,char(old_SEQ{i1}),total_results(i1));
end % for i1

fprintf(fid_res,'\n');
fflush(fid_res);

for i_iter=1:Niter

    system('rm -rf batch??/*');     % clear last results

    fid_thisiter=fopen(sprintf('results_%03d',i_iter),'wt');

    %% winning sequence has a second go
    curr_SEQ=old_SEQ;

    %% but it mutates
    Nmut=0;
    Mutate=rand(length(curr_SEQ),1);
    index=find(Mutate<(Pnomut.*(sum(bound_res')'+1)));
        % the more bases forming structures, the more mutation

    for i1=1:length(index)
        index2=find(rand(seqlen,1)<(Pmutate.*(bound_res(i1,:)'+1)));
        Nmut=Nmut+length(index2);
        if (length(index2)>0)
            seq=curr_SEQ{index(i1)};
            seq(index2)=rna_bases(ceil(4*rand(1,length(index2))));
            curr_SEQ{index(i1)}=seq;
        end % if sum
    end % for i1

    curr_SEQ=unique(curr_SEQ);
    oldsize=length(curr_SEQ);
    newsize=oldsize+oldsize*Nbreed;     % number of new sequences
    N=length(curr_SEQ)+1; curr_SEQ{newsize}={};
        % copy and pre-allocate memory
        % make sure we don't have too much incest

    %% 'breeding' of sequences (crossover)
    disp(sprintf('\n\n***\niteration: \t %3d\nnew size:\t%3d\n***\n\n',i_iter,newsize))
    fprintf(fid_thisiter,'iteration:\t%3d\ninput size:\t%3d\n',i_iter, oldsize);
    fflush(fid_thisiter);

    for i1=1:oldsize
        index=ceil(oldsize*rand(1,Nbreed)); % randomly chose Nbreed

        seq1=curr_SEQ{i1};
        for i2=1:Nbreed
            X=round(seqlen/10*randn+seqlen/2);  % where is the cross-over
            if X<2, X=2; end
            if X>(seqlen-2), X=seqlen-2; end

            if (rand(1)>0.5)
                curr_SEQ{N}=char([seq1(1:X), curr_SEQ{index(i2)}((X+1):end)]);
            else
                curr_SEQ{N}=char([curr_SEQ{index(i2)}(1:X), seq1((X+1):end)]);
            end % if rand
            N=N+1;
        end % for i2
    end % for i1

    curr_SEQ=unique(curr_SEQ);  % don't run on identical sequences
    N=length(curr_SEQ)+1;

    %% add new ones if necessary
    if (length(curr_SEQ)<Nseq)
        Nmissing=Nseq-length(curr_SEQ);
```

```
    for i1=1:Nmissing
        curr_SEQ{N}=rna_bases(ceil(4*rand(1,seqlen)));
        N=N+1;  % new random sequence
    end % for i1
else
    Nmissing=0;
end % if (N<Nseq)

fprintf(fid_res,'Run: %3d\n\tsequences:\t%d\n',i_iter,length(curr_SEQ));
fprintf(fid_res,'\t\t(%d new, %3d mutations)\n',Nmissing, Nmut);

fprintf(fid_thisiter,'sequences:\t%3d\nmutations:\t%d\n',length(curr_SEQ),Nmut);
fflush(fid_thisiter); fflush(fid_res);

for i1=1:length(curr_SEQ)

    seq_b=curr_SEQ{i1};
    sequences=generate_sequences(seq_b);

    for i2=1:Ntests
        fid=fopen(sprintf('batch%02d/seq_%04d_%c.seq', i2, i1, '@'+i2),'wt');
        fprintf(fid,'%s',sequences{i2});
        fclose(fid);
    end % for i2
end % for i1

clear pid;
%% run analysis
for i1=1:Ntests
    [in, out, thispid]=popen2('./analyze_data',sprintf('batch%02d',i1));
    pid(i1)=thispid;
    % start parallel analysis, only works in linux (octave)
end % for i1
for i1=1:Ntests
    waitpid(pid(i1));   % wait for analysis to finish
%   pclose(pid(i1));
end % for i1

clear run_best;

run_results=zeros(length(curr_SEQ),Ntests);
bound_res=zeros(length(curr_SEQ),seqlen);

for i1=1:Ntests
    fid=fopen(sprintf('batch%02d/results',i1));
    fid2=fopen(sprintf('batch%02d/results_bound',i1));
    res=[]; file_no=[]; b_res=[];
    while ~feof(fid)
        s=fgetl(fid); s2=fgetl(fid2);
        if length(s)>1
            res=[res;str2double(s(12:22))];
            file_no=[file_no;str2double(s(27:30))];
            if (length(s2)>0)
                b_res=[b_res; (s2((end-seqlen+1):end)=='X')];
            else
                b_res=[b_res; zeros(1,seqlen)];
            end % if length s2
            % read dG and file number (4 digits)
            % as well as which bases were forming structures
        end % if length
    end % while not EOF
    fclose(fid); fclose(fid2);

    for i2=1:length(curr_SEQ)
        ind=find(file_no==i2);
        if (length(ind))
            run_results(i2,i1)=min(res(ind));
            bound_res(i2,:)=sum(b_res(ind,:));
            % the smaller, the better binding
            % so we are selecting the 'worst' case
        else
```

```
                run_results(i2,i1)=no_loop_value;
            end % if length
        end % for i2
    end % for i1

    total_results=min(run_results')';   % the 'worst' of all tests

    [total_results,ind]=sort(total_results,'descend');
    cutoff_val=total_results(Nbest);
    ind2=(total_results>=cutoff_val);

    fprintf(fid_res,'\t surviving sequences (%d, dG >= %5.2f)\n',sum(ind2),cutoff_val);
    fprintf(fid_thisiter,'surviving sequences (%d, dG >= %5.2f)\n',sum(ind2),cutoff_val);

    old_SEQ=curr_SEQ(ind(ind2));
    bound_res=bound_res(ind(ind2),:);

    for i1=1:sum(ind2)
        fprintf(fid_res,'\t\t%3d: %s (%.2f)\n',i1,char(old_SEQ{i1}),total_results(i1));
        fprintf(fid_thisiter,'\t\t%3d:
%s(%.2f)\n',i1,char(old_SEQ{i1}),total_results(i1));
    end % for i1

    fprintf(fid_res,'\n');
    fflush(fid_res);
    fclose(fid_thisiter);

end % for i_iter

fclose(fid_res);

%% End evoltest script
```

A.2.2 Function generate_sequences.m

```
%=========================================================================
% Written by Gerhard A Blab & K Jordan
%=========================================================================

function [varout]=generate_sequences(seq_target, seqlen)

rna_bases='AUCG'; seqlen=19;

dna_complement('A')='T';dna_complement('U')='A'; dna_complement('Q')='Q';
dna_complement('C')='G';dna_complement('G')='C';

if (nargin<2)
    seqlen=19;
elseif (isempty(seqlen))
    seqlen=19;
end % if isempty seqlen
if (nargin<1)
    seq_target=rna_bases(ceil(4*rand(1,seqlen)));
elseif (isempty(seq_target))
    seq_target=rna_bases(ceil(4*rand(1,seqlen)));
end % if isempty seq_target

seq_a_star='AUUCUAUCCUCCUUUCACUUAGU'; % found by trial (no binding to hammerhead)
seq_A=fliplr(dna_complement(seq_a_star)); % old DNA primer, v2

old RNA sequence
seq_hammer='AUCCCGUCUGUUGUAUYY'; % new RNA minus complement for B (19 bases)
seq_a=[seq_hammer,seq_a_star];
fillersequence=char('Q'*ones(1,25)); % spacer with non-base-forming elements

seq_B=fliplr(dna_complement(seq_target)); %  DNA complement of attachment
seq_b=[seq_hammer,seq_target]; %  generate full RNA strand (hammer head + attachment)
seq_b_dimer=[seq_b,fillersequence,seq_b]; % must not form homogenous dimers
```

```
seq_B_dimer=[seq_B,fillersequence,seq_B]; % ditto
seq_ab_cross=[seq_a,fillersequence,seq_b];% RNAs must not crosslink
seq_Ab_cross=[seq_A,fillersequence,seq_b];% RNA b must not attach to DNA A
seq_aB_cross=[seq_a,fillersequence,seq_B];% RNA a must not attach to DNA B

varout{1}=seq_b_dimer;
varout{2}=seq_B_dimer;
varout{3}=seq_ab_cross;
varout{4}=seq_Ab_cross;
varout{5}=seq_aB_cross;
```

A.2.3 Script: analyze_data

The following script calls on *mfold* to predict the secondary structure of the generated sequences at T=22˚C and 0.6 mM Na^{2+} concentration. All other conditions are left to default, but can be changed by modifying this script. This script copies out all of the dG values determined for the various sequences tested in *mfold* and saves to a results file. All *mfold* output .pdf files are then placed in a pdfs/ folder.

```
#!/bin/bash

export MFOLDBIN=/opt/mfold/bin
export MFOLDDAT=/opt/mfold/dat
export PATH=$PATH:$MFOLDBIN

cd $1
#if [-e results ;] then
        rm -rf results* pdfs
#end
mkdir pdfs
for i in *seq; do
        j=`basename $i .seq`
        mfold SEQ=${i} T=22 NA_CONC=0.6 &>/dev/null
        for k in *ct; do
                head --lines=1 $k >> results
               while read -r dummy dummy dummy dummy bound dummy; do
                       if [ ${bound:0:3} != 'seq' ]; then
                               if [ $bound -gt 0 ]; then
                                       echo -n X >> results_bound
                               else
                                       echo -n O >> results_bound
                               fi
                       fi
               done < $k
               echo >> results_bound
        done
        mv $i done_$i
       mv $j*pdf pdfs/
        rm $j*
done
```

A.2.4 Sequence Generator for Manual *mfold* Testing

```
%=========================================================================
% Program to generate files for MFOLD to analyze from "best" linker regions
% as determined by evoltest.m (run 05/16/06)
%
% Written by K Jordan
%=========================================================================

clear

ORS = 'UACCCGUCUGUUGUAUUCAUUCUAUCCUCCUUUCACUUAGU'; %Old RNA Sequence
OD = 'ACTAAGTGAAAGGAGGATA'; %Old DNA Sequence
R = 'AUCCCGUCUGUUGUAUYY'; %Region complementary to HHT5
x = 'QQQQQQQQQQQQQQQQQQQQQQQQQQQQQQ'; %Spacer

bases = 'UAGC'; N = 19;
compl('A')='T'; compl('U')='A';compl('C')='G';compl('G')='C';

NLR = 'CCAAAAAAAAAAAGCCGUAAACU'; %New linker region to test
%  NLR = 'CCAAAAAAAAAAAGCCGUAAAUU';

ND = fliplr(compl(NLR)); %New DNA primer

% Generate the sequence combinations to test
A = [R,NLR,x,R,NLR];
B = [R,NLR,x,OD];
C = [ORS,x,R,NLR];
D = [ORS,x,ND];
E = [ND,x,ND];

filename_A = sprintf('sequence_1_A.seq',i);
filename_B = sprintf('sequence_1_B.seq',i);
filename_C = sprintf('sequence_1_C.seq',i);
filename_D = sprintf('sequence_1_D.seq',i);
filename_E = sprintf('sequence_1_E.seq',i);

% Open file for each sequence
fidA = fopen(filename_A,'w');
fidB = fopen(filename_B,'w');
fidC = fopen(filename_C,'w');
fidD = fopen(filename_D,'w');
fidE = fopen(filename_E,'w');

% Write appropriate sequence to its own unique file
fprintf(fidA,A);
fprintf(fidB,B);
fprintf(fidC,C);
fprintf(fidD,D);
fprintf(fidE,E);

% Close files
fclose(fidA);
fclose(fidB);
fclose(fidC);
fclose(fidD);
fclose(fidE);

%end
```

APPENDIX B
PROTOCOLS

B.1 Labeling Modified RNA

For fluorophore-labeled RNA, take care to work in the dark (keep tubes wrapped in foil) as much as possible. This will limit the amount of photobleaching that can occur during the preparation stage. Also, store RNA in the -80˚C freezer. This will also increase its shelf-life.

B.1.1 RNA Deprotection

1) Add 800µl triethylamine trihydrofluoride (TEA 3HF) and 200µl dimethyl formamide (DMF). Vortex.
2) Shake at RT for 20-24hours.
3) Quench reaction with 200µl ddH2O.
4) Transfer to Falcon tube and add 5ml 1-butanol. Mix and chill the solution at -80˚C for at least 45min. This can safely be left overnight.
5) Centrifuge at 3000rpm for 10min. Decant.
6) Dry RNA in SpeedVac, taking care to not dry out too much.

B.1.2 15% Polyacrylamide Gel Electrophoresis

Next, the RNA must be gel purified. The following protocol includes steps for both analytical and purification gel electrophoresis.

1) Set up gel plates (use the short plates for analytical gel and long plates for purification).
2) Add:

	15% Gel		20% Gel	
	Analytical	Purification	Analytical	Purification
Urea	24.0 g	48.0 g	24.0 g	48.0 g
40% Acrylamide	18.75 ml	37.50 ml	25.0 ml	50.0 ml
5xTBE	16.25 ml	32.5 ml	10.0 ml	20.0 ml

3) Microwave 20 sec. Stir until dissolved and cooled.
4) Add 90µl each 50% APS and TEMED for analytical gel, 130 µl each for a gel purification.
5) Pour gel MMEDIATELY and let set.
6) Re-suspend RNA in ddH2O and determine concentration.

7) For an analytical gel, extract 4µg into eppendorf tube. For purification, take half of the RNA stock. Dry down excess and store in the -70°C.
8) Set up the gel, remembering to pre-run (at 25W for analytical, 45W for purification).
9) Add equal volume of appropriate dye. For the analytical gel, use FA-LB + BPB + XC. This will give Bromophenol Blue (at about 8 bases for 20% gel) and Xylene Cyanol (at about 38 bases for 20% gel) bands. For the gel purification, use FA-LB +BPB, that only contains Bromophenol Blue, so as to not contaminate the RNA with dye.
10) Place in 90°C heat bath 2 min then ice bath 10min.
11) Load RNA onto gel. Cover. Let run 1-2 hours (or until there is sufficient dye separation).
12) Disassemble gel.
13) For analytical only: Leave gel in Ethinium Bromide solution 10-15min. Recycle Ethinium Bromide. Wash. Leave in water 15-20min to quench the reaction.
14) View results under UV light source. Photograph.

B.1.3 RNA Extraction Post Gel Purification

1) Cut out RNA band from gel. Chop and load into column. Fill with 4-6ml 1mM EDTA. Use just enough buffer to cover the gel bits. Tumble at 4°C overnight.
2) Extract buffer into Falcon tubes.
3) Chloroform Extract:
   a) Add equal volume of bottom chloroform layer. Mix. Centrifuge at 9000rpm 5-10min.
   b) Extract supernatant (top layer).
   c) Add about 5µl of 100mM ATP
4) Ethanol Precipitate:
   a) Add 10% total volume of 3M NaOAc (Sodium Acetate)
   b) Add 3x volume cold Ethanol.
   c) Leave in -70°C at least 3 hours (can sit overnight). Centrifuge tubes at 9000rpm for 20 min. Pipette off EtOH.
5) Dry down pellet(s) and store in -70°C.

B.1.4 HPLC Purification

1) Re-suspend RNA in about 105µl. Only 100µl can be loaded into the HPLC for purification. The excess 5µl should be extracted and diluted in ddH_2O to total volume of 100µl and injected for the analytical run.
2) Start up HPLC:
   a) Make entry in HPLC logbook.
   b) Check the waste container is not full and that there is plenty of Buffers A and B. Also check that Buffer A is free from contamination.
   c) Turn on the power strip behind the instrument and then turn on the computer.

d) Open the release valve (it should be in the closed position when not in use).
e) Ramp the pumps to 50% B at 6ml/min over 1 min ramp. Watch the pump line (from the release valve) and continue flow until the bubbles disappear (takes about 5 min and the bubbles never totally disappear).
f) Ramp the pumps to 100% B at 3ml/min over 1 min for about 30 sec.
g) Stop the pumps and close the release valve.

3) Run the method STARTUP (run time is 31min). The column is now ready for an injection.
4) To run a sample:
   a) Activate your method/gradient from the file menu (C_8 for Cy5+3 or reallyslowGradient or C_{18} for long_doubly_labeled_RNA work well depending on which column, C_8 or C_{18} is in use).
   b) First do an analytical run:
   c) Click the "Run" command in the system control software.
   d) Put the injection valve in the "Load" position.
   e) Clean the injection syringe with ddH_2O 4 times before loading your sample
   f) Load sample, injecting syringe until you feel the second stop. Turn the valve to "Inject"
   g) Clean the injection syringe and the injection valve (while still in the "Inject" position) with ddH_2O.
   h) Wait 80min for the method to finish. This is a good time to load the fraction collector for the preparative run.
5) Wait 10min between multiple runs to ensure system returns to initial state.
6) From the graph output from the analytical run, determine the peak(s) corresponding to the RNA and calculate the appropriate collection time and number of fractions to collect. (A 42-mer singly labeled with Cy5 is expected around 30min, while a doubly labeled 42-mer is expected around 32min. Collection between 26min and 34:16min in 24 fractions (20 sec each fraction and a 16 sec delay) should be sufficient.)
7) The preparative run (the purification run):
   a) Load the fraction collector with eppendorf tubes, if not already done. Remember that the collection pattern is serpentine.
   b) Program the fraction collector:
      i) Type = time windows,
      ii) Rack Type = microtubes,
      iii) Pattern = standard,
      iv) Fraction by time,
      v) Fraction = 20sec,
      vi) Flow Delay = 16sec,
      vii) Nonpeak/Window = divert,
      viii) Restart = none.
   c) The window should show RUN over the "A" button before loading the sample.
   d) As above, click the "Run" command in the system control software and put the injection valve in the "Load" position.

e) Load sample, injecting syringe until you feel the second stop. Turn the valve to “Inject”. Simultaneously hit “Start” on the fraction collector.
f) Clean the injection syringe and the injection valve (while still in the “Inject” position) with ddH_2O.
g) Wait 80min for the method to finish, collecting fractions when necessary.

8) Wait 10min between multiple runs to ensure system returns to initial state.
9) To shut down the HPLC:
   a) Activate and run the method SHUTDOWN. This will take 21min.
   b) Complete the HPLC logbook entry
   c) Shut down the computer, and then flip off the power strip behind the instrument.
   d) DO NOT open the release valve.
10) NEVER open the release valve when the column is under pressure.

B.1.5 Removal of Triethylamine from HPLC Purification Pre Labeling

1) Dissolve RNA in 100μl ddH_2O and chloroform extract one to two times.
2) Ethanol precipitate.
3) Dry in speedvac

B.1.6 Cy3 Labeling Post HPLC Purification

1) Combine:
   a) 14μl DMSO, containing 200μg dye succinimidyl ester (Cy3 Mono-Reactive dye pack)
   b) 75μl 0.1M $Na_2B_4O_7$-HCl, pH 8.5 (or 10μl 1M $NaHCO_3/NaCO_3^-$, pH 8.3)
   c) 11μl ddH_2O containing up to 100μg oligonucleotide
   d) Fill with ddH_2O to total volume of 100μl.
2) Incubate at RT in the dark overnight or for 16 hours.
3) EtOH precipitate.
4) HPLC purify.

B.2 Modified DNA Protocol

DNA is much easier to work with than RNA. It can be stored at -20°C and does not need to be dried. There is also no deprotection protocol to be followed here. However, the DNA must be desalted before use.

1) Desalt using a NAP-10 column (DNA with a 5’ Cy3 label):
   a) Note that NAP-5 or NAP-10 is prepackaged Sephadex G-25 column (5ml bed volume) from Pharmacia for desalting and buffer change.
   b) Rinse with 5 column volumes of buffer of interest (for desalting use ddH2O)
   c) Apply 0.5ml of sample (for NAP-10, use 1ml).
   d) Elute with 1ml of buffer of interest or water and collect (for NAP-10 use 1.5ml).
   e) Recover column by rinsing with 5 column volumes of buffer/ddH2O.

2) For 5' biotinolated DNA, dissolve in ddH_2O.
3) Measure the concentration.
4) Run an analytical gel to check purity. Most likely the gel will not show degradation so purification (gel and HPLC) will not be necessary.

B.3 In Vitro Transcription Protocol for HHT5 Hammerhead

1) Prepare the reaction solutions:
   a) 4X Reaction Buffer (total V=2500μl):
      i) 1200μl 1M HEPES-KOH pH 7.5
      ii) 300μl 1M $MgCl_2$
      iii) 20μl 1M Spermidine
      iv) 400μl 1M DTT
      v) 100μl 1% Triton X-100
      vi) 480μl ddH_20
   b) Reaction Solution (total V=1106.25μl):
      i) 131.25μl ddH_2O
      ii) 375μl 4X Reaction Buffer
      iii) 300μl 40% PEG
      iv) 150μl each 3μM concentrated top and bottom strands
2) Heat reaction solution in 90˚C heat bath for 3min then cool on ice.
3) Combine:
   a) 66.25 μl ddH_2O
   b) 1106.25 μl of reaction solution
   c) 60 μl of each 100mM ATP, UTP, CTP, GTP
   d) 37.5 μl PPi 0.1 u/μl (Pyrophosphatase inorganic)
   e) 50 μl T7 Polymerase (T7 His) 0.5mg/ml)
4) Heat for at least 3 hours at 37˚C (This can stay overnight)
5) Add 160μl 0.5M EDTA to stop reaction (This can stay in the -20˚C overnight.)
6) Phenol/Chloroform extract:
   a) Add 1.5ml phenol/chloroform
   b) Vortex then centrifuge for 15min
   c) Transfer top layer to new tube
   d) Add 1.5ml chloroform
   e) Vortex then spin to separate layers
   f) Transfer top layer to new tube
7) Concentrate with centricon column 3000 – this will take 2-4 hours
   a) Centrifuge 4000-6500G at 4˚C until volume is low enough to load on a gel (200-400μl)
   b) For ~2min at 300-1000G at 4C to collect RNA/DNA into the cap
8) Prepare and run (small) 20% denaturing gel to separate full transcripts:
   a) Load samples with BPB+XC and run at 25W
   b) Allow XC to run to the bottom of the gel (2-3 hours)
9) Recover the transcribed RNA:
   a) Tumble in 1mM EDTA

b) Chloroform extract with 3ml chloroform twice
c) EtOH precipitate
d) Dry and resuspend in ddH_2O

B.4 Sample Preparation for Single-Molecule TIR-FRET Experiments

1) Buffers needed:
   a) Standard Buffer:
      i) 50 mM Tris-HCl pH 7.5
      ii) 20 mM $MgCl_2$
      iii) dilute to 10ml
   b) Standard Buffer + 10%Glucose (Glucose Buffer):
      i) 50 mM Tris-HCl pH 7.5
      ii) 10 mM $MgCl_2$
      iii) 1 g Dextrose
      iv) dilute to 10ml & sterile filter
   c) Sodium Buffer:
      i) 50 mM Tris-HCl pH 7.5
      ii) 200 mM NaCl
   d) Oxygen Scavenger System (OSS):
      i) 12.5 μl Catalase
      ii) 50 μl equivalent volume Glucose Oxydase
      iii) 100μl of Buffer containing 50 mM Tris-HCl and 50 mM NaCl, pH 7.5
      iv) Mix lightly with pipette (do not shake) and do not to introduce air bubbles
   e) OSS Buffer:
      i) 192 μl Glucose Buffer
      ii) 2 μl OSS
      iii) 4 μl βME (Beta-mercapto-ethanol)
2) Slide Preparation:
   a) Cut pipette tips to the appropriate size
   b) Pipette 50μl BSA into channel. Take care to remove pipette tip without introducing air into the channel.
   c) Seal each hole with drop of ddH_2O and let sit for 5min.
   d) In the meantime, prepare Solution A:
      i) 1 μl R_Cy3_Cy5
      ii) 0.411 μl D_19_B
      iii) 7.60 μl Standard Buffer
      iv) 1 μl βME
   e) Let sit in 90C bath for 30sec
   f) Let cool to RT for about 5min.
   g) Inject:
      i) ~80 μl Sodium buffer
      ii) ~80 μl Streptavidin
   h) Seal with a drop of ddH_2O and wait 5 min.
   i) In the meantime, prepare 5 nM solution (Solution B):

i) 2 μl Solution A
ii) 4 μl βME
iii) 194 μl Standard Buffer

3) Set up calibration laser as per Walter Lab protocol
4) Prepare 100 pM solution (Solution C):
   i) 4 μl Solution B
   ii) 4 μl βME
   iii) 192 μl Standard Buffer
5) Inject slide with ~80 μl Standard Buffer and let sit
6) Inject ~80 μl Solution C
7) Start single molecule measurements as per Walter Lab protocol
8) Inject ~100 μl Ribozyme Buffer (OSS+R_z):
   i) 250 nM HHT5
   ii) Fill to 100 μl with OSS Buffer
9) Continue single molecule measurements, including injection of analyte buffer(s) and analyze as per current Walter Lab protocols.

B.5 Spectrophotometer Calculations

To determine the concentration of an oligo, specifically of a 1/100 dilution of RNA, the following equations are used:

$$c' = 3.7A \tag{5.4}$$

$$c = \frac{c'}{330n} \times 10^6 \tag{5.5}$$

where *c'* = concentration of RNA (μg/μL), *c* = molar concentration of RNA (μM), *A* = (absorbance at 260 nm – absorbance at 320 nm), *n* = number of bases, 330 = average molecular weight of base, and 3.7 = estimated multiplier for RNA (for single-stranded DNA, use 4.0).

The molar concentration (M) of Cy3 and Cy5 of a 1/100 dilution is given by

$$c = \frac{A}{\varepsilon b} \times 100 \tag{5.6}$$

where *c* = Concentration of fluorophore (M), *A* = Absorbance (at 550 nm for Cy3 and at 650 nm for Cy5), ε = Molar extinction coefficient (150000 /M/cm at 550 nm and 250000 /M/cm at 650 nm), and *b* = Path length, known to be 1 cm.

B.6 Preparation of Slides for Microarray Printing

The spotter uses split quills to print the slides. Up to 8 constellations (array of spots) can be printed on a normal 25 x 75 mm slide using 8 quills. For one constellation, only one quill is necessary.

1) Using a 384 well plate, fill the wells with 3μl of oligo/spotting solution.

2) The printing order is as follows:
   a) For the first quill (or one quill):
      i) A1, A2, B1, B2, A13, A14, B13, B14, C1, C2, D1, D2, C13, C14, D13, D14, E1, E2, etc...
   b) For the remaining quills, just shift over:
      i) For quill 2: A3, A4, B3, B4, A15, A16...etc.
      ii) For quill 3: A5, A6, B5, B6, A17, A18...etc.
      iii) For quill 4: A7, A8, B7, B8, A19, A20...etc.
3) Unfortunately, there is no repeat type functionality with the printer, thus, for every repeated spot, you will need 3µl volume in the 384 well plate.

B.7 Microarray Sample Preparation Protocol

1) First, ensure the following buffers are available.

   a) Buffer A (Blocking Buffer):

Final Composition	Volume	Initial Composition
5X SSC	1.25 ml	20X SSC
0.5% SDS	0.05 ml	10% SDS
0.1 mM EDTA	1.0 ml	10 mM EDTA
1% BSA	0.05 g	BSA
Fill to 5ml ddH_2O	Fill to 5.0 ml	ddH_2O

   b) Buffer C (Hybridization Buffer):

Final Composition	Volume to add	Initial Composition
50% formamide	40 ul	formamide
5X SSC	20 ul	20X SSC
0.1% SDS	0.8 ul	10% SDS
1/40 herring sperm DNA	2.0 ul	herring sperm DNA
1/10 RNA substrate	8.0 ul	RNA substrate
Fill to 90ul ddH_2O	19.2 ul	ddH_2O

   c) Wash Buffers:

Buffer	Composition	20X SSC	10% SDS	ddH2O	Final V
I	1X SSC 0.2% SDS	1.0 ml	400 ul	18.6 ml	20 ml
II	0.1X SSC 0.2% SDS	100 ul	400 ul	19.5 ml	20 ml
III	0.1X SSC	100 ul	0	19.9 ml	20 ml
IV	ddH2O	0	0	20 ml	20 ml

2) Prepare Buffer A and stamped slides for blocking (~30 min)
3) Incubate Buffer A at 42˚ for 30min
4) Label stamped slides to be used with diamond knife, carefully indicating locations of constellations to be used as they will no longer be visible post-blocking.
5) Place hybridization (HybriWell or homemade) chamber around constellations.
6) Blocking (~30 min)
   a) Spot Buffer A onto constellations, cover with coverslip.
   b) Let sit in a humid environment at 42˚C for 30 min.
7) Washing step (~10 min)

a) Place slides in Coplin jar filled with H_2O and shake for 1-2 min.
b) Repeat 4 times.
c) Place slides in Coplin jar filled with isopropanol and shake for 1-2 min.

8) Let slides air dry (Can lightly flow air over slides to speed up process).
9) Prepare for hybridization (~5 min)
   a) Make small hybridization chambers out of double-sided taped and place around constellations (this is to hold hybridization buffer in place and isolate the constellations for the duration of hybridization).
10) Add DNA and RNA to Buffer C as appropriate
11) Heat Buffer C to 90˚C for 2 min
12) Cool on ice for ~ 30 sec.
13) Hybridization
   a) Spot Buffer C as appropriate, ensuring there is enough liquid that evaporation will not be a problem.
   b) Let sit in a dark, humid environment at RT for hybridization time
      i) RNA-DNA hybridization time: 6 hours
      ii) DNA-DNA hybridization time: 1.5 hours
14) Post-hybridization (~30 min)
   a) Leave coverslips in wash buffers I, II, III, and IV for 5 min each while agitating.
   b) Dry slides and store in dark slide box in 4˚C
15) Create flow cell around constellations
   a) Cut out pattern for flow cell using parafilm
   b) Cover with a coverslip that has been washed (and plasma cleaned – optional) to ensure it is hyrophyllic
   c) Use a soldering iron to melt the parafilm, securing the coverslip
16) Introduce appropriate measurement buffer
   a) Standard buffer + HHT5 hammerhead (+ theophylline)
17) Close off inlet and outlet of flow cell using vacuum grease to ensure experimental conditions do not change during scanning.
18) Image slides using microarray scanner
   a) Appropriate starting settings:
      i) Focus: -50
      ii) PMT gain: 80%
      iii) Power: 75%
      iv) Resolution: use 50μm for focusing and calibrating, increase to 10μm to take data
   b) Adjust settings to ensure signal is not saturated

B.8 Spin Coating a 30μm Layer of PDMS Onto a Coverslip

This protocol calls for a 10:1 ratio of A:B where A is PDMS (RTV615A) and B is the curing agent (RTV615B). This ratio can be varied from 10:1 to 10:4

depending on the layer properties desired. These volumes yield approximately 16 coated 18mm^2 coverslips.

1) Weigh out materials as follows and mix well:
   a) Pour 10g of A into a weighboat
   b) Zero scale
   c) Add 1g of B (for a 10:1 ratio). Mix well with stir stick.
2) Degas the mixture, being careful to not to let it overflow. Do not degas for more than 45min or the PDMS will start to set.
3) If mixed too well, large bubbles will form. If this happens, let off on the vacuum and lightly shake the chamber until the bubbles pop, then turn the vacuum back on.
4) Make sure the oven is on at 80˚C.
5) When bubbles are mostly gone, close chamber valve and remove from lines.
6) Ensure spin coater vacuum lines are open before turning on the spin coater. Run the spin coater 3 times for several seconds to warm it up.
7) Slowly release valve on vacuum chamber and allow to come to equilibrium
8) Center the coverslip on the peg, deposit a drop of PDMS mixture onto the coverslip and start spin cycle, using Recipe 1 settings for a 30μm layer.
9) Recipe 1:
   a) 10 sec at 500rpm to spread out the PDMS
   b) ~45 sec at 2000rpm to spin it down
10) Leave coated coverslips in oven for approximately 30 min to cure.
11) Use razor blade or scalpel to cut desired channels into PDMS.

Note that the thickness of the PDMS near the center of the coverslips is approximately 30μm but along the edges, there is a raised lip and the thickness is about 60-120μm. Normally, this raised area can be cut off, but I exploit this and use it as a lifterslip.

B.9 Plasma Cleaning of Coverslip

The surface of PDMS spin-coated slides will be hydrophobic and slides must be plasma cleaned before use in a fluid environment. The following is the protocol used with the Harrick PDC-32G Basic Plasma Cleaner (does not include the PlasmaFlo Gas Flow Mixer). If the unit has not been in use recently, moisture and air contaminants may accumulate in the chamber, preventing the vacuum from reaching appropriate levels for plasma generation. Therefore, cleaning the vacuum chamber may be necessary. Otherwise, skip step 1.

1) Clean the vacuum chamber
   a) Carefully remove glass chamber from cleaner housing by first unscrewing stopper at the back of the unit.
   b) Wash thoroughly with isopropanol.
   c) Dry and replace chamber. Attach vacuum line and make sure vacuum pump main switch is on.
   d) Turn on vacuum and pump down for approximately 45 min.

    e) Turn off vacuum and return to atmosphere. The unit is now ready to be used as a cleaner.
2) Make sure vacuum pump is attached to the plasma cleaner.
3) Insert samples to be cleaned into the chamber. Remember that only the side facing up will be cleaned, so using a simple sample holder is advantageous.
4) Turn on vacuum and pump down for 10-15 min.
    a) Hold chamber door in place (make sure release valve is fully closed) and flip the red vacuum switch on (This is the switch above the door to the pump, not the switch on the plasma cleaner.)
5) Generate and sustain plasma.
    a) Turn all switches on the plasma cleaner to the “On” position and turn the RF frequency to “High”.
    b) After about 10 seconds, you should see a purple glow coming from the coil in the chamber.
    c) Begin to very slowly open the release valve so that the glow is brightest (magenta).
    d) Open and close this valve to maintain maximum plasma brightness for at least 30 sec (I do 1 min).
6) Turn off all switches and slowly release air valve to return to atmosphere.
7) Cover chamber to minimize contaminants that may affect cleaner performance.

Note: Surface properties are only guaranteed to remain altered due to plasma cleaning for about 30 min, depending on environmental factors such as humidity and air purity. This is important for microfluidic chip generation because PDMS will revert to its hydrophobic properties. However, for use in the microarray, only the glass surface is of concern and glass will maintain sufficient hydrophilicity for an indefinite period after cleaning.

REFERENCES

Abb07 Abbott Laboratories Diagnostic Division, www.abbott.com

Ame07 Amersham Biosciences, www.amersham.com

Ans00 R. M. Anson, E. Hudson, V. A. Bohr, *Mitochondrial endogenous oxidative damage has been overestimated*, FASEB J **14**, 355 (2000).

Axe01 D. Axelrod, *Total Internal Reflection Fluorescence Microscopy in Cell Biology*, Traffic **2**, 764 (2001).

Bee02 D. J. Beebe, G. A. Mensing, and G. M. Walker, *Physics and Applications of Microfluidics in Biology*, Annu. Rev. Biomed Engin. **4**, 261 (2002).

Beh02 B. Behesti, P.C. Park, I. Braude, J.A. Squire, *Microarray CGH,* Molecular Cytogenetics: Protocols and Applications (Humana Press, New Jersey, 2002).

Ben00 A. Benkert, F. W. Scheller, W. Schössler, C. Hentschel, B. Micheel, O. Behrsing, G. Scharte, W. Stöcklein, A. Warsinke, *Development of a Creatinine ELISA and an Amperometric Antibody-Based Creatinine Sensor With a Detection Limit in the Nanomolar Range*, Anal. Chem**. 72**, 916 (2000).

Ben05 J. A. Benn, J. Hu, B. J. Hogan, R. C. Fry, L. D. Samson, T. Thorsen, *Comparative Modeling and Analysis of Microfluidic and Conventional DNA Microarrays*, Annal. Biochem. **348**, 284 (2006).

Ber01 C. Berens, A. Thain, R. Schroeder, *A Tetracycline-Binding RNA Aptamer*, Bioorg. & Med. Chem. **9**, 2549 (2001).

Bie94 F. F. Bier, R. Jockers, R. D. Schmid*, Integrated Optical Immunosensor For s-triazine Determination: Regeneration, Calibration and Limitations*, Analyst **119**, 437 (1994).

Bre97 R. R. Breaker, *In Vitro Selection of Catalytic Polynucleotides*, Chem. Rev. **97**, 371 (1997).

Bre02 R. R. Breaker*, Engineered Allosteric Ribozymes as Biosensor Components*, Curr. Opin. Biotech. **13**, 31 (2002).

Bro99 P. O. Brown and D. Botstein, *Exploring the New World of the Genome with DNA Microarrays*, Nat. Genet. **21**, 33 (1999).

Bru99 J. G. Bruno and J. L. Kiel, *In Vitro Selection of DNA Aptamers to Anthrax Spores with Electrchemiluminescence* Detection, Biosens. Bioelectron. **14**, 457 (1999).

Cec81 T. R. Cech, A. J. Zuag, P. J. Grabowski, *In Vitro Splicing of the Ribosomal RNA Precursor of Tetrahymena: Involvement of a Guanosine Nucleotide in the Excision of the Intervening Sequence*, Cell **27**, 487 (1981).

Cec92 T. R. Cech, *Ribozyme Engineering,* Curr. Opin. Struct. Biol. **2**, 605 (1992).

Cer02 L. Cerchia, J. Hamm, D. Libri, B. Tavitian, V. de Franciscis, *Nucleic Acid Aptamers in Cancer Medicine,* FEBS **528**, 12 (2002).

Che03 H. Chen, D. Acharya, A. Gajraj, J.-C. Meiners, *Robust Interconnects and Packaging for Micofluidic Elastomer Chips*,, Anal. Chem. **75**, 5287 (2003).

Che04a H. Chen and J.-C. Meiners, *Topological Structure for Microfluidic Mixing*, Application for U.S. and international utility patents pending. (2004).

Che04b H. Chen, and J.-C. Meiners, *Topologic Mixing on a Microfluidic Chip*, Applied Physics Letters **84**, 2193 (2004).

Che06 W. Chen and D. Foran, *Advances in Cancer Tisue Microarray Technology: Towards Improved Understanding and Diagnostics,* Analytica Chemica Acta **564**, 74 (2006).

Cho06 E. J. Cho, J. R. Collet, A. E. Szafranska, A. D. Ellington, *Optimization of Aptamer Microarray Technology for Multiple Protein Targets,* Analytica Chemica Acta **564**, 82 (2006).

Clo97 B. Clouet d'Orval and O. C. Uhlenbeck, *Hammerhead Ribozymes with a Faster Cleavage Rate,* Biochem. **36**, 9087 (1997).

Col05 J. R. Collet, E. J. Cho, J. F. Lee, M. Levy, A. J. Hood, C. Wan, A. D. Ellington, *Functional RNA Microarrays for High-Throughput Screening of Antiprotein Aptamers,* Anal. Biochem. **338**, 113 (2005).

Cos05 J. Costello, M. Sentmanat, K. Bogart, *DGRC Hybridization Trouble Shooting Guide* (Indiana University, Bloomington, 2005).

DeR96 J. DeRisi, L. Penland, P. O. Brown, M. L. Bittner, P. S. Meltzer, M. Ray, Y. Chen, Y. A. Su, J. M. Trent, *Use of a cDNA Microarray to Analyse Gene Expression Patterns in Human Cancer,* Nature Genet. **14**, 457(1996).

DeS98 A. DeSaizieu, U. Certa, J. Warrington, C. Gray, W. Keck, J. Mous, *Bacterial Transcript Imaging by Hybridization of Total RNA to Oligonucleotide Arrays,* Nature Biotechnol. **16**, 45(1998).

Dou02 J. A. Doudna and T. R. Cech, *The Chemical Repertoire of Natural Ribozymes,* Nature **418**, 222 (2002).

Duc97 M. W. Ducey, A. M. Smith, X. Guo, M. E. Meyerhoff, *Competitive nonseparation electrochemical enzyme binding/immunoassay (NEEIA) for small molecule detection*, Anal Chim Acta **357**, 5 (1997).

Duf98 D. C. Duffy, J. C. McDonald, O. J. A. Schueller, G. M. Whitesides, *Rapid Prototyping of Microfluidic Systems in Poly(dimethylsiloxane),* Anal. Chem. **70**, 4874 (1998).

Edw03 E. Oosterbroek and A. van den Berg, Lab-on-a-Chip: Miniaturized Systems for (Bio)chemical Analysis and Synthesis, Second Edition (Elsevier Science, 2003)

Ela03 M. Elangovan, H. Wallrabe, Y. Chen, R. N. Day, M. Barroso, N. Periasamy, *Characterization of One- and Two-Photon Excitation Fluorescence Resonance Energy Transfer Microscopy,* Methods **29**, 58 (2003).

Eri07 Erie Scientific Company Microarray, www.eriemicroarray.com

Fei96 J. Feigon, T. Dieckmann, F. W. Smith, *Aptamer Structures from A to ζ,* Chemistry & Biology **3**, 611 (1996).

Fei04 J. Feigon and C. Bustamante, *Nucleic Acids – Controlling Biology and Controlled by Biophysics,* Curr. Opin. Struct. Biol. **14**, 333 (2004).

Fer04 A. Ferguson, R. M. Boomer, M. Kurz, S. C. Keene, J. L. Diener, A. D. Keefe, C. Wilson, S. T. Cload, *A Novel Strategy for Selection of Allosteric Ribozymes Yields RiboReporter Sensors for Caffeine and Aspartame*, Nucleic Acids Research **32**, 1756 (2004).

Fis07 N. O. Fischer, T. M. Tarasow, J. B.-H. Tok, *Aptasensors for Biosecurity Applications*, Curr. Opin. Struct. Biol. **11**, 316 (2007).

Foo98 MAFF UK – Survey of Caffeine and Other Methylxanthines in Energy Drinks and Other Caffeine-Containing Products (March 1998) http://archive.food.gov.uk/maff/archive/food/infsheet/1998/no144/144caff.htm

For48 T. Forster, *Intermolecular Energy Migration and Fluorescence*, Annal. Physik. **2**, 55 (1948).

Ges99 R. F. Gesteland, T. R. Cech, and J. F. E. Atkins, The RNA World, Second Edition (Cold Spring Harbor Laboratory Press, Cold Spring Harbor, 1999).

Gil86 W. Gilbert, *Origin of Life: The RNA World,* Nature **319**, 618 (1986).

Gop06a S. C. Gopinath, T. S. Misono, K. Kawasaki, T. Mizuno, M. Imai, T. Odagiri, P. K. Kumar, *An RNA Aptamer That Distinguishes Between Closely Related Human Influenza Viruses and Inhibits Haemagglutinin-Mediated Membrane Fusion,* J. Gen. Virol. **87**, 479 (2006).

Gop06b S. C. Gopinath, Y. Sakayamaki, K. Kawasaki, P. K. Kumar, *An Efficient RNA Aptamer Against Human Influenza B Virus Hemagglutinin,* J. Biochem. **139**, 837 (2006).

Ha01 T. Ha, *Single-Molecule Fluorescence Resonance Energy Transfer,* Methods **25**, 78 (2001).

Ha03 T. Ha, J. Xu, *Photodestruction Intermediates Probed by an Adjacent Reporter Molecule,* Phys. Rev. Lett. **90**, 223002 (2003).

Han00 R. Hanna, and J. Doudna, *Metal Ions in Ribozyme Folding and Catalysis*. Curr Opin Chem Biol **4**, 166 (2000).

Hen83 L. Hendeles, M. Weinberger, *Theophylline. A "State of the Art" Review,* Pharmacotherapy **3**, 2 (1883).

Hen85 L. Hendeles, M. Weinberger, G. Mila Vetz, M. Hill 3d, L. Vaughan, *Food-Induced "Dose Dumping" From a Once-a-Day Theophylline Product and a Cause of Theophylline Toxicity*, Chest 87, 758 (1985).

Hua06 Z. Huang, D. Ji, S. Wang, A. Xia, F. Koberling, M. Patting, R. Erdmann, *Spectral Identification of Specific Photophysics of Cy5 by*

Means of Ensemble and Single Molecule Measurements, J. Phys. Chem. A **110**, 45 (2006).

Hun94 C. L. Huntoon, P. A. Whitson, and C. F. Sams, Hematologic and Immunologic Functions. In: Space Physiology and Medicine (Lea & Febiger, Philadelphia,1994).

IUP07 International Union of Pure and Applied Chemistry, Compendium of Chemical Terminology, Internet edition http://goldbook.iupac.org/

Kir04 R. Kirby, E. J. Cho, B. Gehrke, T. Bayer, Y. S. Park, D. P. Neikirk, J. T. McDevitt, A. D. Ellington, *Aptamer-Based Sensor Arrays for the Detection and Quantitation of Proteins,* Anal. Chem. **76**, 4066 (2004).

Klu94 S. J. Klug, and M. Famulok, *All you wanted to know about SELEX,* Mol. Biol. Rep. **20**, 97 (1994).

Koi99 M. Koizumi, G. A. Soukup, J. N. Q. Kerr, R. R. Breaker, *Allosteric Selection of Ribozymes that Respond to the Second Messengers cGMP and cAMP,* Nature Struct. Biol. **6**, 1062 (1999).

Kon07 X. Kong, E. Nir, K. Hamadani, S. Weiss, *Photobleaching Pathways in Single-Molecule FRET Experiments,* J. Am. Chem. Soc. **129**, 4643 (2007).

Kri01 R. V. Krishnan, R. Varma, S. Mayor, *Fluorescence Methods to Probe Nanometer-Scale Organization of Molecules in Living Cell Membranes*, J. Fluorescence **11**, 211 (2001).

Lak99 J. R. Lakowicz, Principles of Fluorescence Spectroscopy, Second Edition (Kluwer Academic, Norwell, 1999).

Lee05 H. J. Lee, A. W. Wark, L. Yuan, R. M. Corn, *Fabricating RNA Microarrays with RNA-DNA Surface Ligation Chemistry,* Anal. Chem. **77**, 7832 (2005).

Lev07 H. Levine and M. Nilsen-Hamilton, *A Mathematical Analysis of SELEX*, Comput Biol Chem. **9**, 17218151 (2007).

Lim05 D. V. Lim, J. M. Simpson, E. A. Kearns, M. F. Kramer, *Current and Developing Technologies for Monitoring Agents of Bioterrorism and Biowarfare,* Clin. Microbiol. Rev. **18**, 583 (2005).

Loc00 D. J. Lockhart and E. A. Winzeler, *Genomics, Gene Expression and DNA Arrays,* Nature **405**, 827 (2000).

Lor94 J. R. Lorsch J. W. Szostak, *In Vitro Selection of RNA Aptamers Specific for Cyanocobalamin.* Biochemistry. **33**, 973 (1994).

McC03 T. G. McCauley, N. Hamaguchi and M. Stanton, *Aptamer-Based Biosensor Arrays for Detection and Quantification of Biological Macromolecules,* Anal. Biochem. **319**, 244 (2003).

Mic00 A. Michienzi, L. Cagnon, I. Bahner, J. J. Rossi, *Ribozyme-Mediated Inhibition of HIV 1 Suggests Nucleolar Trafficking of HIV-1 RNA,* PNAS **97**, 8955 (2000).

Min88 M. Minsky, *Memoir on Inventing the Confocal Microscope*, Scanning **10**,128 (1988).

Mis05 T. S. Misono and P. K. Kumar, *Selection of RNA Aptamers Against Human Influenza Virus Hemagglutinin Using Surface Plasmon Resonance,* Anal. Biochem. **342**, 312 (2005).

Moo02 P. B. Moore and T. A. Steitz, *The Involvement of RNA in Ribosome Function,* Nature **418**, 229 (2002).

Mur98 J. B. Murray, A. A. Seyhan, N. G. Walter, J. M. Burke, W. G. Scott, *The Hammerhead, Hairpin and VS Ribozymes are Catalytically Proficient in Monovalent Cations Alone*. Chem Biol **5**, 587. (1998).

Nav06 N. K. Navani and Y. Li, *Nucleic Acid Aptamers and Enzymes as Sensors,* Curr. Opin. Chem. Biol. **10**, 272 (2006).

Oly07 Olympus Microscopy Resource Center: Advanced Techniques in Fluorescence Microscopy http://www.olympusmicro.com/primer/techniques/fluorescence/fluorhome.html

Osu02 C. K. O'Sullivan, *Aptasensors--the future of biosensing?* Anal. Bioanal. Chem. **372**, 44 (2002).

Pan05 Q. Pan, X. L. Zhang H. Y. Wu P. W. He, F. Wang, M. S. Zhang, J. M. Hu, B. Xia, J. Wu, *Aptamers that Preferentially Bind Type IVB Pili and Inhibit Human Monocytic-Cell Invasion by Salmonella entericaserovartyph*,. Antimicrob Agents Chemother. **49**, 4052 (2005).

Pat97 D. J. Patel, A. K. Suri, F. Jiang, L. Jiang, P. Fan, R. A. Kumar, S. Nonin, *Structure, Recognition and Adaptive Binding in RNA Aptamer Complexes,* J. Mol. Biol. **272**, 645 (1997).

Per02 M. J. Pereira, D. A. Harris, D. Rueda, N. G. Walter, *Reaction Pathway of the Trans-Acting Hepatitis Delta Virus Ribozyme: A Conformational Change Accompanies Catalysis*, Biochem. **41**, 730 (2002).

Per05 D. R. Perez, E. M. Sorrell, R. O. Donis, *Avian Influenza: An Omnipresent Pandemic Threat*, Pediatr. Infect. Dis. J. **24**, S208 (2005).

Pot98 R. A, Potyrailo, R. C. Conrad, A. D. Ellington, G. M. Hieftje, *Adapting selected nucleic acid ligands (aptamers) to biosensors,* Anal. Chem. **70**, 3419 (1998).

Pyl02 A. M. Pyle, *Metal Ions in the Structure and Function of RNA*, J Biol Inorg Chem **7**, 679 (2002).

Ras06 I. Rasnik, S. A. McKinney, T. Ha, *Non-Blinking and Long-Lasting Single Molecule Fluorescence Imaging,* Nat. Methods **3**, 891 (2006).

Ris97 J. Rishpon and D. Ivnitski, *An amperometric enzyme-channeling immunosensor,* Biosens Bioelectron **12** 195 (1997).

Rob94 D. E. Robbins and T. C. Yang, Radiation and Radiobiology. In: Space Physiology and Medicine (Lea & Febiger, Philadelphia,1994).

Rue05 D. Rueda and N. G. Walter, *Single Molecule Fluorescence Control for Nanotechnology,* J. Nanoscience and Nanotechnology **5**, 1 (2005).

Rue06 D. Rueda and N. G. Walter, *Fluorescence Energy Transfer Readout of an Aptazyme-Based Biosensor,* Meth. Mol. Biol. **335**, 289 (2006).

Rxl07 RxList: Theodure Indications & Dosage http://www.rxlist.com/cgi/generic/theosr_ids.htm

Sch96 M. Schena, D. Shalon, R. Heller, A. Chai, P. O. Brown, R. W. Davis, *Parallel Human Genome Analysis: Microarray-Based Expression Monitoring of 1000 Genes,* PNAS **93**,10614 (1996).

Sch01a F. W. Scheller, U. Wollenberger, A. Warsinke, F. Lisdat, *Research and Development in Biosensors*, Curr. Opin. Biotech. **12**, 35 (2001).

Sch01b I. Schmerold and H. Niedermuller, *Levels of 8-hydroxy-2'-deoxyguanosine in cellular DNA from 12 tissues of young and old Sprague-Dawley rats*, Exp. Gerontol. **36**, 1375 (2001).

Sco07 W. G. Scott, *Ribozymes,* Curr. Opin. Struct. Biol. **17**, 280 (2007).

Sek02 P. T. Sekella, D. Rueda, N. G. Walter, *A Biosensor for Theophylline Based on Fluorescence Detection of Ligand-Induced Hammerhead Ribozyme Cleavage*, RNA **8**, 1242 (2002).

Sem05 D. Semwogerere and E. R. Weeks, *Confocal Microscopy*, Encyclopedia of Biomaterials and Biomedical Engineering (2005).

Set94 R. S. Sethi, *Transducer Aspects of Biosensors*, Biosensors & Bioelectronics **9**, 243 (1994).

Shu97 A. P. Shuber, L. A. Michalowsky, G.S. Nass, J. Skoletsky, L.M. Hire, S. K. Kotsopoulos, M. F. Phipps, D. M. Barberio, K. W. Klinger, *High-Throughput Parallel Analysis of Hundreds of Patient Samples for More Than 100 Mutations in Multiple Disease Genes,* Hum. Mol. Genet. **6**, 337 (1997).

Sil03 S. K. Silverman, *Rube Goldberg goes (ribo)nuclear? Molecular switches and sensors made from RNA*, RNA **9**, 377 (2003).

Sou99a G. A. Soukup and R. R. Breaker, *Design of Allosteric Hammerhead Ribozymes Activated by Ligand-Induced Structure Stabilization,* Structure **7**, 783 (1999).

Sou99b G. A. Soukup and R. R. Breaker, *Engineering Precision RNA Molecular Switches,* PNAS **96**, 3584 (1999).

Sou00a G. A. Soukup and R. R. Breaker, *Allosteric Nucleic Acid Catalysts,* Curr. Opin. Struct. Biol. **10**, 318 (2000).

Sou00b G. A. Soukup and R. R. Breaker, *Altering Molecular Recognition of RNA Aptamers by Allosteric Selection,* J. Mol. Biol. **298**, 623 (2000).

Sou01 G. A. Soukup, E. C. DeRose, M. Koziumi, R. R. Breaker, *Generating New Ligand-Binding RNAs by Affinity Maturation and Disintigration of Allosteric Ribozymes,* RNA **7**, 524 (2001).

Sta98 T. K. Stage-Zimmerman and O. C. Uhlenbeck, *Hammerhead Ribozyme Kinetics,* RNA **4**, 875 (1998)

Sto07 R. Stoltenburg, C. Reinemann, and B. Strehlitz, *SELEX-A (r)evolutionary Method to Generate High-Affinity Nucleic Acid Ligands*, Biomol. Engin. **24**, 381 (2007).

Tay03 S. Taylor, S. Smith, B. Windle, A. Guiseppi-Elie, *Impact of Surface Chemistry and Blocking Strategies on DNA Microarrays,* Nuc. Acid. Res. **31**, (2003).

Tin05 R. Tinsley, Ph.D. dissertation, University of Michigan, Ann Arbor (2005).

Tom05 S. Tombelli, M. Minunni, E. Luzi, M. Mascini, *Aptamer-Based Biosensors for the Detection of HIV-1 Tat Protein,* Bioelectrochemistry **67**, 135 (2005).

Tow06 M. B. Townsend, E. D. Dawson, M. Mehlmann, J. A. Smagala, D. M. Dankbar, C. L. Moore, C. B. Smith, N. J. Cox, R. D. Kuchta, K. L. Rowlen, *Experimental Evaluation of the FluChip Diagnostic Microarray for Influenza Virus Surveillance*, J. Clin. Microbiol. **44**, 2863 (2006).

Ung99 M. Unger, E. Kartalov, C.-S. Chiu, H. A. Lester, S. R. Quake, *Single-Molecule Fluorescence Observed with Mercury Lamp Illumination,* BioTechniques **27**, 1008 (1999).

Vog06 S. S. Vogel, C. Thaler, and S. V. Koushik, *Fanciful FRET*, Science's stke **2**, 33 (2006).

Vol03 F. Vollmer, S. Arnold, D. Braun, I. Teraoka, A. Libchaber, *Multiplexed DNA Quantification by Spectroscopic Shift of Two Microsphere Cavities,* Biophys. J. **85**, 1974 (2003).

Wal98 N. G. Walter, K. J. Hampel, K. M. Brown, J. M. Burke, *Tertiary Structure Formation in the Hairpin Ribozyme Monitored by Fluorescence Resonance Energy Transfer*, The EMBO J. **17**, 2378 (1998).

Wal00 D. R. Walt, *Bead-Based Fiber-Optic Arrays,* Science **287**, 451 (2000).

Wal01 N. G. Walter, *Structural Dynamics of Catalytic RNA Highlighted by Fluorescence Resonance Energy Transfer*, Methods **25**, 19 (2001).

Wal02a N. G. Walter and D. R. Engelke, *Ribozymes: Catalytic RNAs That Cut Things, Make Things, and Do Odd and Useful Jobs*, The Biologist **49**, 200 (2002).

Wal02b N. G. Walter, *Probing RNA Structural Dynamics and Function by Fluorescence Resonance Energy Transfer*, Curr. Prot. Nuc. Acid Chem. **11.10**, 11.10.1 (2002).

Wal03a H. Wallrabe, M. Elangovan, A. Burchard, A. Periasamy, M. Barroso, *Confocal FRET Microscopy to Measure Clustering of Ligand-Receptor Complexes in Endocytic Membranes*, Biophys. J. **85**, 559 (2003).

Wal03b H. Wallrabe, Y. Chen, A. Periasamy, M. Barroso, *Issues in Confocal Microscopy for Quantitative FRET Analysis,* Microscopy Res. Tech. **69**, 196 (2006).

Wil92 C, Wilson and J. W. Szostak, *Ribozyme Catalysis,* Curr. Opin. Struct. Biol. **2**, 749 (1992).

Wil99 D. S. Wilson and J. W. Szostak, *In Vitro Selection of Functional Nucleic Acids,* Annu. Rev. Biochem. **68**, 611 (1999).

Zay05a N. V. Zaytseva, V. N. Goral, R. A. Montagna, A. J. Baeumner, *Development of a Microfluidic Biosensor Module for Pathogen Detection,* Lab Chip **5**, 805 (2005).

Zay05b N. V. Zaytseva, R. A. Montagna, A. J. Baeumner, *Microfluidic Biosensor for the Serotype-Specific Detection of Dengue Virus RNA,* Anal.Chem. **77**, 7520 (2005).

Zim98 G. R. Zimmermann, T. P. Shields, R. D. Jenison, C. L. Wick , A. Pardi, *A Semiconserved Residue Inhibits Complex Formation by Stabilizing Interactions in the Free State of a Theophylline-Binding RNA,* Biochem. **37**, 9186 (1998).

Zim00 G. R. Zimmermann, C. L. Wick, T. P. Shields, R. D. Jenison, A. Pardi, *Molecular Interactions and Metal Binding in the Theophylline-Binding Core of an RNA Aptamer,* RNA **6**, 659 (2000).

Zhe02 B. Zhen, Y. J. Song, Z. B. Guo, J. Wang, M. L. Zhang, S. Y. Yu, R. F. Yang, *In Vitro Selection and Affinity Function of the Aptamers to Bacillus Anthracis Spores by SELEX*, Sheng Wu Hua Xue Yu Sheng Wu Wu Li Xue Bao (Shanghai) **34**, 635 (2002).

Zhu02 X. Zhuang, H. Kim, M. J. B. Periera, H. P. Babcock, N. G. Walter, S. Chu, *Correlating Structural Dynamics and Function in Single Ribozyme Molecules,* Science **296**, 1473 (2002).

Zuk99 M. Zuker, D. H. Mathews, and D. H. Turner, *Algorithms and thermodynamics for RNA secondary structure prediction: A practical guide, RNA Secondary Structure*, RNA Biochemistry and Biotechnology, (NATO ASI Series, Kluwer Academic Publishers, 1999).

Zuk03 M. Zuker, *Mfold web server for nucleic acid folding and hybridization prediction*, Nucleic Acids Res. **31**, 3406 (2003).